P-13-42

Äspö Task Force on modelling of groundwater flow and transport of solutes

Task 7 – Subsurface flow and transport modelling of hydraulic tests and in situ borehole flow measurements conducted at Olkiluoto Island

Andrew Frampton, Stockholm University

Hrvoje Gotovac, University of Split

David Holton, Serco Assurance, Harwell

Vladimir Cvetkovic, Royal Institute of Technology (KTH)

October 2015

Svensk Kärnbränslehantering AB
Swedish Nuclear Fuel
and Waste Management Co

Box 250, SE-101 24 Stockholm
Phone +46 8 459 84 00

ISSN 1651-4416
SKB P-13-42
ID 1413213
October 2015

Äspö Task Force on modelling of groundwater flow and transport of solutes

Task 7 – Subsurface flow and transport modelling of hydraulic tests and in situ borehole flow measurements conducted at Olkiluoto Island

Andrew Frampton, Stockholm University

Hrvoje Gotovac, University of Split

David Holton, Serco Assurance, Harwell

Vladimir Cvetkovic, Royal Institute of Technology (KTH)

Abstract

This report summarises work conducted by the SKB-KTH modelling group within Task 7 of the Äspö Task Force on Modelling of Groundwater Flow and Transport of Solutes. An overarching theme for Task 7 is to address the issue of performance uncertainty in hydrogeological models for groundwater flow in sparsely fractured rock. A central aspect is to assess whether the uncertainty of the performance of such models can be reduced by making use of certain flow measurements, in particular the Posiva Flow Log device. As such, this work investigates and develops means by which directional, fracture-specific flow information can be used to improve and possibly reduce the uncertainty of the performance of hydrogeological models of water flow in bedrock. Based on the analysis and results obtained in this work, the use of flow-log data such as the type obtainable from Posiva Flow Log measurements can improve the design and performance of hydrogeological groundwater flow models for the scales considered.

Task 7 is subdivided into three subtasks each with specific aims and objectives addressing the overarching theme and additional specific hydrogeological research questions. Each subtask makes use of different but related data sets representing various spatial and temporal scales obtained from investigations at the island of Olkiluoto in Finland. The first sub-task, denoted as Task 7A, focuses on investigating a long-term pump test at a regional scale of a few kilometres comprising the entire island. The second, Task 7B, focuses on multiple cross-borehole interference tests at a block-scale of about 100 metres located close to the centre of the island, and the third, Task 7C, focuses on a single fracture scale of a few metres located close to repository depth.

The analysis conducted in Task 7A indicates that it is still very challenging to directly capture measured flows at the large scale without the use of formal model calibration methods. Questions are also raised whether formal calibration methods can be used for these hydrogeological systems as unique solutions are unlikely to be obtainable. However the use of flow measurements is favoured against sole use of pressure head measurements since flows can provide more detailed information on hydraulic pathways in the bedrock and indirectly provide information on heterogeneity and possibly also on connectivity.

This becomes more evident from the analysis conducted in Task 7B, where flow responses to multiple hydraulic pump tests are used to characterise and simulate in greater detail the flow complexity of a relatively small block-scale region of the sparsely fractured bedrock. A method which can be used to incorporate directional fracture-specific flows in discrete fracture network modelling is developed, demonstrated and applied with field measured flows. Flow responses are interpreted to indirectly provide indications on heterogeneity, primarily at the network scale but to some extent also at the single-fracture scale.

The analysis conducted in Task 7C demonstrates a possible downscaling method for which flow-log measurements complemented by additional detailed inflow measurements into a tunnel or shaft, or more detailed directional borehole measurements, may be used to develop conceptual models for single fractures. It is then shown how such an approach can be used together with numerical simulations of single heterogeneous fractures to analyse and compare results with field measurements, both on a quantitative as well as a qualitative basis.

Furthermore, a need to further develop improved conceptual fracture models and approaches for discrete fracture network flow modelling which can be used to combined flow and pressure data obtained in situ under field conditions is identified. The Posiva Flow Log device allows for direct, in situ flow measurements involving both flow direction and magnitudes and may therefore require new conceptual approaches for making efficient use directional flow data in groundwater modelling of sparsely fractured rock.

Sammanfattning

Denna rapport är en sammanfattning av arbete utfört av modelleringsgruppen SKB-KTH för modelleringsuppgiften Task 7 inom Äspö Task Force on Modelling of Groundwater Flow and Transport of Solutes. Ett övergripande tema inom Task 7 är att adressera osäkerhetsprestandan i hydrogeologiska modeller för grundvattenflöde i glest sprickigt berg. En central aspekt är att undersöka huruvida osäkerheten i sådana modeller kan minskas genom att utnyttja flödesmätningarna såsom Posivas differensflödeslogg. Detta arbete undersöker och utvecklar metoder som kan använda sprick-specifika flödesmätningar för att förbättra och möjligen minska osäkerheten i hydrogeologiska modeller av vattenflöde i berggrunden. Baserat på analyserna och resultaten som gjorts i denna studie kan användningen av differensflödesdata förbättra utformningen och prestandan av hydrogeologiska modeller för grundvattenflöde för skalorna som har analyserats.

Task 7 är indelat i tre deluppgifter med enskilda och specifika målsättningar som dels adresserar det övergripande temat samt belyser ytterligare specifika hydrogeologiska forskningsfrågor. Deluppgifterna använder sig av flera dataset motsvarande olika spatiala och temporala skalor från en mängd undersökningar på ön Olkiluoto i Finland. Den första deluppgiften är Task 7A och fokuserar kring att studera ett prolongerat pumptest och representerar en studie av vattenföring i berggrund i den regionala kilometerskalan som innefattar hela ön. Den andra är Task 7B som fokuserar kring en serie av borrhålsinterferenstester i de centralt belägna delarna av ön och representerar en blockskala om ca 100 meter. Den tredje är Task 7C som fokuserar kring en enskild spricka i slutförvarsdjup och motsvarar meterskalan.

Analyserna som utförts inom Task 7A belyser svårigheter med flödeskonditionering i den regionala skalan som utförs utan formella kalibreringsmetoder. Å andra sidan finns det frågetecken kring huruvida formella kalibreringsmetoder verkligen kan användas för dessa hydrogeologiska problem eftersom parametersviden omöjliggör unika lösningar. Flödesmätningar ger dock en kompletterande och mer detaljerad informationsbild av flödessystemet som inte kan åstadkommas från enbart tryckmätningar i borrhål. Flödesmätningarna kan även i viss mån ge indikationer kring heterogenitet och möjligen även systemets konnektivitet.

Det sistnämnda undersöks i större grad genom analyserna som utförts inom Task 7B, där flödesresponser från flera hydrauliska interferenstester används för att karakterisera och i större detaljgrad simulera flödeskomplexiteten i spricknätverket i blockskalan. En metod för att inkludera sprickspecifika flödesmätningar i diskret sprickmodellering utvecklas, demonstreras och appliceras med flödesmätningar från fältet. Tolkningar av flödesresponser är att dessa ger indikationer om systemets heterogenitet, främst i nätverksskalan men även i viss mån i den enskilda sprickskalan.

Analyserna som utförs inom Task 7C demonstrerar en möjlig nerskalningsmetod som kan användas för att utveckla konceptuella modeller för enskilda sprickor där man kan använda differensflödesmätningar samt mätningar av inflödet i tunnlar och detaljerade mätningar av flödesriktningen i borrhål. Metoden kan sedan användas tillsammans med numeriska simuleringar för enskilda heterogena sprickor för att analysera och jämföra resultat både kvantitativt och kvalitativt med fältmätningar.

Ett behov har identifierats för att utveckla förbättrade konceptuella modeller för sprickor samt tillvägagångsätt för diskret sprickmodellering som kan använda sig av kombinerade flödes- och tryckdata från in situ fältmätningar. Posivas differensflödeslogg erbjuder direkta, in situ flödesmätningar med både flödesriktning och flödesmängd och kan därför behöva nya konceptuella metoder för att kunna använda riktad flödesdata i grundvattenmodellering av sprickigt berg.

Contents

1 Introduction and objectives

This report summarises work conducted by the SKB-KTH modelling group for Task 7 in the Äspö Task Force on Modelling of Groundwater Flow and Transport of Solutes.

The background of Task 7, as well as a description of its scope and objectives, is documented in the overall Task 7 Description Document (Vidstrand et al. 2015). The following contains a brief summary of the background, scope and objectives of Task 7 with an emphasis of the main aspects of interest from the perspective of the SKB-KTH modelling group.

1.1 Background

The work conducted within Task 7 concerns hydrogeological modelling at several spatial and temporal scales of the Olkiluoto Island in Finland. The reason for conducting hydrogeological modelling is in relation to the on-going site characterisation programme of the Island, as well as in combination with the construction of the Onkalo underground facility and planned future deep repository site, which provides vast amounts of field and site data. In particular, hydrogeological information collected during the construction of the deep repository may be useful as it may provide additional information and complement traditional surface and borehole studies. Here, the overall aim is to improve the characterisation of the hydraulic properties of the bedrock, which in turn may be useful in reducing characterisation and performance assessment uncertainty.

Thus the focus is on a relatively broad setting, with an over-arching aim at addressing safety assessment issues based on field characterisation information stemming from site investigations. One specific aspect is making use of flow measurements obtained in boreholes, both during long term and short term pump tests, as well as for non-pumped conditions, in order to improve the understanding of the behaviour of the hydrogeological flow system and its responses at both small and large spatial scales.

1.2 Scope and objectives of Task 7

The main motivation of this work is to improve the understanding the hydraulic system of a region prior to and during the construction of a deep subsurface repository for spent nuclear fuel. Therefore, an overall objective is to learn how the uncertainty of the hydraulic characterisation of the subsurface hydrogeological flow system can be reduced, through a combination of field investigations, conceptual modelling, and numerical modelling. One specific objective is exploring new ways in which the Posiva Flow Log (PFL) measurement instrument can be used in modelling. The PFL tool is a quick and efficient means of characterising subsurface hydraulic flow responses in open boreholes, and can be used both during non-pumped and pumped conditions. It can measure flow rates over a wide range of values and can resolve individual flowing features with high spatial resolution, as well as determine the flow direction in terms of flow entering or leaving the borehole.

That is, the PFL tool can provide high quality and detailed characterisation data of the subsurface, and a general objective is to understand how this type of characterisation data can be used efficiently, accurately and in novel ways, both for conceptual and numerical modelling of the subsurface. Hence, the overall objective previously stated may be rephrased as to understand how a reduction in characterisation uncertainty can be achieved, primarily by maximising the use of measurement techniques such as the PFL. Hence, for the work conducted herein, one particular emphasis is on understanding and maximising the potential and use of the PFL instrument and the information it can deliver.

2 Task specifications

The description of the Task 7 specifications is documented in the Task 7 Description Document (Vidstrand et al. 2015), which also contains details of the description of subtasks Task 7A, 7B and 7C. The following contains a brief summary of the specifications of Task 7A, Task 7B and Task 7C with an emphasis of the main aspects of interest for the SKB-KTH modelling group.

2.1 Task 7A – Regional scale

The focus of Task 7A is on understanding and interpreting a long-term pumping experiment conducted at the Olkiluoto Island in Finland. The main objective is aimed at simulating the hydraulic responses measured during a long-term pumping test carried out in borehole KR24 in the spring of 2004.

The focus is on increasing the understanding of the major fracture zones acting as boundaries for bedrock compartments and the interaction between these possibly isolated compartments and the major flow system. The work as a whole is intended to further provide a bridge between site characterisation and safety assessments. The long-term pump test is provides responses at a spatial scale of kilometres. The Posiva Flow Log (PFL) device is used to measure flow in the pumped borehole as well as flow responses in open boreholes. Also, conventional pressure observations are made in open and packed-off boreholes distributed throughout the Island.

Hence there is potential at understanding the large scale responses due to a long-term pump test and obtain a general understanding of the large scale hydrogeological flow and transport processes. This may be of relevance for safety and performance assessment as flow pathways and transport may occur over large spatial scales and encompass significant temporal scales.

2.2 Task 7B – Block scale

The focus of Task 7B is on understanding and interpreting a series of cross-borehole pumping experiments in a block-scaled region of the Olkiluoto Island conducted in the winter of 2002, which represents spatial scales of a few hundred metres. The main objective is aimed at simulating the hydraulic responses measured during each of the cross-borehole pump tests, which are performed in sequence for the five boreholes KR14–KR18, and each for a sufficiently long time period such that steady-state conditions are obtained. Here PFL measurements are also conducted, both in pumped boreholes as well as observation boreholes.

The focus is on understanding the hydrogeological flow system at an intermediate spatial scale denoted as the block-scaled fracture network. Furthermore, the focus is also on how PFL flow measurements can be used to create a suitable hydrogeological model at this scale. The main objective is to create a model which is easily configured and not inconsistent with available measurements. A notable challenge in this task is making use of detailed flow response data in neighbouring observation boreholes for each pump test. Since multiple tests are conducted, which means the same hydrogeological system is forced with different drawdowns and at different spatial locations, the system is being forcing with multiple non-symmetric gradients, thereby potentially provided additional information of its hydrogeological behaviour.

Hence, here an overall aim is also to attempt to reduce uncertainty in the performance of a hydrogeological model, primarily based on the use of PFL measurement information.

2.3 Task 7C – Single-fracture scale

The focus of Task 7C is on understanding and interpreting flow measurements obtained in a single fracture intersecting an open ventilation shaft, which were conducted in August 2009. This is

performed during the construction phase of the Onkalo facility in Olkiluoto Island. The main objective is aimed at simulating the observed heterogeneity of the inflow measurements obtained at the circumference of intersection of the shaft wall with the fracture.

The focus is on understanding the variability in flow measurement data at a single fracture scale, and addressing internal fracture heterogeneity for a fracture with very low transmissivity. Here numerical simulations combined with conceptual models of fracture heterogeneity structures are used to identify possible heterogeneity structures which can be consistent with measured data. The shaft inflows are not measured with a tailor-made device, not with the PFL instrument. However, PFL measurement data from previous boreholes intersecting the fracture prior to shaft excavation are used to assign a mean fracture transmissivity. Thereafter the main constraining parameters are flow magnitudes measured along an internal circumference of the fracture intersection with the shaft wall, measured with a relatively coarse resolution under a relatively short time scale.

3 Task 7A

3.1 Modelling Approach

3.1.1 Overall approach

The overall approach for the modelling work conducted in Task 7A is to attempt to reduce the performance assessment uncertainty of a regional scale hydrogeological model of Olkiluoto based on using data obtained from hydraulic tests conducted on the island. This is done by comparing field measured drawdown and flow responses obtained during the long-term pump test conducted at borehole KR24 with simulated drawdown and flow responses. The simulated model is first configured as a forward model, based on a general understanding of the field characterisation data. It is thereafter revised and modified according to general interpretations of the performance of the model. Thereby, uncertainties or inherent unknowns in the model configuration can be revised and updated. Thereafter new simulated results can be compared with appropriate field measurements. As such, a 'trial-and-error' approach is used to attempt to adjust various aspects of the model, both in terms of conceptual assumptions and variations in parameters which cannot be determined directly from field data, in order to obtain an improved model which is not inconsistent with field data.

In the modelling work performed within Task 7A, the fracture system and hydrogeological properties of the entire Olkiluoto Island is represented with a discrete fracture network (DFN) model. In this model, only deterministic fractures are employed. At the scale of the Olkiluoto Island, this includes the relatively large hydraulic zones which are known or believed to be known, and tend to transect large parts or most of the subsurface domain of the island. For simplicity, stochastic features or background fractures in the deep subsurface are not considered.

The main objective of the work conducted is to make use of flow log data obtained from the Posiva Flow Log (PFL) instrument. First, it is necessary to get acquainted with the flow log data obtained from PFL instrument in terms of understanding how field measurements are conducted and what data is provided and how such data should be interpreted. Thereafter, an objective is to evaluate how the PFL flow log data can be used for constructing and modifying a numerical model of the hydrogeological flow system. That is, to evaluate if PFL data could be useful for condition a model, and if so, how this could be achieved. Thereafter, an objective is to apply PFL data to model construction and conditioning and evaluate to what extent the model may have been improved. The final objective is to study the impact of resulting flow systems in terms of advective transport and retention properties in order to attempt to describe the long-term performance of model improvement based on PFL data.

3.1.2 Data usage and interpretation

A general understanding of the field characterisation data, based on the Task Definition Document and an aggregated data analysis of the multiple Data Deliveries for Task 7A, has been a basis for conducting the modelling in Task 7A. The main data used to construct the DFN hydrogeological model is listed in the following. A more detailed description of the model and how the data is implemented is provided in Section 3.2.2.

- The lateral sides of the model domain are defined by the hydraulic conductors in contact with Baltic Sea, obtained from Data Delivery 8c, file "boundaries.txt".
- The top surface of the domain has a boundary condition based on surface elevation, which is obtained from Data Delivery 9, file "topo2.dat", together with the description of the data from Data Delivery 10c, file archive "topography-grid-format.zip".
- Geometries of fracture zones are obtained from Data Delivery 8c, files "smallFaces4.txt" and "largeFaces4.txt".
- Hydraulic properties of fractures are obtained from "Promemoria 2007-01-31" (page 8).

- Geometries of boreholes, including casing depths and packed-off sections, are obtained from Data Delivery 8b, file archive “TF_taskdefinition7a_lev1/borehole-xyz-data.zip/” and file “TF_taskdefinition7a_lev1/measuring sections of packed-off boreholes.xls”.
- Flow data measured in boreholes is obtained from Data Delivery 8b, files “TF_taskdefinition7a_lev1/KR14-flow.xls”, etc.
- Drawdown data measured in boreholes is obtained from Data Delivery 6, files in directory “pumping-test-pressure responses”.
- Heads and pumping rates for the long-term pumping test in KR24 are obtained from Data Delivery 8b, files “heads in pumping borehole KR24.xls” and “pumping-rate-KR24.xls”.

3.2 Conceptual Model

3.2.1 Main assumptions and simplifications

A discrete fracture network (DFN) approach is used and matrix flow is not considered. The domain is three-dimensional and each fracture is represented by a two-dimensional rectangular surface or conduit with an assigned transmissivity. This can be seen as flow through parallel plates with a given void space (fracture aperture) or as Darcy flow through a thin slab of porous media with an effective transmissivity (hydraulic conductivity integrated over the fracture aperture). The advantage of the latter is effective fracture transmissivity is easier to obtain from field investigations than effective aperture.

The simulations are used to evaluate long-term (steady-state) conditions during pumping; that is, in this study transient responses during the early pumping phases are not considered. The steady-state, constant density groundwater flow equation is used to obtain fluid pressure at the intersections of the fracture network.

Volumetric flow Q through each fracture is obtained from the gradient of the pressure field grad(P) between intersections by assuming a homogenous transmissivity T (or hydraulic conductivity K with aperture $2b$) within each fracture (between intersections), which results in

$$Q = w\, T\, \mathrm{grad}(P) / (\rho\, g)$$

for a fracture plane of width w, and where ρ = 1,000 kg/m^3 is fluid density of water assumed to be constant and g = 9.81 m/s^2 is the gravitational constant.

When designing a DFN, both fracture geometrical and hydraulic properties are needed. In this work, fracture zones have a defined geometry provided by the data deliveries of Task 7A. The geometries are obtained (inferred) from extensive field characterization work. The hydraulic properties of fractures, here primarily fracture transmissivity, is also obtained from the data deliveries of Task 7A. These stem from hydraulic tests and flow measurements conducted during field characterization. As such, effectively homogenous fracture transmissivity is generally assumed.

3.2.2 Geometrical description

Domain

The domain is a three-dimensional closed region forming in a generalised sense a polyhedron structure. The lateral sides of the model domain are defined by the hydraulic conductors in contact with Baltic Sea. The top surface is at elevation z = 0 m.a.s.l., and the bottom surface is at elevation z = –1,000 m.a.s.l.. The domain size is approximately of the scale 7 km by 4 km by 1 km.

The top surface has a sub-grid (x, y, z) division of 100 by 100 by 10 boxes based on a square domain of 7,800 m by 7,800 m by 1,000 m. Thus the top surface has a resolution of size 78 m by 78 m, which means the top surface BC is averaged over these 78 m by 78 m squares.

Fractures

Fractures are two-dimensional planar surfaces formed by rectangular polygons. All deterministic fracture zones are included as specified. That is, the large versions are used, and several of these extend to the model boundaries, and zones HZ19B and HZ20B are not used. The transmissivity T of each fracture zone is constant (that is, effectively homogeneous fractures are assumed), and the values used for assigning T are the given geometric mean values of T (page 8 of Promemoria 2007-01-31). The source files for the fracture geometry data is given in Data Delivery 8, in the subdirectory "pkg4/", as ASCII text files with fracture zones defined by triangulated surfaces.

All fractures in our model are rectangular fractures defined by the ConnectFlow / Napsac ASCII format, and they are tessallated to a 100 m length scale. They are further tessallated to a 10 m length scale in the vicinity (100 m radius) of the borehole – fracture intersections. The FEM has a resolution of approximately 10 by 10 elements for each tessallated fracture; thus in the case of 100 m tessallation, the FEM resolution is of the order of 10 m by 10 m, and in the case of 10 m tessallation, the FEM is of the order of 1 m by 1 m.

A near-surface DFN is generated as a random network of fractures with uniform orientations and a homogeneous areal density (P32 density). Each fracture has a constant size of 50×50 m^2 and transmissivity of $T = 1E{-}5.9$ m^2/s, such that the effective hydraulic conductivity is 1E–7 m/s. The spatial extent of the near-surface DFN extends horizontally over the entire domain and vertically down to a depth z > = –70 m.

Boreholes

All boreholes are used as specified. Boreholes are implemented as one-dimensional features and are defined by given sets of (x, y, z) coordinates. The top of the borehole (x, y, z) coordinates are defined by the bottom of the borehole casings. The casings and packed-off sections are given in Data Delivery 8 in the file "measuring sections of packed-off boreholes.xls" as distance along borehole. The borehole coordinates and distance along borehole are given in the .pth files contained in Data Delivery 8 in the sub-directory "TF_taskdefinition7a_lev1/borehole-xyz/". Therefore, it was necessary to interpolate the borehole coordinate data using the appropriate distances along boreholes, in order to obtain the correct (x, y, z) coordinates for each of the packed-off sections of boreholes and borehole casings.

For the simulations requiring no boreholes, the boreholes are implemented as above, but assigned a low permeability value. Section 3.4.2 describes a sensitivity study of the use of assigning low permeability values to boreholes.

Borehole KR24 is implemented in two ways. The first approach is as three hydraulically connected boreholes; the top section has radius $r_t = 0.0757$ m, the middle section has radius $r_m = 0.002$ m, and the bottom section has radius $r_b = 0.0757$ m. Then, whenever extraction is simulated in KR24, a pumping rate is assigned to the top part of KR24 only. Thus, the by-pass packer is implemented in borehole KR24 as suggested in *Option 1* of the Task description (page 8 of Task7A; Part 1; Version 3.0; dated 2006-11-01). However, no consideration has been taken to the fact that in reality, the flow through this bypass packer is probably in the turbulent regime.

The second approach is as two disconnected boreholes; both the top and bottom sections have radius $r = 0.0757$ m but they are separately defined by their respective (x, y, z) coordinates. Then whenever extraction is simulated in KR24, different pumping rates are assigned to the top and bottom parts, as suggestion in *Option 2* of the same Task description.

Figure 3-1 illustrates the domain setup for the base case scenario, showing the top surface boundary condition where head is equal to elevation, the domain boundaries which have head set to zero and are in contact with the Baltic Sea, as well as the inside of the model domain with the major fracture zones as discrete features, coloured by transmissivity. Figure 3-2 shows the resulting head distribution after solving for the pressure field for simulation SS02a (natural flow with conductive boreholes) as well as for simulation SS04a (pumping in KR24 with conductive boreholes).

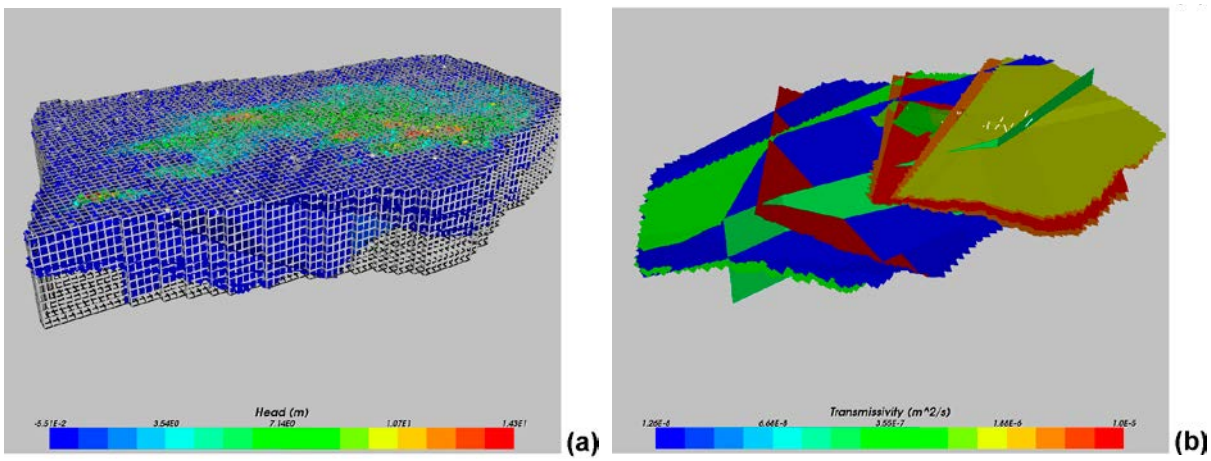

Figure 3-1. *Illustration of domain. (a) Domain boundaries trimmed to hydraulic conductors in contact with the Baltic Sea, coloured by head (illustrates top surface BC). (b) Deterministic fracture zones coloured by transmissivity.*

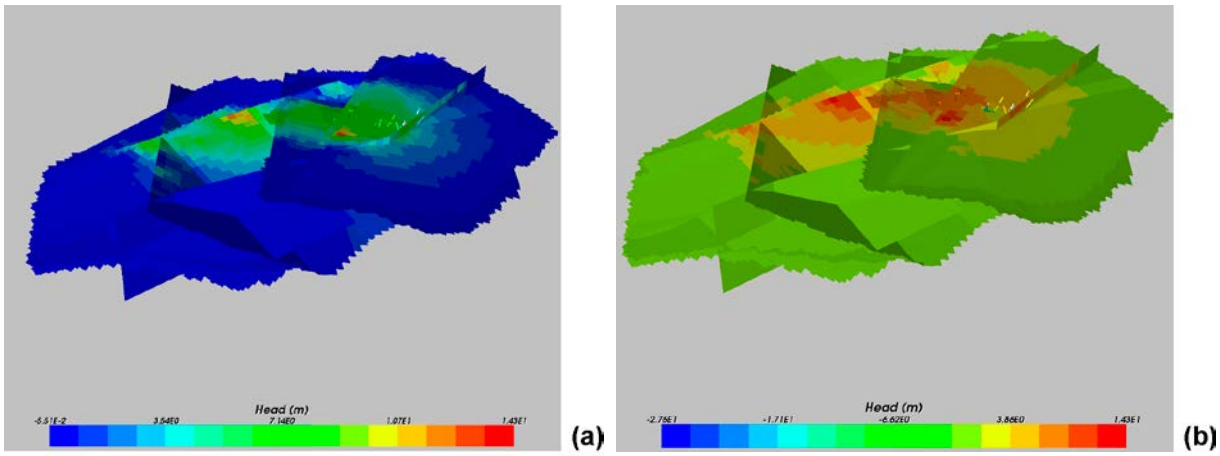

Figure 3-2. *Illustration of domain. (a): Head distribution for SS02a (natural conditions with conductive boreholes) with top surface DFN removed. (b): Head distribution for SS04a (pumping with conductive boreholes) with top surface DFN removed.*

3.2.3 Processes considered

Fluid properties are that of fresh water with constant density. Steady-state conditions are assumed throughout, that is, the initial transient responses during pumping are ignored. Thus possible processes such as saltwater intrusion and density-dependent effects are not considered. Also, temporal effects such as infiltration and a variable groundwater table in the unsaturated regime are not considered.

However, the fracture network is explicitly accounted for by the inclusion of a DFN representing the main hydrogeological features of the island. Thus, large-scale heterogeneity in sparsely fractured media is to some extent accounted for. Thus, resulting flow and advective transport in a large-scale heterogeneous formation are included.

3.2.4 Boundary and initial conditions

The top surface has head equal to elevation; h(top) = z. The file used for elevation is “topo2.zip” from Data Delivery 9 (aided by explanations in Data Delivery 10).

The lateral sides which are in contact with the Baltic Sea have head set to zero; h(sides) = 0. The file which defines the geometry of the lateral sides is is "pkg4/boundaries.txt" obtained from Data Delivery 8.

The bottom surface is at z = –1,000 m and has a no-flow BC.

3.3 Model Implementation

3.3.1 Numerical model

The software used for the simulations which are presented in this report is ConnectFlow, provided by Serco Assurance, Harwell, UK. ConnectFlow is a finite element (FEM) code for solving flow and transport in porous media which incorporates both continuum porous media (CPM) and discrete fracture media (DFN) approaches. A detailed technical description of the software is provided by Hartley and Holton (2008a, b) and Hartley et al. (2008a, b).

In the modelling currently performed only the DFN (Napsac, v9.4) approach was used. In the Napsac code, fractures are discretized in the fracture plane by a regular finite-element mesh. Fracture intersections are approximated by the nearest FEM nodes. Thereafter the pressure field is solved at each node of the system by applying boundary conditions at relevant nodes of the domain. Once the pressure field is solved for, the flow field in the fracture system is obtained by applying Darcy's law.

In particular, boreholes are implemented as one-dimensional lines and such that they act as hydraulically conductive features by connecting nodes along the fractures they intersect. A borehole (well) model is used to correct for the pressure in the borehole relative to the pressure in the fracture plane. If P_W is the pressure in the borehole node and P_{PE} is the pressure in the FEM node corresponding to the location of the borehole, then

$$P_W = P_{PE} + \frac{Q}{\Gamma}$$

where Γ is a function which depends on the fracture transmissivity and on skin, and Q is the flow in the fracture plane, given by

$$Q = \int_{n \in \Omega} \nabla \phi_n \frac{T}{\rho g} \nabla h$$

where the integral is over elements containing n.

3.3.2 Parameters

The main model parameters are geometric and hydraulic fracture properties, in particular fracture transmissivity. For model conditioning, the parameter which is varied is fracture aperture. Fracture aperture *2b* is directly related to fracture transmissivity *T* by the cubic law relationship, $T = \rho\, g\, (2b)^3 / (12\, \mu)$, where μ = 0.001 kg/ms is fluid viscosity, ρ =1,000 kg/m^3 is fluid density, and g = 9.81 m/s^2 is the gravitational constant.

When presenting results, the labelling convention used for boreholes is shown in Table 3-1, and the convention used for borehole-fracture intersections is shown in Table 3-2.

3.3.3 Model conditioning and calibration

A trial-and-error approach is adapted to attempt to improve the first (forward) model configuration. The model parameter which is varied is fracture aperture, where fractures are maintained homogenous. The objective is not to perform a robust calibration procedure, but rather attempt to obtain a reasonable range of valid/consistent apertures and hence transmissivities, based on PFL data and assuming homogenous fracture zones.

Table 3-1. The labelling for the boreholes shown in figures with pressure head results (Figure 3-4, Figure 3-6, Figure 3-8, etc).

Label	Borehole	Label	Borehole
0	KR01T2	10	KR22
1	KR01T4	11	KR23T2
2	KR01T6	12	KR25T1
3	KR01T7	13	KR25T3
4	KR01T8	14	KR25T4
5	KR04	15	KR25T6
6	KR07	16	KR25T7
7	KR08	17	KR25T8
8	KR10	18	KR27
9	KR14	19	KR28

Table 3-2. The labelling for the borehole – fracture intersections shown in figures with flow results (Figure 3-3, Figure 3-5, Figure 3-7, etc).

Label	Borehole	Fracture	Label	Borehole	Fracture
0	KR04	HZ19A	21	KR22	HZ20A
1	KR04	HZ19A	22	KR22	HZ20A
2	KR04	HZ19A	23	KR22	HZ20B_ALT
3	KR04	HZ19C	24	KR27	HZ004
4	KR04	HZ19C	25	KR27	HZ19A
5	KR04	HZ19C	26	KR27	HZ19A
6	KR04	HZ20A	27	KR27	HZ19A
7	KR04	HZ20A	28	KR27	HZ19C
8	KR04	HZ20B_ALT	29	KR27	HZ19C
9	KR04	HZ20B_ALT	30	KR27	HZ20A
10	KR14	HZ002	31	KR28	HZ19A
11	KR14	HZ002	32	KR28	HZ19A
12	KR14	HZ19A	33	KR28	HZ19A
13	KR14	HZ19C	34	KR28	HZ19A
14	KR14	HZ19C	35	KR28	HZ19C
15	KR14	HZ19C	36	KR28	HZ19C
16	KR14	HZ19C	37	KR28	HZ19C
17	KR14	HZ19C	38	KR28	HZ19C
18	KR22	HZ19A	39	KR28	HZ20A
19	KR22	HZ19A	40	KR28	HZ20B_ALT
20	KR22	HZ19C	41	KR28	HZ20B_ALT

3.4 Results

3.4.1 Reference case with boreholes: SS02a

Here results from the reference/base case scenario SS02a are shown. Boreholes are open and free to conduct flow shows a comparison of the simulated and measured flows as well as the absolute differences between the simulated and measured flows, for selected borehole and fracture intersections. Figure 3-4 shows a comparison of the simulated and measured head values in selected boreholes and packed-off sections in boreholes. The labelling used for boreholes is provided in Table 3-1, and for borehole-fracture intersections is provided in Table 3-2.

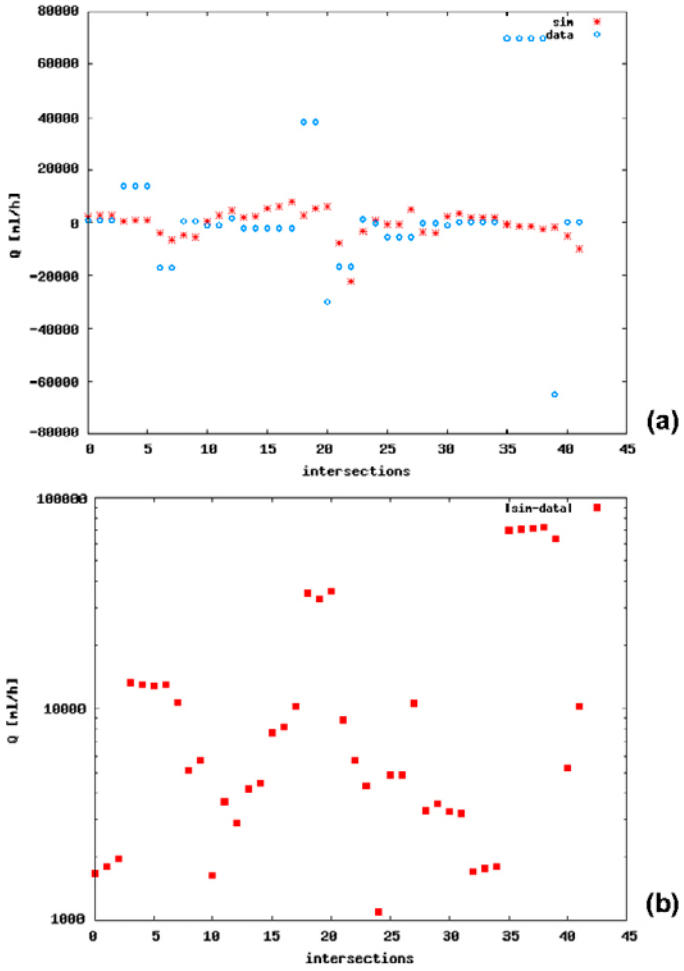

Figure 3-3. *SS02a flows: Boreholes are open and free to cross-flow; no permeability is assigned, instead boreholes are defined by their radius. The horizontal axes indicates measurement points in BHs which have been assigned to a specific fracture intersection. The vertical axes is the flow rate measured or simulated in units ml/h (positive value means flow from fracture to borehole). (a) Simulated results vs given measurements. (b) Absolute difference of (a). See Table 3-2 label numbering.*

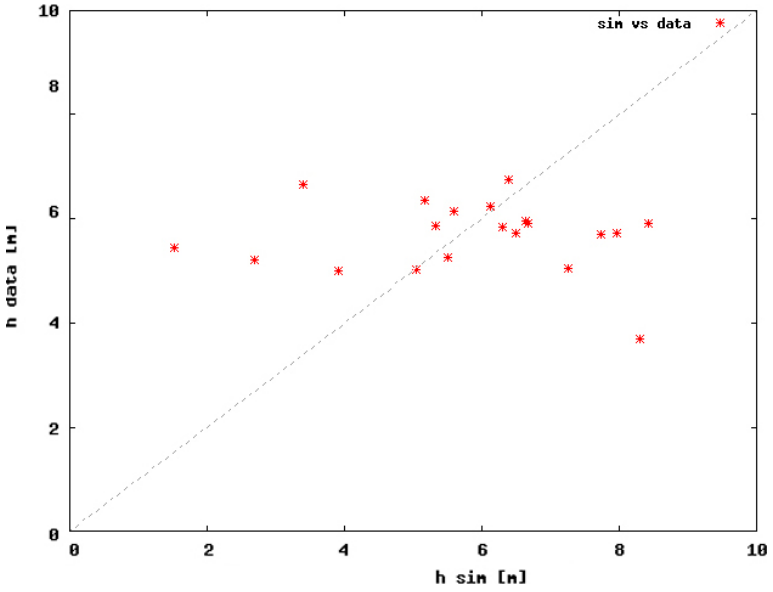

Figure 3-4. *SS02a heads: Boreholes are open and free to cross-flow; no permeability is assigned, instead boreholes are defined by their radius and flow in an open smooth pipe is assumed. Simulated head (horizontal axis) vs given measurements (vertical axis). See Table 3-1 for label numbering scheme.*

3.4.2 Reference case with no boreholes: SS01

The results from the scenario with no boreholes, ie SS01, are shown in Figure 3-5 (flows) and Figure 3-6 (heads). The implementation of "no boreholes" is done by assigning a low permeability value to the borehole, such that there is essentially no flow along (up/down/across) the borehole. The permeability assigned is $\kappa = 1E{-}15\ m^2$.

Also, to check the sensitivity of assigning a low permeability value to the boreholes, several simulations with varying borehole permeabilities have been conducted. The results from these simulations are shown in Figure 3-7 (flows) and Figure 3-8 (heads), where the permeabilities assigned are in increasing order $\kappa = 1E{-}17\ m^2$, $\kappa = 1E{-}15\ m^2$, $\kappa = 1E{-}13\ m^2$, $\kappa = 1E{-}11\ m^2$, $\kappa = 1E{-}9\ m^2$, $\kappa = 1E{-}7\ m^2$, and $\kappa = 1E{-}5\ m^2$.

As can be seen from Figure 3-7 and Figure 3-8, as the permeability increases the simulated results exhibit greater variation in flow values, and the variation approaches that of the simulation with open boreholes (see Section 3.4, Figure 3-3). The threshold is at around $\kappa = 1E{-}5\ m^2$ since the variation is exactly the same as the simulation with open boreholes (cf. Figure 3-3).

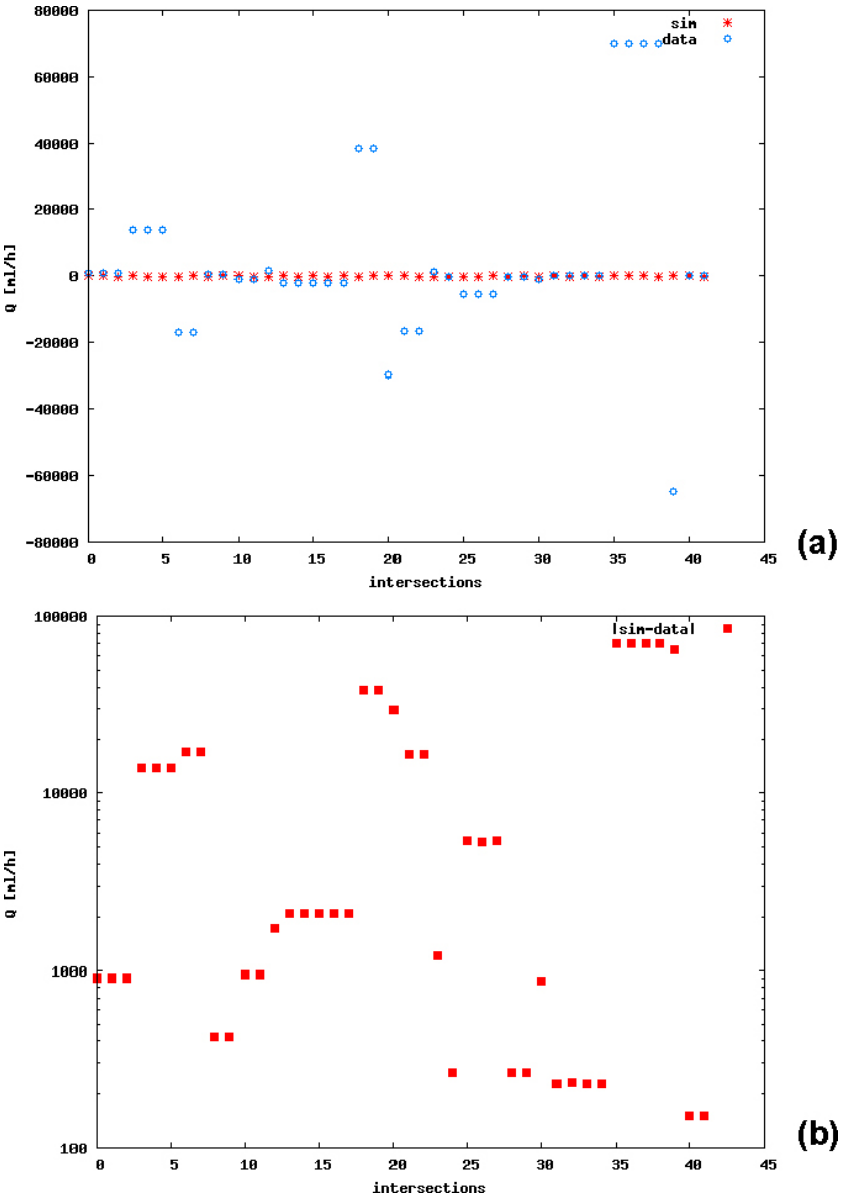

Figure 3-5. *SS01 flows: Boreholes are not open and free to cross-flow; boreholes are defined by a low permeability* $\kappa = 1E{-}15$. *(a) Simulated results vs. given measurements. (b) Absolute difference of simulated results and given measurements. See Table 3-2 for label numbering scheme.*

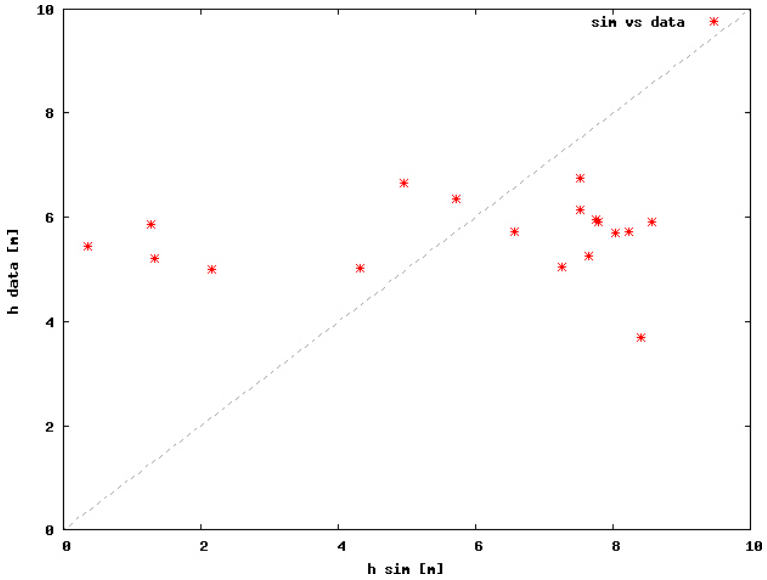

Figure 3-6. *SS01 heads: Boreholes are not open and free to cross-flow; boreholes are defined by a low permeability* κ *= 1E–15. Simulated head (horizontal axis) vs. given measurements (vertical axis). See Table 3-1 for label numbering scheme.*

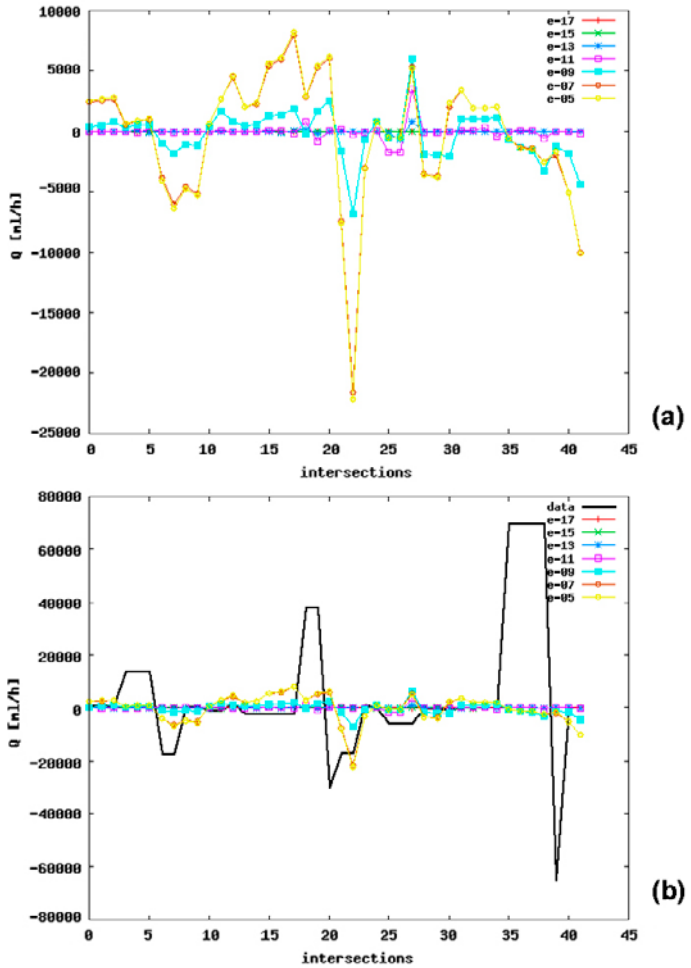

Figure 3-7. *SS01 flows: Sensitivity study of assigning borehole permeability* κ*. Shown are values of* κ *= 1E–17 m², κ = 1E–15 m², κ = 1E–13 m², κ = 1E–11 m², κ = 1E–9 m², κ = 1E–7 m², and κ = 1E–5 m². Note that as* κ *increases, the simulated results converge to the simulation results of SS02a. (a) Comparison of various choices of* κ*; simulated results only. (b) Comparison of various choices of* κ*; simulated results vs. given measurements (solid black line). See Table 3-2 for label numbering scheme.*

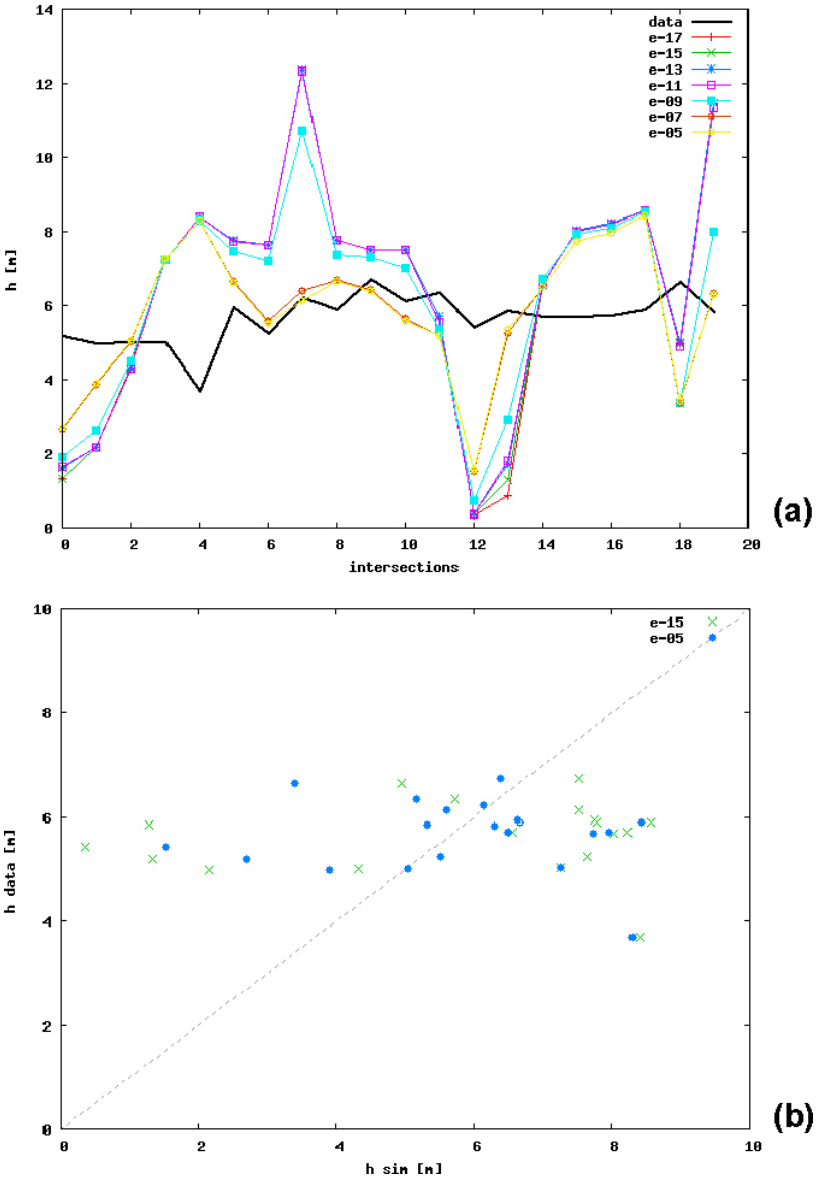

Figure 3-8. *SS01 heads: Sensitivity study of assigning borehole permeability* κ*. Shown are values of* κ *= 1E–17 m², κ = 1E–15 m², κ = 1E–13 m², κ = 1E–11 m², κ = 1E–9 m², κ = 1E–7 m², and κ = 1E–5 m². Note that as* κ *increases, the simulated results converge to the simulation results of SS02a. (a) Comparison of various choices of* κ*; simulated results vs given measurements. (b) Simulated head (horizontal axis) vs. given measurements (vertical axis); comparison of* κ *= 1E–15 (green cross) and* κ *= 1E–5 (blue asterisks). Note that* κ *= 1E–15 exhibits slightly more spread in head compared with* κ *= 1E–5, that is, the addition of boreholes show a homogenization of the responses as connectivity increases. See Table 3-1 and Table 3-2 for label numbering scheme.*

3.4.3 Variations of reference case: SS02b

Figure 3-9 through Figure 3-14 show results from the scenario based on the reference case scenario, but with a trial-and-error approach to calibration/varying model parameters, here the parameter which is varied is fracture aperture. Here boreholes are open and free to cross-flow. The objective here is not to perform a robust calibration procedure, but rather to get a feel of the valid parameter range for aperture, assuming homogenous fracture zones.

However, a complication when varying transmissivity or aperture for homogenous fracture zones is the fact that the absolute differences of simulated and measured flow or head values vary depending on fracture-to-borehole intersections. That is, for a given fracture, its intersection with one borehole may produce a small absolute difference in say head or flow and in another borehole a large absolute difference. Thus it may be difficult, if not impossible, to obtain a more accurate match for all borehole-to-fracture intersections when assuming homogenous fractures.

Nevertheless, the first and second attempts at varying parameters for homogenous fractures has been to increase the value of the hydraulic aperture of fracture zone HZ19C which seems to have the greatest absolute difference obtained in simulation SS02a (cf. Figure 3-3). The results of an increase of the aperture of HZ19C by a factor of 2 is shown in Figure 3-9, and an increase by a factor of 10 is shown in Figure 3-10. Even though the increase of a factor of 2 does for some intersections produce better matches, there are still many intersections which are not closely matched.

The third through sixth attempts at varying parameters for homogenous fractures has been to increase or decrease the value of the hydraulic aperture of all fracture zones simultaneously (Figure 3-11 to Figure 3-14). As can be seen, when the fracture apertures are increased or decreased by a factor of 10 (Figure 3-11 and Figure 3-12 respectively), the matches are generally worse. For the increase of a factor of 2 however (Figure 3-13), the results seem to be improved, as discussed below.

3.4.4 Variation attempt 5: SS02b-5

For the fifth attempt, there is a significant increase in the variability of the flows for the scenario where the fracture aperture is increased by a factor of 2 (Figure 3-13).

Even though this variation attempt does not produce more accurate absolute errors than the reference case (Figure 3-3 of Section 3.4), it does produce greater variability which is within the ranges observed for given measurements. Thus this may imply that the given transmissivities are in general too low.

Sample statistics for variation attempt 5 are shown in Table 3-3 and compared with statistics from the reference case simulation SS02a as well as with the given measurements. This clearly indicates that the increase of fracture aperture by a factor of 2 (ie an increase in fracture transmissivity by a factor of $2^3 = 8$, since we are assuming the cubic law for flow) produces a better model description than the base case, at least in a statistical sense. As can be seen in Table 3-3, the range of flow values obtained from the site data, ie both the minimum and maximum flow values, are more closely captured by simulation SS02b-5 than the reference case simulation SS02a. Also, the mean and sample variance of the flow values in simulation SS02b-5 is closer to data than the reference case simulation SS02a. Hence this indicates that better matches are obtained by increasing the fracture transmissivities/apertures.

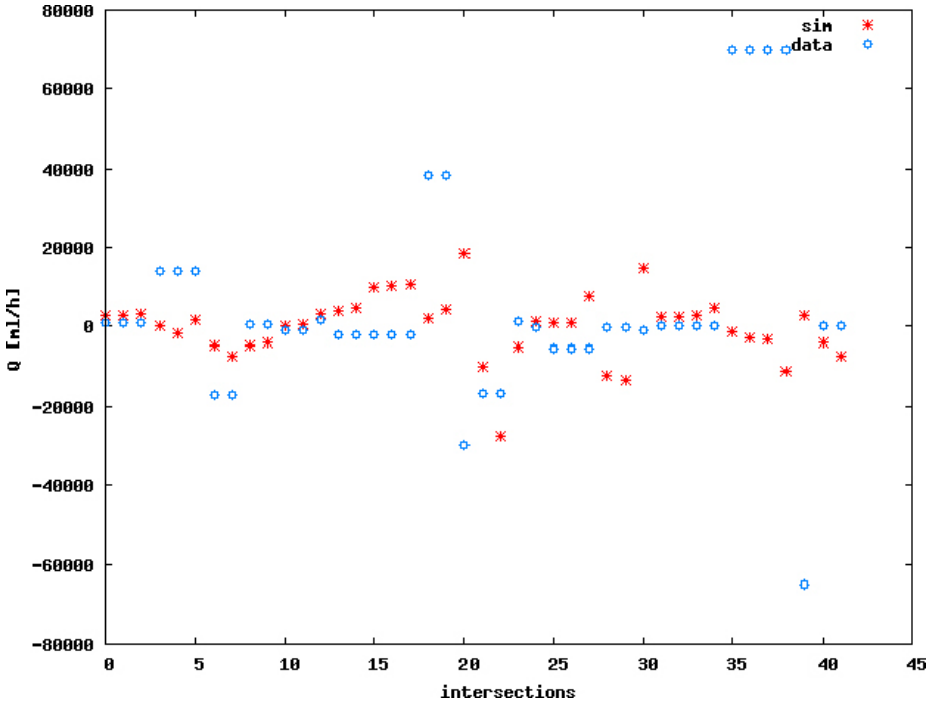

Figure 3-9. *SS02b-1: Variation attempt 1. Increased hydraulic aperture of fracture zone HZ19C by a factor of 2 (from 1.57E–4 to 3.14E–4). Boreholes are open and free to cross-flow. Simulated results vs given measurements.*

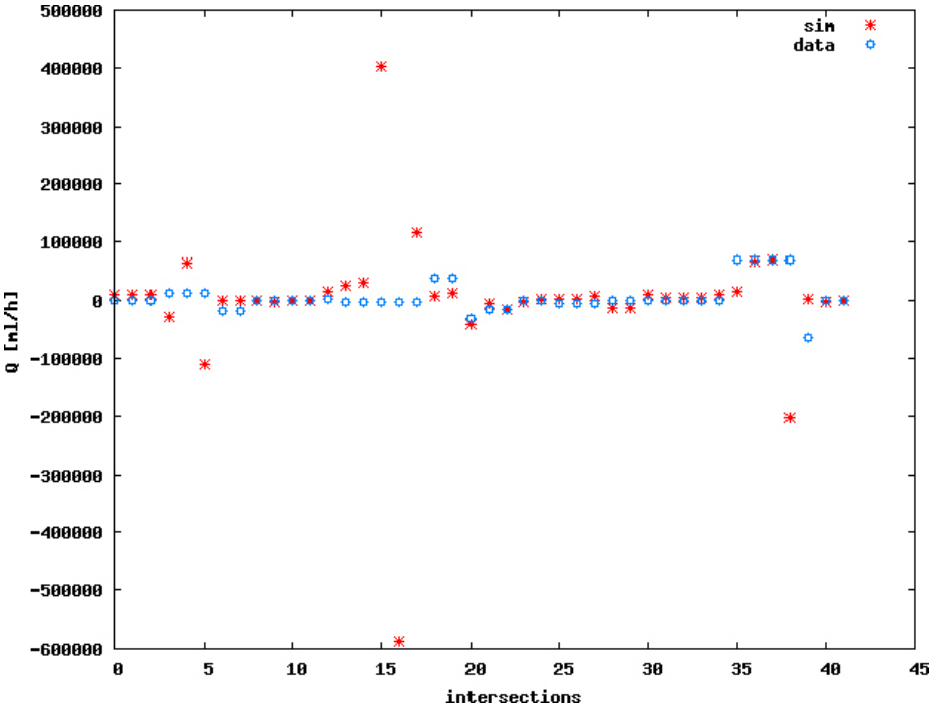

Figure 3-10. *SS02b-2: Variation attempt 2. Increased hydraulic aperture of fracture zone HZ19C by a factor of 10 (from 1.57E–4 to 1.57E–3). Boreholes are open and free to cross-flow. Simulated results vs given measurements. See Table 3-2 for label numbering scheme.*

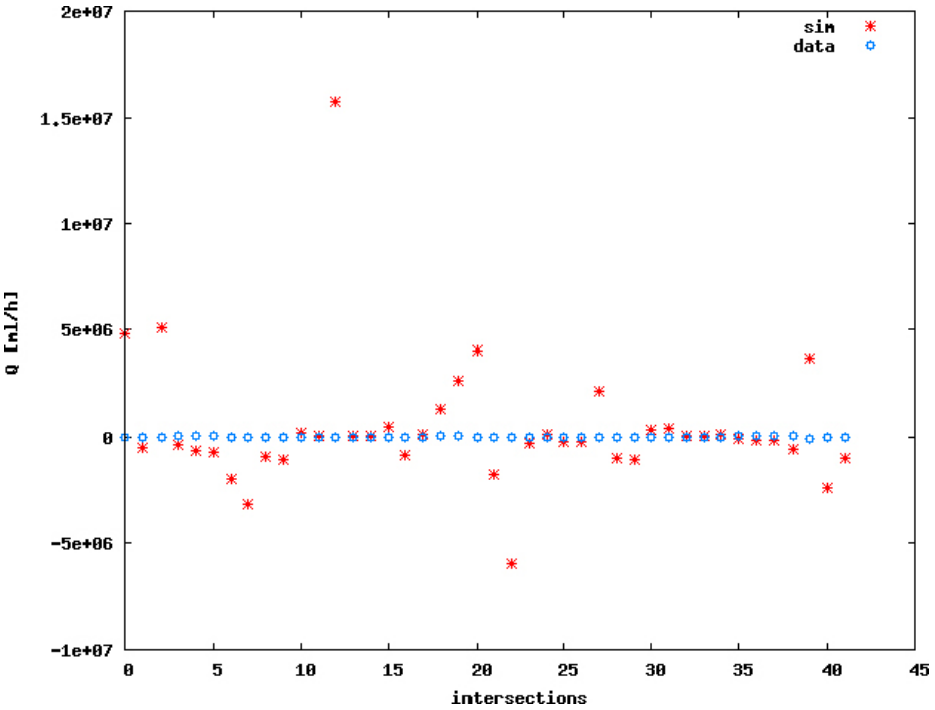

Figure 3-11. *SS02b-3: Variation attempt 3. The hydraulic aperture of all zones has been increased by 1 OM. Boreholes are open and free to cross-flow. Simulated results vs. given measurements. See Table 3-2 for label numbering scheme.*

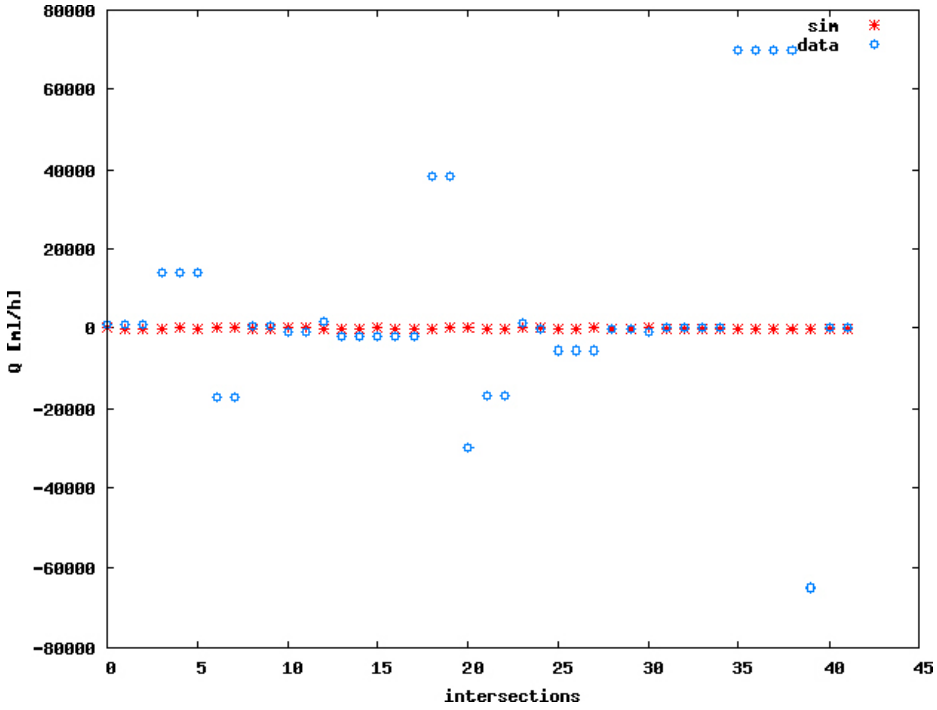

Figure 3-12. *SS02b-4: Variation attempt 4. The hydraulic aperture of all zones has been decreased by 1 OM. Boreholes are open and free to cross-flow. Simulated results vs. given measurements. See Table 3-2 for label numbering scheme.*

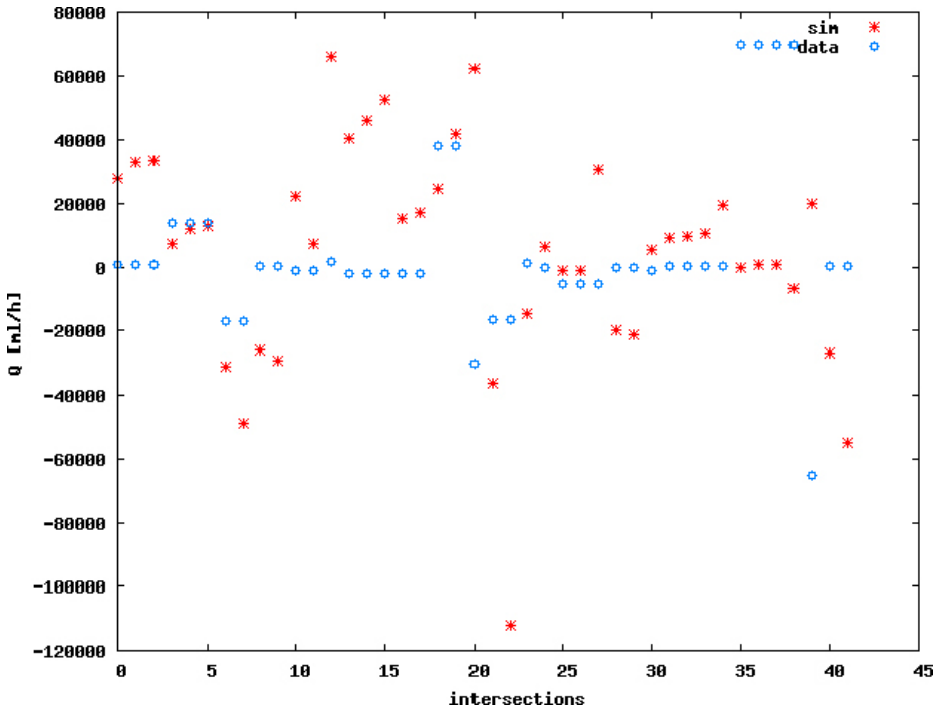

Figure 3-13. *SS02b-5: Variation attempt 5. The hydraulic aperture of all zones has been increased by factor 2. Boreholes are open and free to cross-flow. Simulated results vs given measurements. See Table 3-2 for label numbering scheme.*

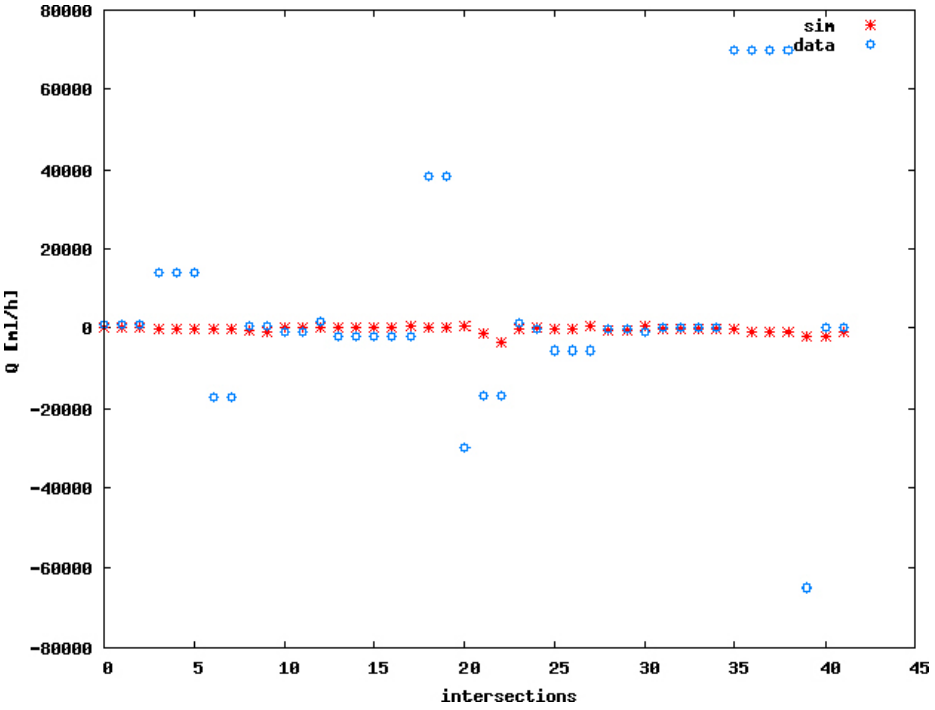

Figure 3-14. *SS02b-6: Variation attempt 6. The hydraulic aperture of all zones has been decreased by factor 2. Boreholes are open and free to cross-flow. Simulated results vs given measurements. See Table 3-2 for label numbering scheme.'*

Table 3-3. Statistics of the flow values for the site data, for simulation SS02b-5 (variation attempt 5).

Flow Q	Min Q	Max Q	Arithmetic mean	Sample variance
Site data	–1.12E+5	6.61E+4	4.99E+3	1.13E+9
SS02b-5	–6.51E+4	6.98E+4	5.07E+3	6.91E+8
SS02a	–2.22E+4	8.19E+3	–2.23E+2	2.85E+7

3.4.5 Pumping with boreholes: SS04a

Figure 3-15 and Figure 3-16 show results from the scenario based on the reference case scenario, but with extraction in borehole KR24 with a pumping rate of 18 l/min assigned to the top part of KR24. Here boreholes are open and free to cross-flow.

Figure 3-17 and Figure 3-18 show results for a similar scenario, except that KR24 is implemented as two disconnected boreholes (no middle section). KR24 is pumped from the top part with Q_U = 12.5 l/min and from the bottom part with Q_L = 5.5 l/min.

It is interesting to notice that the second case, where KR24 is implemented as two disconnected boreholes with different pumping rates, seems to obtain slightly more accurate results in terms of both head and flow values.

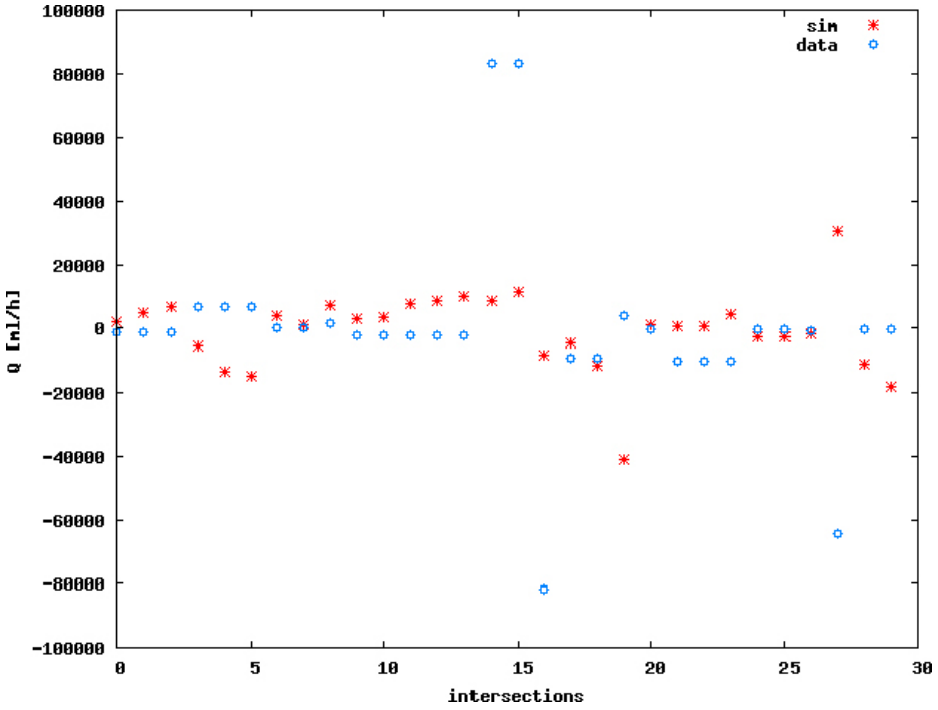

Figure 3-15. *SS04a flows: KR24 is implemented as three hydraulically connected boreholes with the middle section having radius 2 mm; extraction is from the top part only with Q = 18 l/min. All other boreholes are open and free to cross-flow. Simulated results vs given measurements. See Table 3-2 for label numbering scheme.*

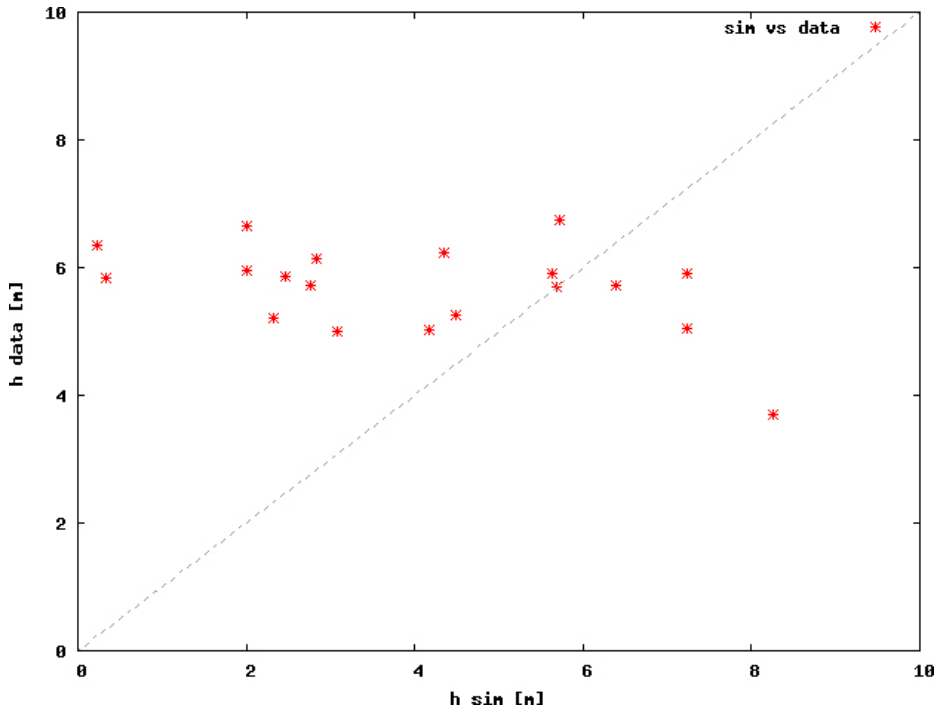

Figure 3-16. *SS04a heads: KR24 is implemented as three hydraulically connected boreholes. Simulated head (horizontal axis) vs given measurements (vertical axis). See Table 3-1 for label numbering scheme.*

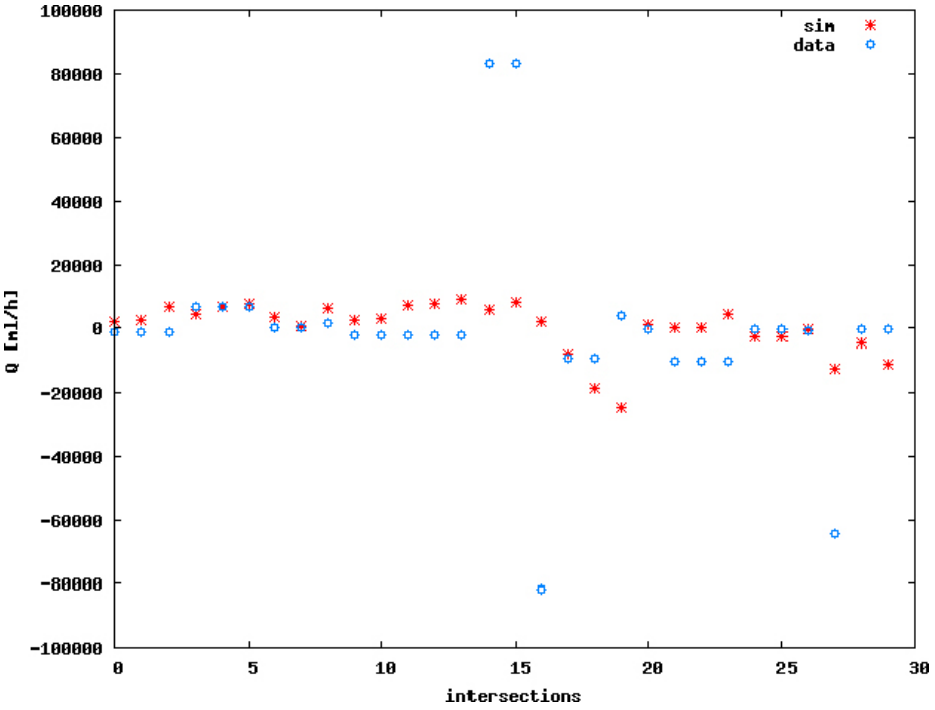

Figure 3-17. *SS04a flows : KR24 is implemented as two disconnected boreholes (no middle section); extraction is from the top part with Q_U = 12.5 l/min and from the bottom part with Q_L = 5.5 l/min. All other boreholes are open and free to cross-flow. Simulated results vs given measurements. See Table 3-2 for label numbering scheme.*

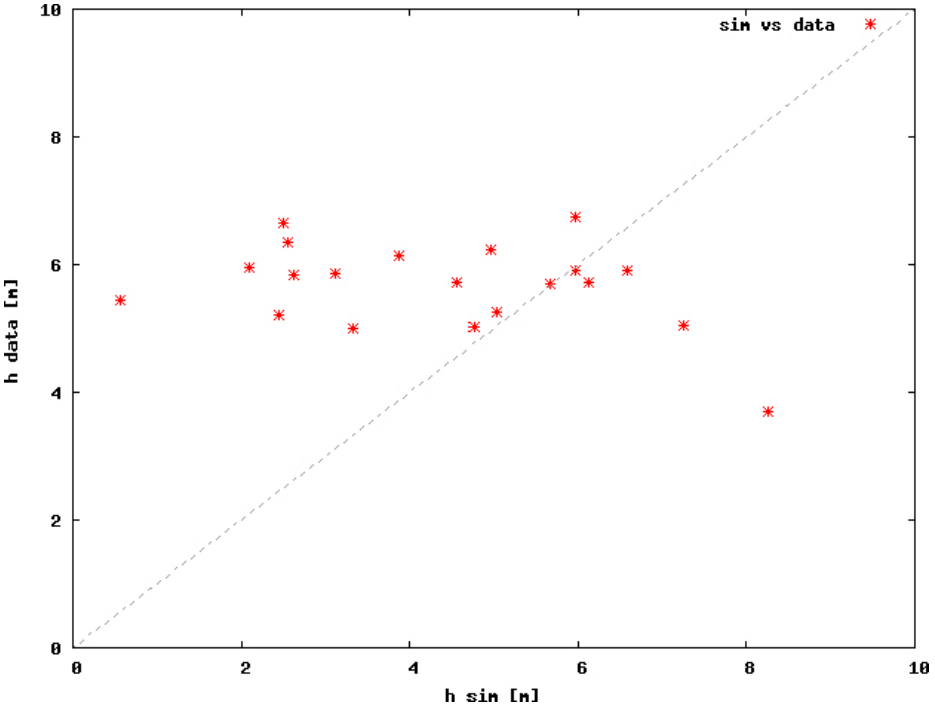

Figure 3-18. *SS04a heads: KR24 is implemented as two disconnected boreholes. Simulated head (horizontal axis) vs given measurements (vertical axis). See Table 3-1 for label numbering scheme.*

3.4.6 Transient simulation with boreholes: TR02a

The model setup for the transient simulation is the reference case setup with KR24 is implemented as two disconnected boreholes, so that pumping is two flow rates Q_U = 12.5 l/min and Q_L = 5.5 l/min. The storativity model for fracture zones is for simplicity represented by $S = 2T$, where T is fracture transmissivity.

Figure 3-19 shows the head distribution over time for four selected boreholes. The "non-physical" response at early time in KR08 (head increase) and also KR14 is likely to be a numerical artefact of the solution scheme due to the choice of time-step, for these very early times.

Figure 3-20 and Figure 3-21 show the flow distribution over time for fracture intersections with two selected boreholes.

As can be seen, asymptotic convergence is obtained in most cases after about 100—200 hours. Of the boreholes depicted in Figure 3-19, the head in KR04 (red) takes longest time to reach a constant value, but less than about 300 hours. For flow, most reach a constant value after about 100 hours, as can be seen in Figure 3-20 and Figure 3-21. Exceptions are zone HZ20A in borehole KR14 (orange, Figure 3-20) and HZ20B_ALT in borehole KR22 (magenta, Figure 3-21), which reach constant values in about 300–400 hours.

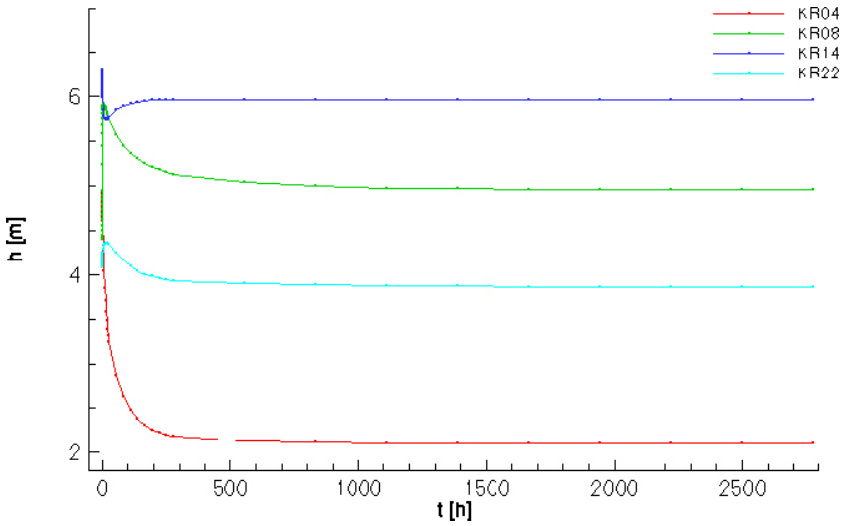

Figure 3-19. *TR02a heads: Head distribution over time for selected boreholes.*

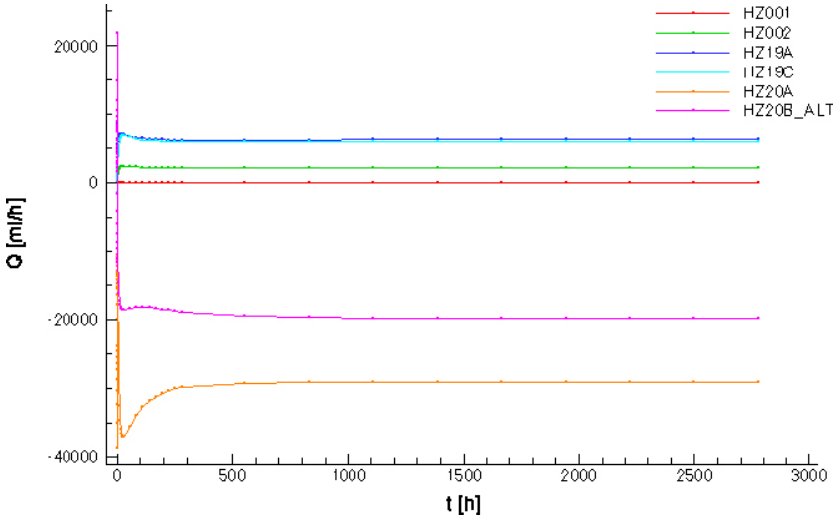

Figure 3-20. *TR02a flows: Flow distribution over time for all fracture intersections in borehole KR14.*

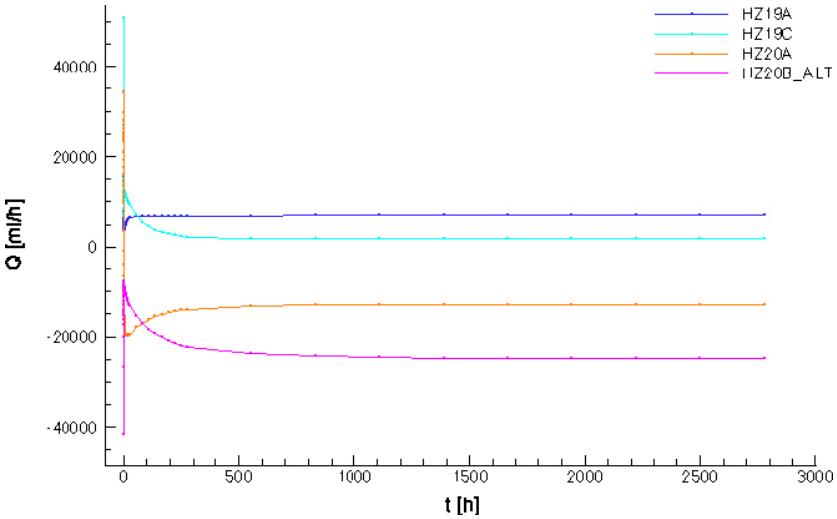

Figure 3-21. *TR02a flows: Flow distribution over time for all fracture intersections in borehole KR22.*

3.4.7 Transport pathway simulation in natural conditions: PA01

The particle tracking simulation is based on simulation SS01 as described in Section 3.4.2; that is, natural conditions where boreholes are assigned a low permeability κ = 1E–15 m^2. The Release Points are as specified in Table 1 of the PDF document "Task 7A; Part 1, Version 3.0" dated 2006-11-01 (where the column heading *Depth of flow (m)* is assumed to be the depth along borehole KR24).

To ensure particles are emitted outside of the borehole location, a radius of 10 m is assigned around the Release Point coordinate (cf. Table 3-4 below). One thousand particles are emitted from each Release Point. The particles considered here are hypothetical non-reactive particles which only follow the advective flow path of the fluid (water), thus forming pathlines.

Figure 3-22 through Figure 3-25 shows the pathlines in the domain resulting from the transport pathway simulation for the various Release Points.

Figure 3-26 shows the complement of the cumulative particle arrival time distributions (CCDs) at any of the domain boundaries from the three Release Points.

Table 3-5 shows some statistics from the particle tracking simulation.

For Release Point 1, cf. Figure 3-23, most particles traverse through fracture zones HZ19C and HZ20A. The total travel times obtained from RP 1 are in general the shortest, indicating faster pathways.

For Release Point 3, cf. Figure 3-25, most particles traverse through fracture zones HZ20A and HZ20B_ALT. The total travel times obtained from RP 3 are in general the longest, indicating slower pathways.

Considering the large percentage of stuck particles emitted from Release Point 2, cf. Table 3-5, it seems that reasonable flow paths out of the domain from this point are more difficult to obtain. In fact, from Figure 3-24 it can be seen that many particles traverse down borehole KR24 (which has a permeability κ = 1E–15 m^2) and out through fracture zone HZ20B_ALT to the domain boundaries. Thus many of the pathways obtained from RP 2 are similar to those obtained from RP 3. Another simulation was performed in which boreholes where completely removed from the system; however then essentially no trajectories where obtained from RP 2.

For all particle trajectories regardless of Release Point, it seems that fracture zone HZ004 acts as a vertical conductor between zones HZ19C, HZ20A, and HZ20B_ALT, and that these latter zones act as major transport pathways to the model boundaries, ie the fracture zones in direct contact with the Baltic Sea.

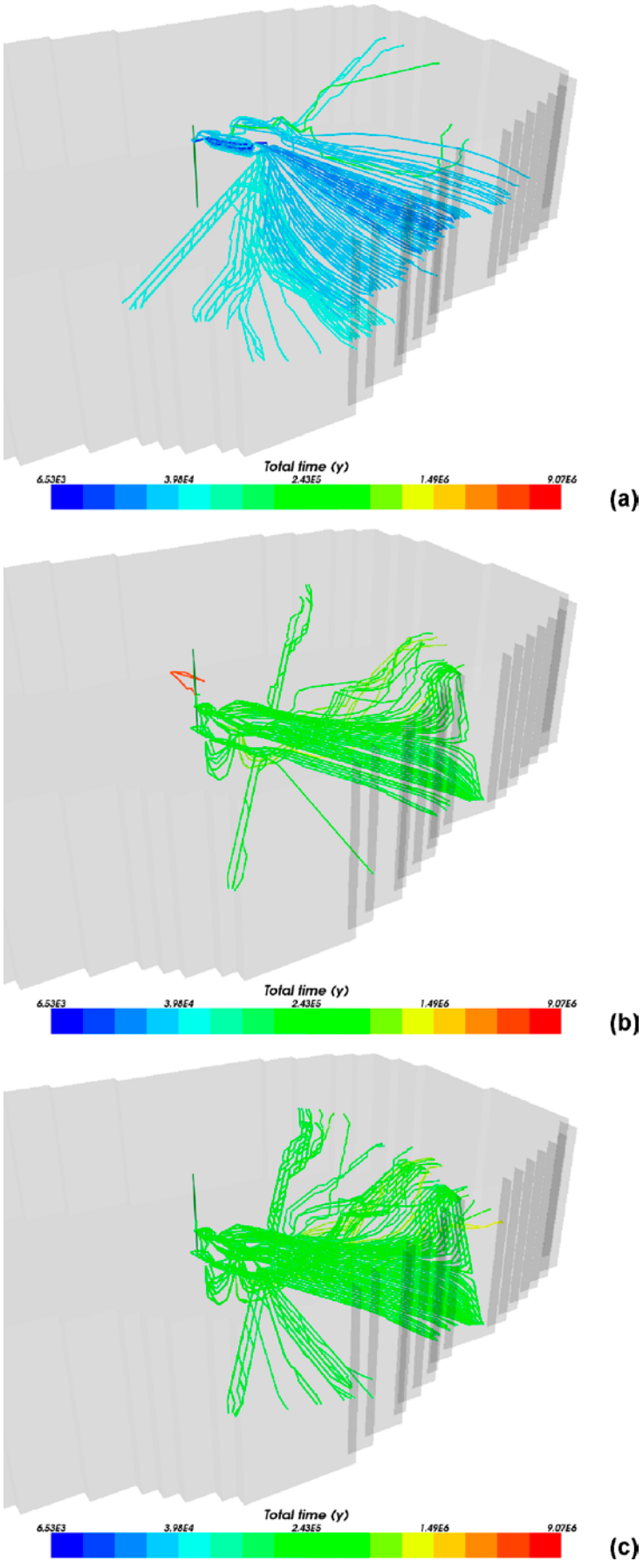

Figure 3-22. *PA01: Location in domain for the three Release Points, pathways coloured by total travel time in years. (a) RP 1. (b) RP 2. (c) RP 3.*

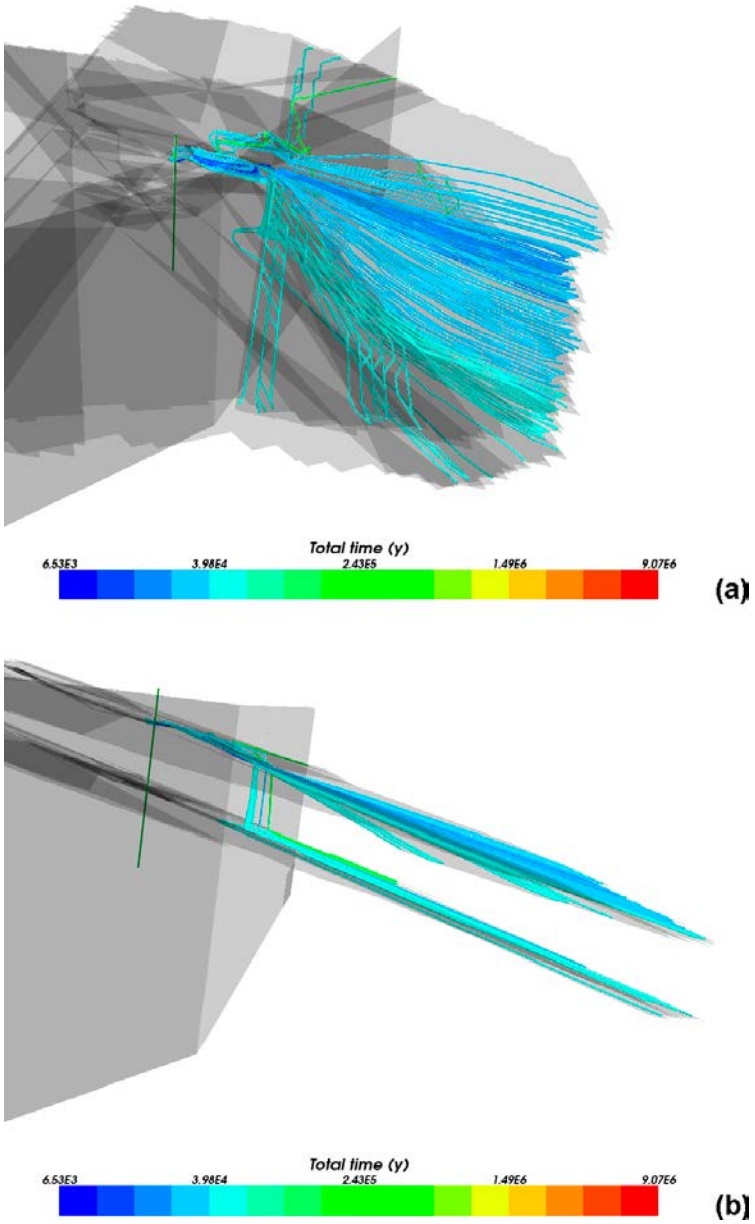

Figure 3-23. *PA01: Release Point 1, detail of fracture zones HZ004, HZ19C, HZ20A. (a) Areal view. (b) Side view.*

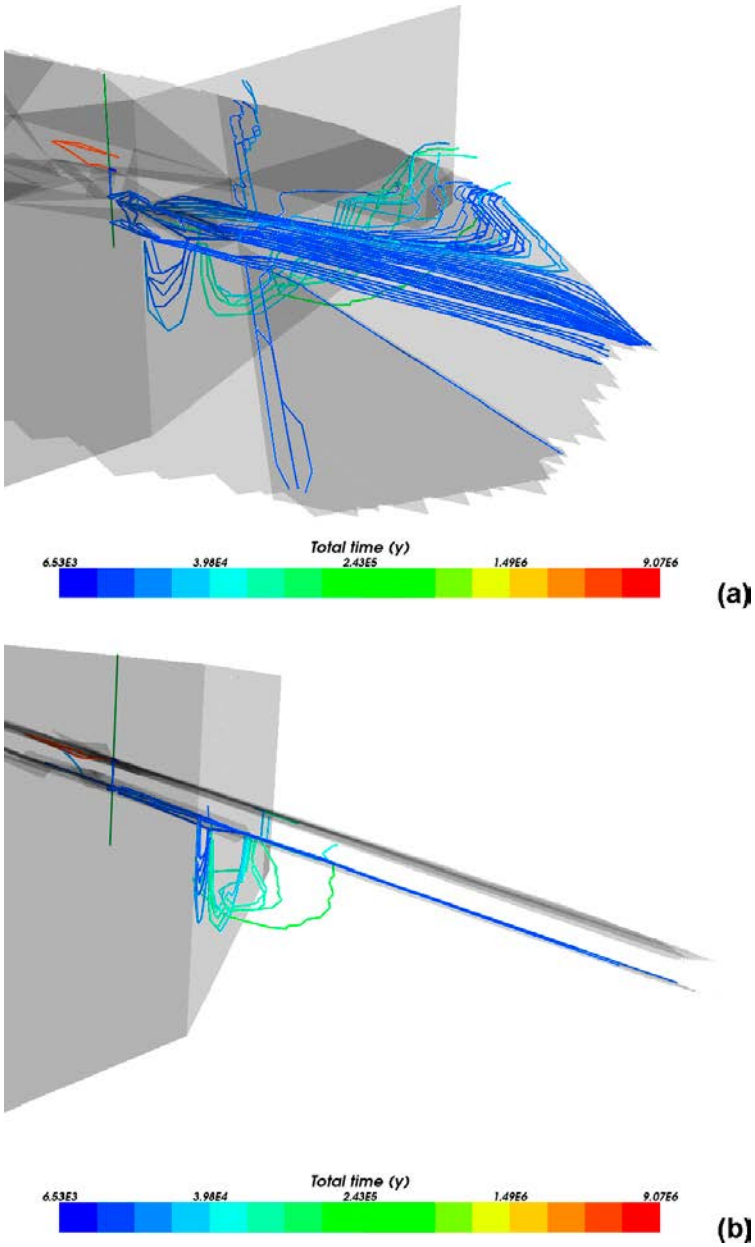

Figure 3-24. *PA01: Release Point 2. (a) Areal view, detail of fracture zones HZ004, HZ20A. (b) Side view, detail of fracture zones HZ004, HZ20A, HZ20B_ALT.*

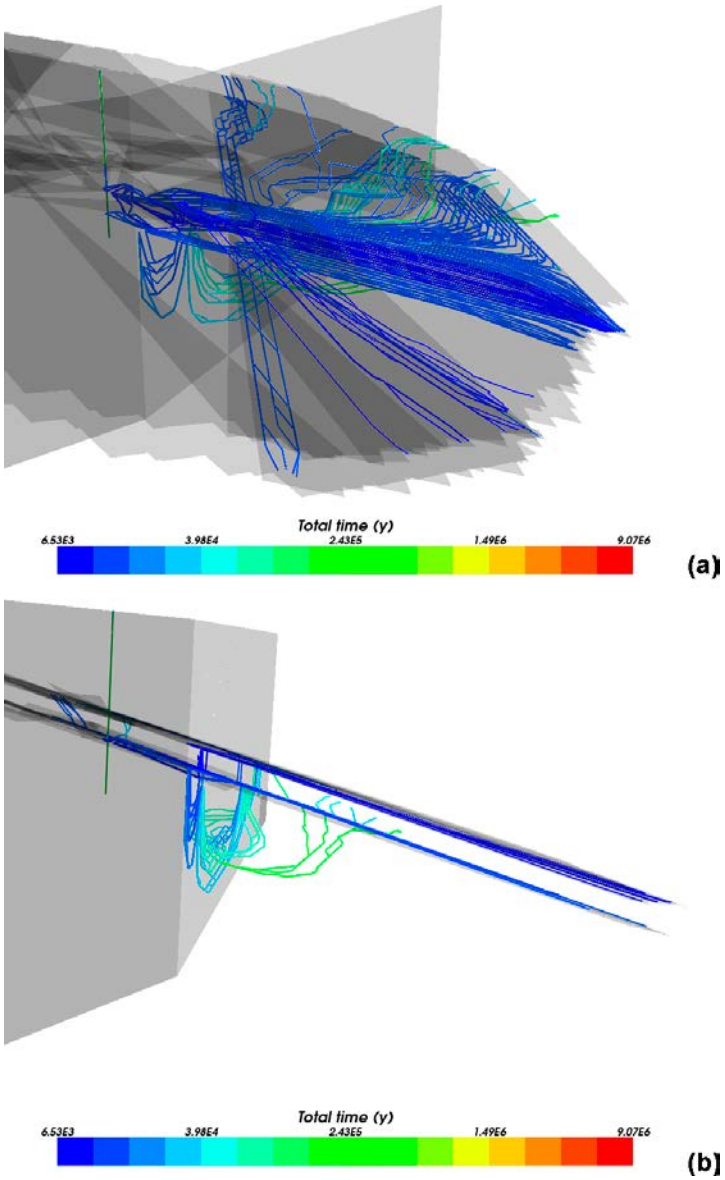

Figure 3-25. *PA01: Release Point 3. Detail of fracture zones HZ004, HZ20A, HZ20B_ALT. (a) Areal view. (b) Side view.*

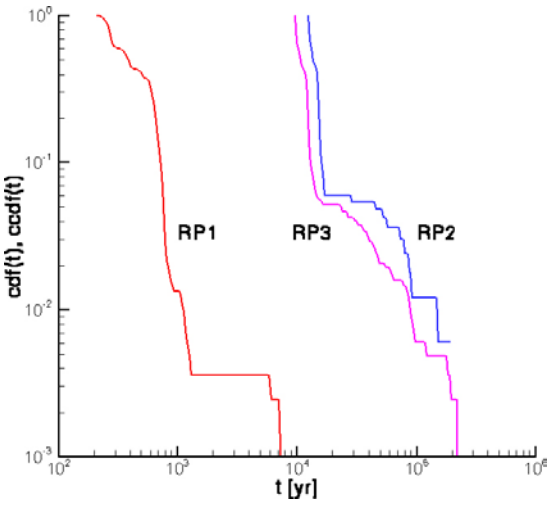

Figure 3-26. *Log-log plot of CCDs of particle arrival times at any of the domain boundaries. The horizontal axis is in units of years, the vertical axis is the normalised number of non-stuck particles.*

Table 3-4. PA01: Location of release point (x,y,z) coordinates (along borehole KR24) and size of radius around coordinate for which particles are emitted. Particles are started from transport nodes nearest to the start point coordinates and within the specified radius.

	X m	Y m	Z m	Radius m
RP 1	1525923.73	6791992.23	–104.26	10.0
RP 2	1525921.63	6791993.64	–293.23	10.0
RP 3	1525921.51	6791993.48	–320.23	10.0

Table 3-5. PA01: Statistics from the particle tracking arrival times.

	Mean	Median	95% bounds	Unit	Stuck particles
RP 1	1.50E+10	1.19E+10	2.40E+10	Seconds	17.7%
	4.77E+02	3.79E+02	7.62E+02	Years	
RP 2	5.74E+11	4.26E+11	1.44E+12	Seconds	83.4%
	1.82E+04	1.35E+04	4.57E+04	Years	
RP 3	4.36E+11	3.35E+11	7.40E+11	Seconds	17.7%
	1.38E+04	1.06E+04	2.35E+04	Years	

3.5 Discussion and conclusions

3.5.1 Discussion and evaluation of results

The current model implementations have provided several interesting observations and results which are discussed in the following.

The manual attempts at varying fracture aperture indicate that if assuming homogenous fracture zones, the given geometric transmissivities are slightly low. In order to obtain statistically better matches with head and flow measurements, the transmissivity of homogenous fracture zones can be increased by up to a factor of about 8, as discussed in Section 3.4.4 and shown in Figure 3-13 and Table 3-3.

The simulations replicate the pumping scenario in a similar way as the non-pumping scenario. From the modelling point of view, it should be noted that the pumping scenario is simply another slightly different model setup (an additional flux boundary condition in the location of the pumping borehole), and results are compared with another, also slightly different, measurement data set (corresponding to dates for which pumping was conducted). A result from the pumping scenario simulations is that the implementation of KR24 as two disconnected boreholes with separate pumping rates (Q_U and Q_L) provides slightly better results than the implementation of KR24 as three hydraulically connected borehole sections.

For transient simulations, it takes about 100–300 hours for the head and flow values of boreholes to converge to constant values, and these constant values are similar to those obtained in the corresponding steady-state simulations.

For particle tracking, release point RP 2 seems to be lacking conductors, i.e. it does not seem to be in the vicinity of any fracture zones. Hence, for a pure DFN model, particles released here have no viable transport path out of the domain. For RP 1 and RP 3 however, most travel paths are towards the South-East, via fracture zone HZ20A and HZ20B_ALT respectively, to the model domain boundaries beneath the sea bed, ie which are in contact with the Baltic Sea. Some pathways deviate towards the North-East and some directly towards the South. The reason particles from RP 2 replicate travel paths from RP 3 is that due to the lack of fracture zones in the RP2 vicinity, particles traverse through the borehole (which thus acts as a conductor) towards the general area of RP 3.

In general, it seems quite challenging to capture the measured flow rates without formal model calibration methods, and even then questionable as hydrogeological systems are typically always under-determined and solutions are likely to be non-unique. It was not possible to conduct a formal calibration due to lack of methodologies and tools. However, based on the scenario tests conducted, several factors could influence the accuracy of the simulated results. For example, it is expected that fracture heterogeneity (by introducing a greater variation in fracture transmissivity) should cause greater variation in simulated fracture flows in the intersections with observation boreholes. Also, including additional conductive features,

such as background fracture networks, and by adjusting the variation in transmissivities of such fractures, should help create additional flow paths which could, at least in principle, be able to reproduce the measured flow data.

It seems that the addition of (conductive) boreholes does influence results such that the simulations are closer to measurements, but to what extent has not been fully answered. However, the sensitivity study on the influence of increasing / decreasing permeability in boreholes clearly shows that the addition of boreholes results in an homogenization of the responses as connectivity increases. That is, the conductive boreholes help connect the DFN, which in these simulations mainly consist of major fracture zones, such that the simulated head response is better matched with the measured head values. This obviously indicates that the inclusion of conductive boreholes is important for a correct model representation. It also indicates that a more correct model representation implies more conductive features (eg background fractures).

From this work is seems that the flow-log (PFL) data is vital in order to produce an accurate groundwater flow model. Clearly, by only using head measurements one could conclude that the reference case model implementation SS02a is a relatively accurate model; it would probably suffice to merely adjust the top surface boundary condition to obtain more accurate simulated values of head. That is, from Figure 3-4 (head results for simulation SS02a) one could draw the conclusion that the model is fairly accurate, and a sufficient model improvement would be to only use the groundwater table instead of the more conservative approximation of using the topography as the top surface boundary condition. However, from Figure 3-12 (flow results for simulation SS02a) it is clear that several of the flow measurements are not close to being correctly captured, and from Figure 3-13 (flow results for simulation SS02b-5) we see that the simulated flow measurements can be radically changed, and more accurate in a statistical sense, by altering transmissivity. Nevertheless, to obtain a more accurate simulation in an absolute sense, it is likely that the flow field requires additional conductive features, such as background fracture sets, or more deterministic fracture zones, possibly vertical zones.

3.5.2 Main conclusions and lessons learned

Based on the work conducted for large scale modelling of Olkiluoto Island within Task 7A, the main conclusions are summarised as follows.

- The Posiva Flow Log data is vital in order to produce a more accurate groundwater flow model. As such, it can be said that Posiva Flow Log data reduces model uncertainty, at least qualitatively.
- There is a clear influence of open boreholes to the hydrogeological flow system. Specifically, the addition of open boreholes results in a homogenization of responses as connectivity increases. That is, the conductive boreholes help connect the discrete fracture network flow system.
- As a consequence, the Posiva Flow Log data measured is based on a flow system which has greater connectivity than the natural (undisturbed) flow system.
- In addition, the inclusion of conductive open boreholes is important for a correct model representation.
- If assuming homogenous fracture zones, the given geometric mean of transmissivities obtained from using the Posiva Flow Log instrument are slightly low. In order to obtain statistically better matches with head and flow measurements, the transmissivity of homogenous fracture zones can be increased by up to a factor of about 8.
- The implementation of the pumping borehole KR24 as two disconnected boreholes with separate pumping rates results in slightly better results than the implementation of KR24 as three hydraulically connected borehole sections.
- For transient simulations, it takes about 100–300 hours for the head and flow values of boreholes to converge to constant (steady-state pumping) values.
- For particle tracking, most pathways are towards the South-East, via two major fracture zones to the fracture zones beneath the sea bed, which are in contact with the Baltic Sea.
- There is a need to develop model conditioning methods. Here a discrete fracture network hydrogeological flow model is used combined with in situ field data obtained primarily from boreholes. The field data consists not only of pressure data but also flow data. Hence, conditioning methods which not only consider pressure (or head) data but also account for flow data are needed.

4 Task 7B

4.1 Modelling Approach

4.1.1 Overall approach

The overall aim is to develop new methods in which flow data, such as measurements obtained from the Posiva Flow Log (PFL) instrument, can be used to characterize and better understand the subsurface flow system for sparsely fractured media. A particular feature of the PFL data is flow rates are provided as a magnitude and direction, in terms of flow entering or leaving the borehole at locations which can be associated with fractures intersecting the borehole.

In the modelling work performed within Task 7B, the fracture system and hydrogeological properties of the region where the KR14–KR18 cross-hole pump tests have been conducted (Figure 4-1, Figure 4-2) is represented with a discrete fracture network (DFN) model. DFN approaches usually employ deterministic features for known fractures, which tend to be large hydraulic zones, and stochastic features for smaller background fractures. Here a compartmentalized fracture growth model is developed. The aim is to model background fracture populations which are known, in the sense of being observed as flowing fractures by the PFL tool, but which may be limited or too small in extent to be considered as hydraulic zones. Thus it may be seen as an attempt at modelling background fracture populations using a non-stochastic approach.

The fracture growth model is developed and evaluated against PFL flow data. It represents a static DFN, based mainly on flowing fractures identified by the PFL tool, with the aim of reproducing PFL flow magnitudes and directions. As such it represents a minimalistic DFN model that can be constructed based primarily on PFL flow data together with associated geometrical fracture information. The main unknowns are the size and geometric structure (orientations) of fractures beyond the immediate vicinity of the borehole, heterogeneity in hydraulic properties, and the connectivity and structure at the network scale. Thus most of the flow system is largely undetermined, as would be expected for any groundwater system. However, the general idea of the approach is that it may enable a study of uncertainties in heterogeneity and connectivity at a relatively small network scale, mainly based on the extent of the cross-borehole configuration tests.

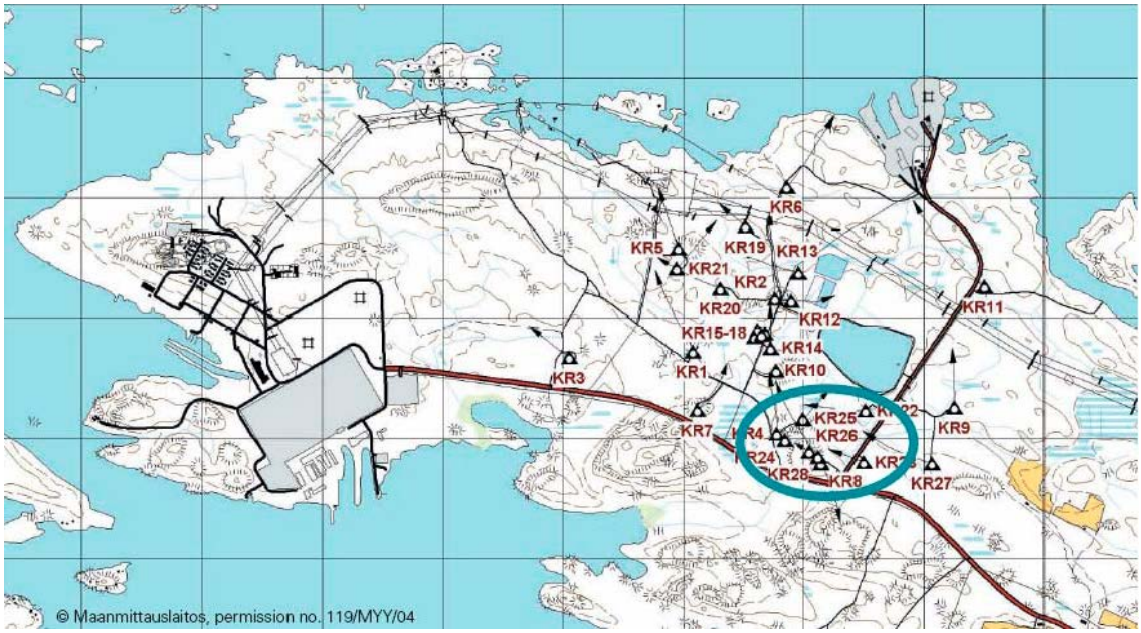

Figure 4-1. *Olkiluoto Island. Showing locations of several core-drilled boreholes (KR1, KR2, etc), as well as the location of the on-going construction of the Onkalo facility (circle, upper image).*

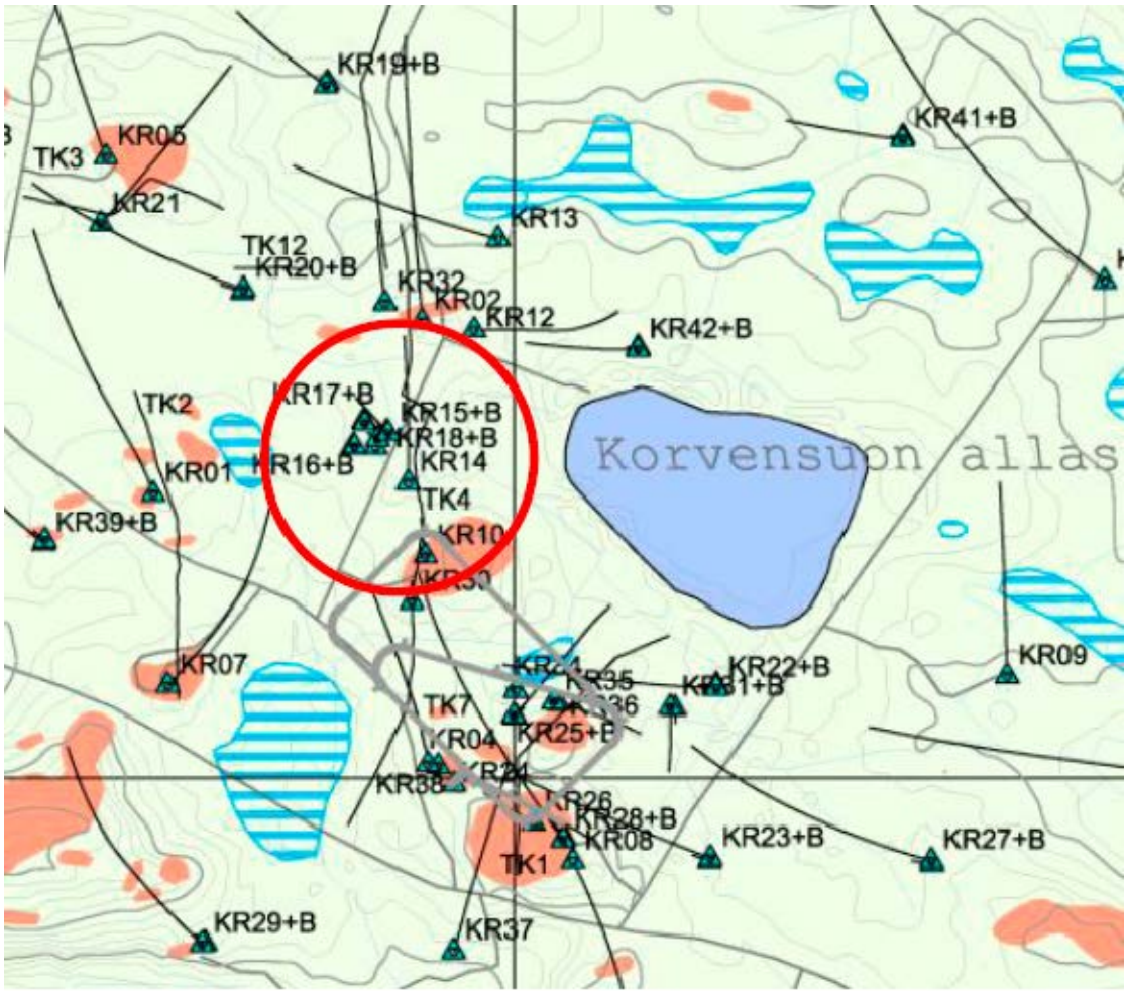

Figure 4-2. *The region of focus of this study is the cross-hole pumping tests conducted in boreholes KR15–KR18, located north-west of the Onkalo facility. The circled region in the lower image has a diameter of about 350 m.*

The modelling procedure is to first construct a forward or 'reference case' model from a general understanding of data from the Olkiluoto site investigations, resulting in a relatively straightforward implementation of the field data. Thereafter, variations are considered by conceptually altering features of the model. Results are then compared against PFL flow data. Several model variants are considered. The models which are deemed to produce better results are then considered as improved or 'conditioned' models. The conceptual features which differ between the forward model and the improved model are discussed, in order to attempt to obtain an improved understanding of the hydrogeological system and of the applicability of the simulation model.

The overall approach of the work conducted is summarised by the following main objectives.

A first objective is to develop a means by which flow measurements can be adopted into a DFN model. The flow data considered are high-resolution PFL measurements, where flow values consist of both a magnitude and direction, in terms of flow either entering the borehole from a fracture or leaving the borehole and entering a fracture. As such these represent a simplified 'binary vector' quantity.

A second objective is to develop and evaluate a new DFN fracture growth model concept, where fractures are generated according to identified PFL flowing fractures, and allowed to extend from the point of observation in boreholes until they intersect with fractures extending from neighbouring boreholes. A prerequisite for this approach is a sufficiently well-characterized region and sufficiently constrained spatial scales.

A third objective is to attempt to constrain the DFN model, combined with the fracture growth concept, by ‘conditioning ‘against PFL flow data. The objective is not to use formal conditioning, calibration or inverse methods, but rather to alter the model using conceptual variants, and evaluate results against PFL data, in order to constrain the model and attempt to improve simulated results in a general sense.

A fourth objective is to conduct an overall analysis of the PFL field measured flow data obtained from the multiple cross-hole interference pumping test, and evaluate the measurements in terms of the usefulness and applicability as ‘binary’ vector information, and what this may indicate in terms of the behaviour of a subsurface flow system in fractured bedrock.

A fifth objective is to study the impact of resulting flow systems in terms of advective transport and retention properties at the network scale.

4.1.2 Data usage and interpretation

A general understanding of the Olkiluoto hydrogeological system, based on previous work, including data analysis and modelling conducted in Task 7A, has been a basis for conducting the modelling in Task 7B.

The data used to construct the DFN model used with Task 7B include the following.

- Borehole fracture data from core logs. This provides fracture locations in boreholes as depth along borehole, which can also be translated to a point coordinate in a suitable coordinate system. The actual data used are the provided fracture point coordinates. Also, core log data provides local fracture strike and dip orientations at the observed location. This is used to define a local fracture surface plan, but of course does not define the size or extent of the fracture. It should be noted that the orientations only represent local measurements and fracture surfaces may not in general be planar, but rather are expected to be rough, irregular surfaces. For simplification however, planar surfaces based on local orientation measurements are adopted.
- PFL detection of flowing features. PFL flows can be cross-correlated to identification of fractures in borehole core logs. Thus, if the core-log observations define one set of fractures, the PFL observations of flowing features generally defines a subset of those fractures. Here, only fractures which are deemed to have flow are used, that is, only the PFL observed fractures are used. Non-flowing fractures are discarded. This may potentially include flowing fractures with flow below the lower limit of the PFL tool.
- PFL transmissivities. The PFL flows can be used to infer effective transmissivity for the fracture. The simulated fractures are assigned a transmissivity value using the PFL inferred transmissivity values. In general, each simulated fracture has a constant, homogenous transmissivity. This is however a parameter which is varied during model conditioning.
- The location, extent and borehole depths. The model domain is 300 m × 300 m × 500 m, which is designed to include all boreholes as well as an extended surface region beyond the boreholes. Thus the borehole locations and extents are indirectly used to define a suitable model region.
- Surface topography is used to define the top surface boundary condition in the forward model and several model variants.
- Hydraulic zones from Task 7A are used in the forward model and in some model variants.
- PFL flows. Flow data is used as the basis to constrain the model during model conditioning. Also, since PFL transmissivites are inferred from the flow values, it should be noted that PFL flows are indirectly used to assign the conductive properties of simulated fractures.

4.2 Conceptual Model

4.2.1 Main assumptions and simplifications

Assumptions are consistent with those used for Task 7A (Section 3.2.1). A discrete fracture network (DFN) approach is used to obtain a description of flow in the subsurface. However, here numerical simulations are only used to evaluate long-term (steady-state) conditions during pumping; that is, transient responses during the early pumping phases are not considered. The steady-state, constant density groundwater flow equation is used to obtain fluid pressure throughout the fracture network.

When designing a DFN, both fracture geometric and hydraulic properties are needed. Typically, due to the large number of unknowns, a stochastic approach is adopted based on statistical information of available fracture characterization. Here a new approach suitable for well-characterized data sets such as that available for the KR14–KR18 cross-hole pump tests is proposed and adopted.

The objective is to use 'hydraulically active fractures' to design the simplest DFN configuration possible to attempt to reproduce measured flow values, considering both flow magnitude and direction. The PFL tool identifies flowing features along the depth of the borehole, and only fractures which can be correlated to PFL flows are used. Thus, a large number of non-active fractures are immediately discarded, as they are deemed to be non-flowing or have flows below the threshold of the PFL measurement limits.

By using PFL flowing fractures, fracture density and location within each borehole is defined. Then the main unknown is fracture size and heterogeneity in the fracture field (both geometric and hydraulic) between boreholes. For this a fracture growth model adopted. The concept is to allow a fracture to grow from its observed location in the borehole along its measured strike and dip directions until it intersects with a fracture from a neighbouring borehole (Figure 4-3 and Figure 4-4). If there are sufficient boreholes, and by allowing fractures to expand simultaneously until they intersect neighbouring fracture sets, a well-connected DFN is generated. The significant advantage of this approach is the constructed DFN honours the field observable measurement locations. Hence, direct comparisons between simulated flows and field measured flows are made possible.

As such, the concept proposed and adopted in this study represents a minimalistic DFN, based mainly on fractures identified by the PFL tool, using the PFL inferred transmissivities, with the aim of reproducing PFL flows. The main unknown is the fracture network behaviour, connectivity and heterogeneity in the regions between boreholes. However, these unknowns greatly complicate model conditioning, even for the simplistic approach used here.

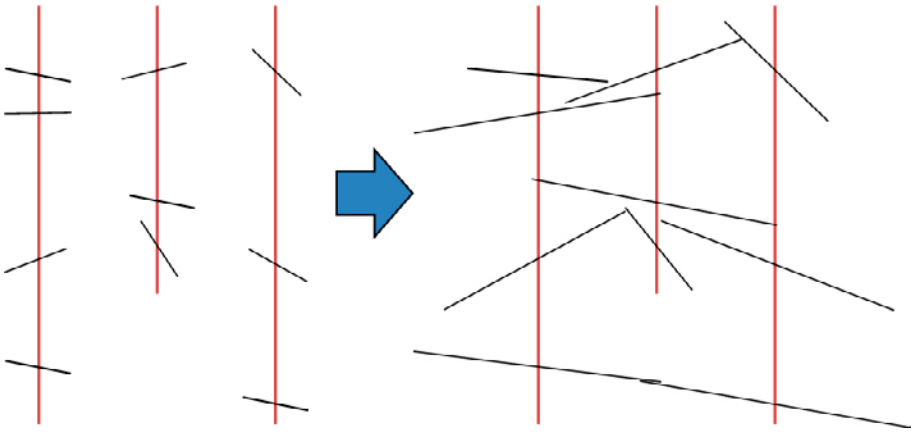

Figure 4-3. *Illustration of the conceptual approach. Fractures are observed in boreholes with imaging, core-logging etc to determine geometrical characteristics (locations and orientations as strike and dip). Flowing fractures are determined by PFL device, and can be matched to core-log occurrence of fracture . Then, by only using PFL-inferred fractures, a DFN model is generated such that fractures are allowed to 'grow' from borehole location in direction of their respective orientations until they intersect neighbouring fractures.*

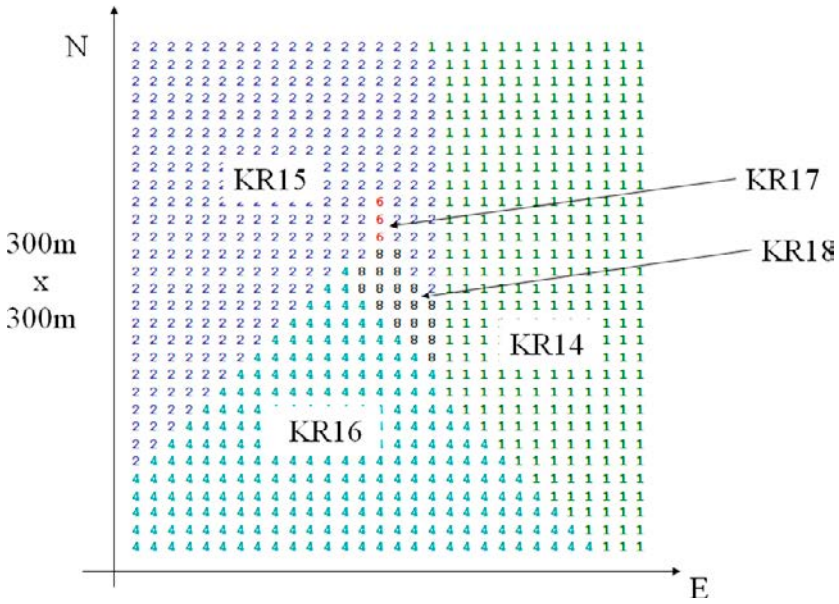

Figure 4-4. *Partitioning scheme. A simplified method of incorporating the fracture growth model is adopted in order to determine regions of intersection, by partitioning boreholes into regions according to their location. A partitioning algorithm is used to subdivide the domain into disjoint regions associated with each borehole. Here each digit represents a block with surface area 10 m by 10 m. Also, some overlap between compartments is needed to obtain connectivity, since the fractures are discrete features and there is no representation of the rock matrix. Fractures are allowed to extend within their respective compartments until they reach a boundary. Fracture density as obtained from the PFL device is thus conserved within its corresponding region.*

4.2.2 Geometrical description

The location of the region where the cross-hole interference tests are conducted on Olkilouto Island is shown in Figure 4-1 and Figure 4-2.

The computational domain is defined as a cuboid with a rectangular surface area of 300 m by 300 m, and depth slightly over 500 m (Figure 4-5). Fractures are two-dimensional planar surfaces. Boreholes are one-dimensional flow conduits. Intersections between two or more fractures and intersections between fractures and boreholes are considered.

Only PFL flowing fractures are used. Hence, fracture density and location within each borehole is obtained directly from the PFL data. The main unknown is fracture size and heterogeneity in the fracture field. The geometric shape of fractures, the connectivity between fractures in the network, as well as hydraulic properties of fractures between boreholes is unknown. For this a compartmentalized fracture growth model concept is adopted. The concept is to allow a fracture to grow from its observed location in the borehole along its measured strike and dip directions until it intersects with a fracture from a neighbouring borehole. If there are sufficient boreholes, and by allowing fractures to 'expand simultaneously' until they intersect neighbouring fracture sets, a connected DFN can be generated. The significant advantage of this approach is the constructed DFN honours the field observable measurement locations. Hence, direct comparisons between simulated flows and field measured flows are made possible.

The implementation of the compartmentalized fracture growth approach is achieved by defining a cuboid region around each borehole which slightly overlaps neighbouring regions (Figure 4-4 and Figure 4-6). This defines compartments associated with each borehole, and in turn defines each fracture set. As there are five boreholes (discarding the B-series of boreholes), there are five compartments and five fracture sets. This implementation method does not necessarily guarantee connectivity between fracture sets, however by adjusting the size of each compartment, connectivity is achieved.

Unless otherwise specified, fractures are rectangular features with an assigned homogenous (constant) transmissivity. Fracture transmissivity is assigned by the inferred PFL transmissivities. In essence, PFL measured flows are converted to transmissivity by adopting the Thiem-Dupuit homogenisation assumptions (Rouhiainen and Sokolnicki 2005). This means fractures are seen as thin slabs of a homogenous porous media, disconnected from a network, and with a constant head at a given distance from the measurement point. In general these assumptions are not valid for fractured rock, however the inferred transmissivities are considered to provide reasonable order-of-magnitude values (Öhberg and Rouhiainen 2000) and hence may be more applicable to sparsely fractured rock.

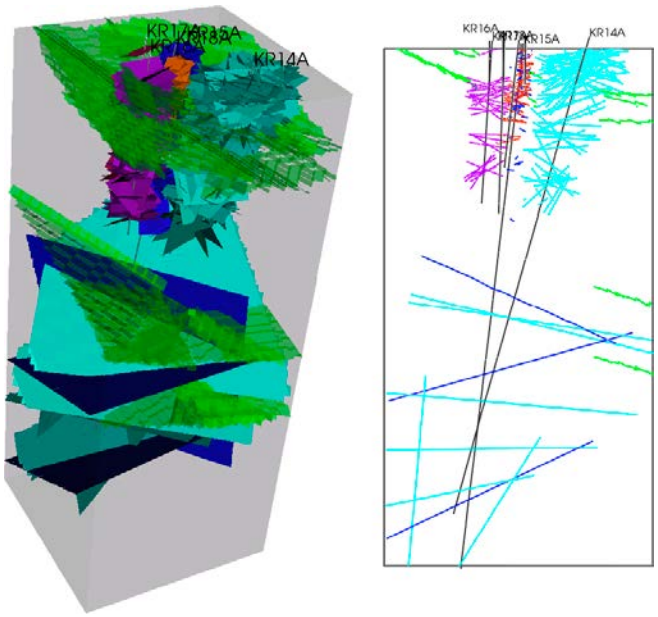

Figure 4-5. *Showing a 3D view (left) and a 2D cross sectional view (right) of fractures in the simulation domain for the reference case (configuration A). In this setup the compartmentalised fracture growth model is not adopted. Instead, fractures are allowed to grow until they intersect each other as well as the hydraulic zones in contact with the Baltic Sea (green), which are the main connectors to the model boundary. Fractures are coloured according to fracture set, where each borehole is associated with a set.*

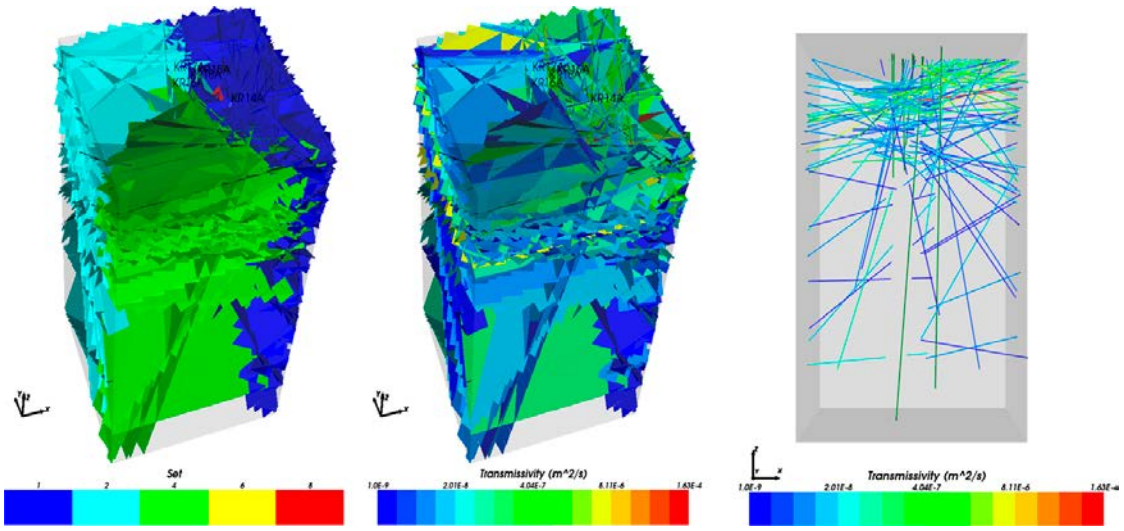

Figure 4-6. *The fracture network in the simulation domain for the improved case (configuration B), where the compartmentalised fracture growth model is adopted. Left: Fractures coloured according to fracture set, where each borehole is associated with a set. (Note the fractures associated with the central boreholes (KR17 and KR18) are not visible). Middle: Fractures coloured according to assigned transmissivity. Right: 2D view of fractures projected of fractures on the vertical (x,z)-plane, coloured by transmissivity.*

4.2.3 Processes considered

Fluid properties are that of fresh water with constant density. Steady-state conditions are assumed throughout, that is, the initial transient responses during pumping are ignored. Thus possible processes such as saltwater intrusion and density-dependent effects are not considered. Also, temporal effects such as infiltration and a variable groundwater table in the unsaturated regime are not considered.

Here, the fracture network is explicitly accounted for based on PFL flowing fractures, which includes large-scaled deformation zones as well as features which typically may be considered as background fractures. Thereby heterogeneity in sparsely fractured media is accounted for at the network scale.

4.2.4 Boundary and initial conditions

Lateral sides have pressure head set to zero. The bottom surface is impermeable to flow, that is it has a no-flow condition. The top surface boundary condition depends on simulation variant; either with pressure head proportional to surface elevation (topography), or set to no-flow.

Pumping is simulated by assigning the field measured drawdown during pumping (Table 4-1). Thus the simulated flow rates obtained during pumping are not calibrated against the field measured (PFL) flow rates.

4.3 Model Implementation

4.3.1 Numerical model

The numerical model used is the ConnectFlow suite, provided by Serco Assurance, Harwell, UK. ConnectFlow is a finite-element code for solving flow and transport in porous media which incorporates both CPM and DFN approaches. Here the Napsac module is used, which is a module for DFN-modelling. The version used is ConnectFlow 9.6 (Hartley and Holton 2008c, Hartley et al. 2008c).

In the Napsac code, fractures are discretized in the fracture plane by a regular finite-element mesh (FEM). Geometrical fracture intersections are found and approximated by the nearest FEM nodes. Thereafter the pressure field at each node along intersections is determined by solving the groundwater flow equation and by applying boundary conditions at relevant nodes intersecting the boundary of the domain. Once the pressure field is solved for, the flow field in the fracture system is obtained by applying Darcy's law.

Further, fractures are subdivided into sub-rectangles, a process denoted as 'tessellation' by the software used. This is for technical reasons in order to implement the fracture growth approach. The effect of tessellating fractures is that a higher-resolution model of the fracture network is obtained, both in terms of geometrical fracture intersections, and of the resulting pressure and flow field. Flow along boreholes is determined using a 1D well model as described in Section 3.3.1.

4.3.2 Parameters

The main model parameters are geometric and hydraulic fracture properties of the discrete fracture network. For model conditioning, various parameters are altered based on the modifications of the conceptual model. There are three main model aspects which are modified, as follows.

Parameters controlling the geometry and size of the domain, as well as boundary conditions such as pressure and flow conditions.

Parameters controlling fracture populations, such as fracture density, connectivity, size and extent. The extent of fractures is mainly based on the extent of local partitioning zones, which defines the size of fractures.

Fracture heterogeneity is implemented by altering fracture transmissivity in confined regions or locations within the model. When fracture transmissivity is altered, the parameter which is modified internally is fracture aperture. As previously (cf. Section 3.3.2 for work conducted within Task 7A) fracture aperture *2b* is directly related to fracture transmissivity *T* by the cubic law relationship,

$T = \rho\, g\, (2b)^3 / (12\, \mu)$

where μ = 0.001 kg/ms is fluid viscosity, ρ = 1,000 kg/m^3 is fluid density, and g = 9.81 m/s^2 is the gravitational constant.

Furthermore, pumping is modelled by assigning the field-measured drawdown during pumping, as listed in Table 4-1.

Table 4-1. The time periods and pumping rates used during the sequence of cross-hole pump tests conducted in boreholes KR14–KR18 at Olkiluoto. Also showing resulting field-measured drawdowns. The drawdown values are used in the simulations to model each pump test. The responses obtained for pumping in KR15 are not delivered as this case is intended to be used as a forward blind prediction.

Pumping rates and resulting drawdowns					
	Pumping period		Pumping rate		Drawdown
Borehole	Start	End	l/min	m^3/s	m
KR14	2002-03-12	2002-03-21	25.0	4.2E–04	6.5
KR15	2002-01-04	2002-01-18	–	–	–
KR16	2002-01-21	2002-02-01	5.9	9.8E–05	10.5
KR17	2002-02-04	2002-02-19	7.7	1.3E–04	10.5
KR18	2002-02-25	2002-03-07	5.3	8.8E–05	10.5

4.3.3 Model conditioning and calibration

The case A configuration is a forward model (illustration shown in Figure 4-5), based on a general understanding of the field data, which is used as a reference configuration. Fracture extent is defined by compartments/regions associated with boreholes, such that they become internally connected only. Additional hydraulic zones from a large scale model are used to connect to model domain boundaries. Top boundary condition is assigned pressure head proportional to surface elevation, and the lateral sides have pressure head set to zero.

There are several test case configurations. These are used for conceptually/manually conditioning the model in order to attempt to improve the configuration. The modifications mainly involve three aspects, as follows:

(i) Alterations related to model boundaries (geometry, size of domain, boundary conditions),

(ii) alterations related to fracture populations (density, connectivity, size and extent, local partitions), and

(iii) alterations related to the heterogeneity of the system (altering fracture transmissivity in confined regions/locations of the model).

The case B configuration is the improved/conditioned model which is used as final configuration. The fractures extend within their respective partitions and out to model domain boundaries; hence no hydraulic zones imported from a large-scale model are needed. Fracture transmissivity is increased by one order of magnitude in the vicinity of boreholes to represent possible skin effects. The top surface of the model domain is assigned a no-flow boundary, and the lateral sides have pressure head set to zero.

4.4 Results

Results are presented in terms of flow entering or leaving boreholes at fracture locations along the depth of the borehole. Both flow directions and flow magnitudes are considered. Each simulation scenario is compared to four field data sets for the corresponding pumping tests, where water is withdrawn from each borehole one at a time (KR14, KR16, KR17 and KR18) until steady-state is reached. For each test, flow of water into or out of the borehole to fractures is monitored, both in the pumping borehole as well as in adjacent boreholes (denoted as response boreholes).

4.4.1 Analysis of PFL flow measurements

The in situ PFL measured flow data as used in this analysis to condition the simulated model is shown in Figure 4-7. Arrows indicate flow directions, using the following convention. Arrows directed upwards indicate flow leaving fractures and entering the borehole (defined as positive values), and arrows directed downwards indicate flow leaving the borehole and entering fractures (defined as negative values). Note the vertical scale for flow is logarithmic to base 10, and flow is in ml/h.

The upper left panel shows PFL flow for the period when pumping is conducted in KR14 (cf. Table 4-1). Note flow occurs in discrete instances, in particular in the sparsely fractured lower regions of boreholes. The flow rates entering the KR14 borehole during pumping varies several orders of magnitude, from about 10 to about 10^6 ml/h. The response in borehole KR15 has flow leaving the borehole in the upper part (40 m to just over 50 m depth), and entering in the remaining bottom part. Similar behaviour is observed for KR16 and KR17, however generally with lower flow magnitudes and fewer flowing features are detected. KR18 appears to have flow leaving the borehole except at three features, close to 50 m depth and 77–80 m depth.

The upper right panel shows PFL flows for the period when pumping is conducted in KR16. The response in KR14 is a significant amount of flow enters the borehole in the upper 50 m of the borehole, and flow leaves the borehole below, with a tendency of decreasing magnitude with depth. In KR15 and KR17 similar patterns occur, with the transition in flow direction occurring at around 55 m depth. Note the flow pattern in KR18 is essentially reversed to the case when pumping is conducted in KR14 (upper left panel).

The lower left panel shows PFL flows for the period when pumping is conducted in KR17. The response in KR14 is flow entering the borehole in the upper 50 m and generally leaving the borehole at depths below. Note the anomaly at around 180 m depth, where flow is apparently circulating, entering and leaving within a small support (less than 1 m) and with similar order of magnitude. As it seems unlikely that natural flow would behave in such a way there is reason to believe this may be a measurement error. Also, this response does not occur in KR14 when other boreholes are being pumped (cf. pumping in KR16 and KR18). The response in KR15 is similar to KR14, with transition in direction occurring at about 50 m depth. Here a small flow anomaly occurs at about 80 m, but is not circulating flow, so may be a correct measurement. The response in KR16 is flow enters the borehole at all depths, with the exception of two exit flows at about 48 m and 135 m. The response in KR18 is also flow entering the borehole throughout, with a single exit flow at about 51 m.

The lower right panel shows PFL flows for the period when pumping is conducted in KR18. The responses in KR14, KR15 and KR16 are generally similar to pumping in KR17. Interesting features include KR14 exhibits a single flow feature entering at about 180 m depth, KR 15 has flow entering at 120–130 m, and KR16 has several exit flows between 50–80 m. For the response in KR17, the upper part has exit flows, and two groups of flows enter at 60–70 m and 125–135 m.

In general, note that many more PFL flowing features are identified when a borehole is being pumped. This is due to the local forcing (drawdown) in borehole. The fractures used to define the DFN model are based on the largest PFL data set, which consists of the features observed during pumping. Hence it may appear that the simulated DFN contains more fractures than measured when analysing response boreholes.

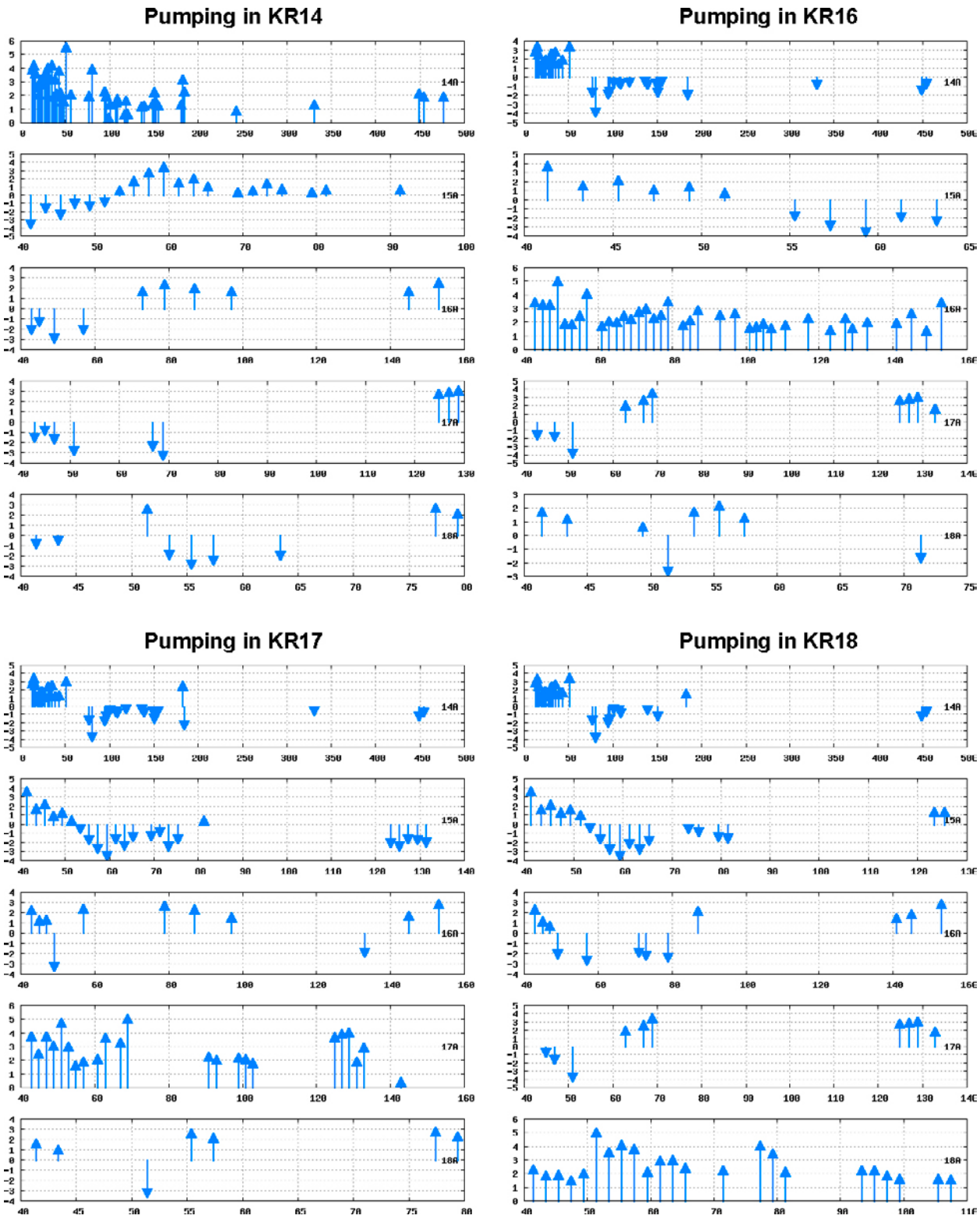

Figure 4-7. *The PFL field measured flow data as used in this analysis. Arrows directed upwards indicate field measured flow entering the borehole (defined as positive values), and arrows directed downwards indicate flow leaving the borehole (defined as negative values). The vertical axis is the base 10 logarithm of flow in ml/h, the horizontal axis is depth along borehole in meters.*

4.4.2 Model conditioning

Configuration A, the reference case forward model

Figure 4-8 shows results from the forward model, the "reference configuration" simulation case A (red arrows) as fracture flow along borehole depth, compared with PFL measured flows (blue arrows). Flow entering the borehole is identified by positive values, and flow leaving the borehole is identified by negative values. Each panel shows one of the four pump tests (KR14, KR16, KR17 and KR18) with corresponding responses in boreholes (rows).

In this forward model, the simulated vs PFL flows correspond surprisingly well for the pumping borehole in all cases. That is, the flows in borehole KR14 match reasonably well when KR14 is pumped (upper left panel, top row), or in KR16 when KR16 is pumped (upper right panel, third row), in KR17 when KR17 is pumped (lower left panel, fourth row), and KR18 when KR18 is pumped (lower right panel, fifth row).

This is also clearly visible in the corresponding plots of cumulative flow (Figure 4-9). Here the vertical axis is linear, and as can be seen the total flows match very well when KR14 and KR16 are pumped, flow in KR17 is slightly over-estimated, and flow in KR18 slightly under-estimated in the pumping boreholes.

Considering the response boreholes, when KR14 is pumped, the response in KR15 is at a correct order of magnitude but generally in the wrong direction (Figure 4-8, upper left panel, second row). Also several minor flows to fractures intersecting the deep end of the borehole occur in the simulation, which are not measured. The responses in KR16, KR17 and KR18 occasionally match but occasionally flow in the incorrect direction. In terms of cumulative flow (Figure 4-9, upper left panel), KR15 is as already noted the correct order of magnitude, but in the incorrect direction, KR16 over-estimated, KR17 within the correct order of magnitude, and KR18 under-estimated.

The response to pumping in KR16, KR17 and KR18 is in a broad sense similar. Flow directions occasionally match, as in KR14 and KR17 when KR16 is pumped (Figure 4-8, right panel), and in KR15 both when KR17 and KR18 is pumped. Otherwise flow directions generally do not match, as in KR18 when KR16 is pumped, KR16 when KR17 is pumped, and KR17 when KR18 is pumped.

An observation common for all cases is the absence of measured PFL flows in the deep end of KR15, and generally there are more simulated fracture flows than there are measured for all boreholes. Also, judging by the cumulative flows (Figure 4-9), flow rates are generally over-estimated in response boreholes.

Intermediate configurations, trial-error testing and conditioning of models

Several configurations are employed in order to test and thereby attempt to condition the forward model, configuration case A. Due to the nature and complexity of the data, formal conditioning approaches have not been attempted. Instead, a manual trial-based approach is adopted, by testing various configurations based on alterations in details of the conceptual model. A multitude of simulation configurations are evaluated; in the following only the main results from these test cases are discussed.

Test case T1 (Figure 4-10 and Figure 4-11):

The hydraulic zones are removed and replaced by fractures extending fully within their respective partitions, and such that the external regions extend to the model domain boundary (cf. Figure 4-4 and Figure 4-6). This causes a notable reduction in the flow rates of pumping boreholes, that is, the flow magnitudes in the pumped boreholes are lower than the field measured values. On the other hand the magnitudes of the flow rates in response boreholes are slightly reduced, and as such the responses are improved. However, the flow directions are not significantly improved, even though several directions are changed with respect to case A.

Test case T2 (figures not shown):

A general observation from both case A and T1 simulations seems to indicate that the simulated system may be over-connected. Therefore, an attempt at reducing the overall fracture density in the T1 model is made. This is achieved by randomly removing fracture surface area with an assigned factor, expressed as a percentage. This is doable since each fracture is tessellated into subfractures. Reducing the fracture density to 90% of case T1 results in negligible differences, however reducing to 75% of case T1 causes a somewhat under-connected system (determined visually). A reduction to 50% causes the system to be essentially disconnected, with only minor flow routes. Thus the overall system does not seem to be significantly over-connected, but could possibly be slightly reduced.

Test case T3 (Figure 4-12 and Figure 4-13):

The top surface boundary condition is changed to a no-flow boundary. When applied to case T1, this results in significantly improved responses, in terms of both flow direction and magnitude. Flow magnitudes in pumping boreholes are however generally under-estimated. Whereas a no-flow top boundary is not expected, the effect in the simulation is water is only extracted from the lateral boundaries of the domain. This effect may be expected due to the large scale highly conductive hydraulic zones which are believed to extend throughout the subsurface of the island.

Test case T4 (figures not shown):

A horizontal near-surface, high-conductivity zone is introduced, based on case T1 (ie the top surface BC is head proportional to elevation). The motivation is that a highly conductive upper zone may drain surface water, and hence mimic a no-flow boundary for the lower part of the domain which is beneath the high-conductive zone. This is implemented by increasing the fracture transmissivity by one order of magnitude for all fractures within elevations –10 m to –20 m. This causes flow magnitudes to be improved in pumping boreholes, but response directions and magnitudes are generally not improved.

Configuration B, the improved model

The final configuration, based on the experience gained in the testing/conditioning configurations is simulation case B, the "improved configuration" model (Figure 4-14 and Figure 4-15). For pumping in borehole KR14, the flow directions in both the pumped borehole KR14 and response boreholes match reasonably well (Figure 4-14, upper left panel). In particular, note the contrast in responses in KR15 between cases A and B (upper left panel, second row in Figure 4-8 and Figure 4-14 respectively); in case A the simulated flow directions opposed the measured flows, whereas in case B they correspond reasonably well.

Similarly, for pumping in KR17 and KR18 the responses have a general tendency to match the measured flow directions. Minor exceptions do occur however, such as in the deep parts of KR14 for pumping in KR17, and in the upper parts of KR17 for pumping in KR18.

For the case B configuration, it is mainly pumping in KR16 which shows the least consistency in flow directions, in particular notable for the responses in KR17 and KR18 and the deep parts of KR14.

The improved match in flow directions is also visible in terms of cumulative flow (Figure 4-15). However, note that the magnitudes of simulated flows in the pumping borehole are under-estimated for all cases; for pumping in KR14 by a factor of about 5, for KR17 by a factor of about 4, and for KR16 and KR18 by a factor of about 3. However, the simulated cumulative flows in the response boreholes have similar shapes and magnitudes as the measured flows. The most notable exceptions would include KR17 for pumping in KR14, KR16 and KR18. Also, the response magnitude in KR14 is generally under-estimated for the upper parts of the borehole for all pumping cases.

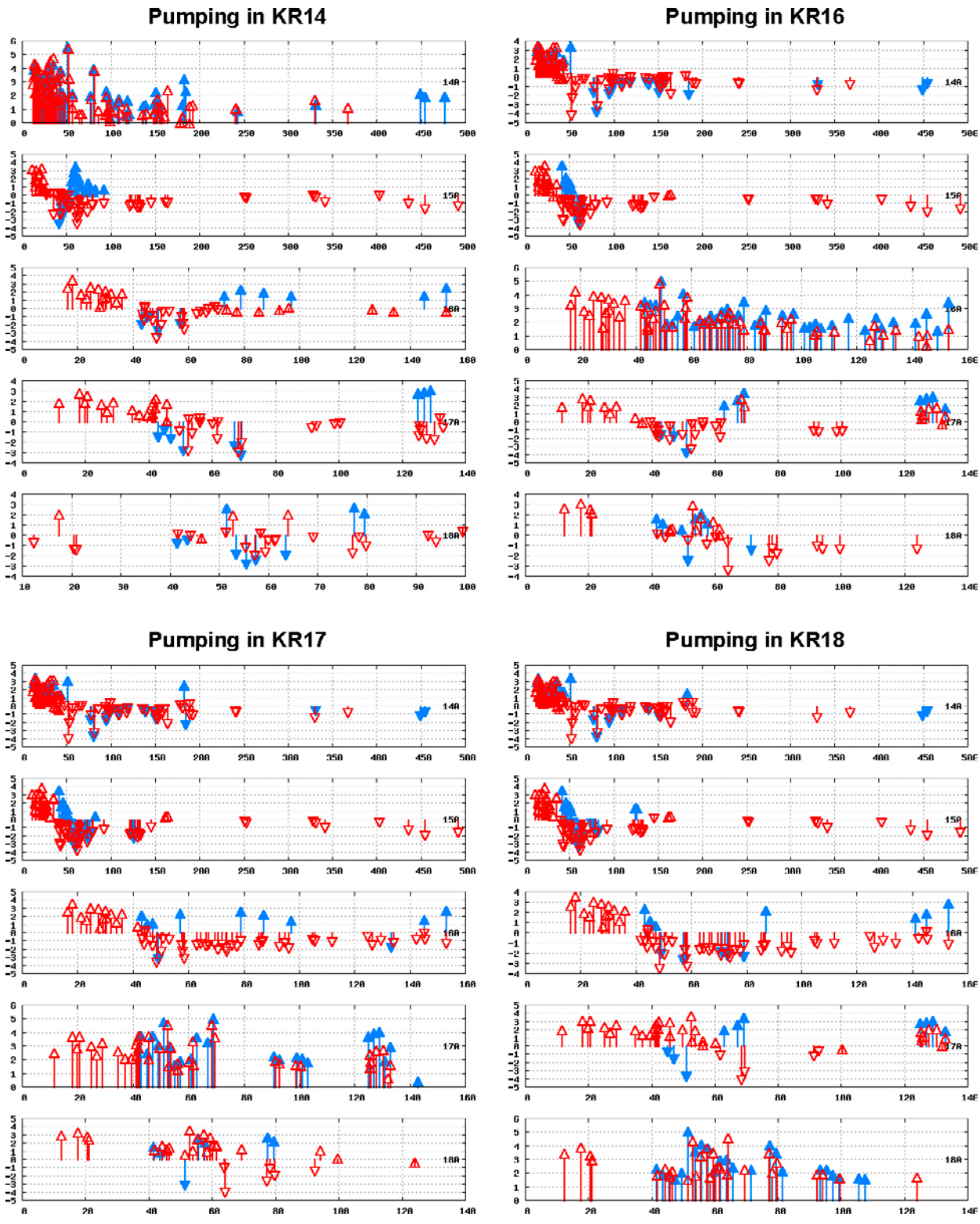

Figure 4-8. *Simulation case A "Reference case". Fracture flow along borehole depth. Blue arrows indicate field measured flow entering (identified by positive values) or leaving (identified by negative values) the borehole along the extent/depth of the borehole, as measured by the PFL device. Red arrows indicate corresponding flows obtained by the simulated model, with configuration according to the Reference case A. Each panel shows one of the four pump tests (KR14, KR16, KR17 and KR18) with corresponding responses in boreholes (rows). The vertical scale is logarithmic to base 10, and units of flow are ml/h*

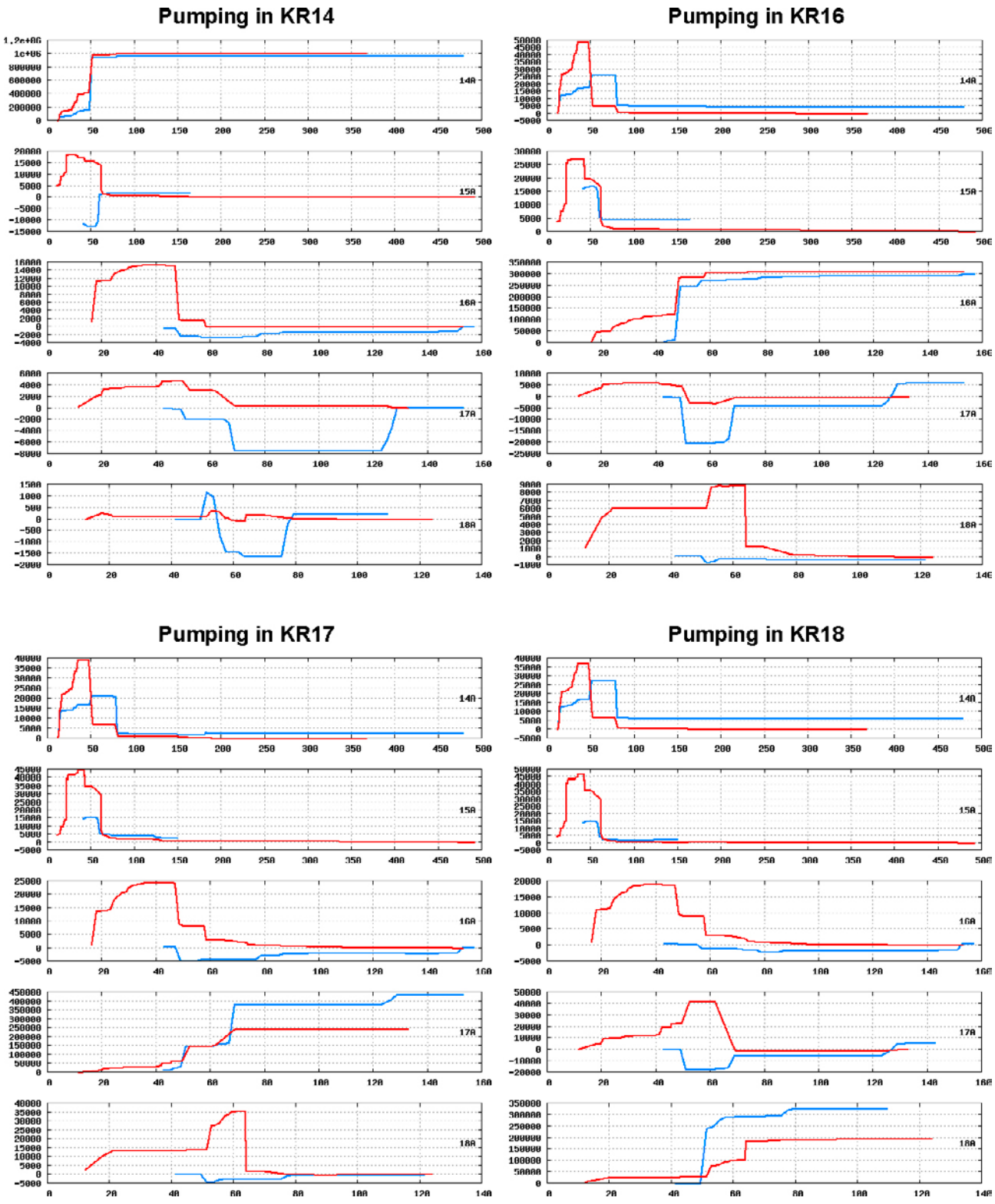

Figure 4-9. *Simulation case A "Reference case". Cumulative fracture flow along borehole depth. The vertical axis is linear.*

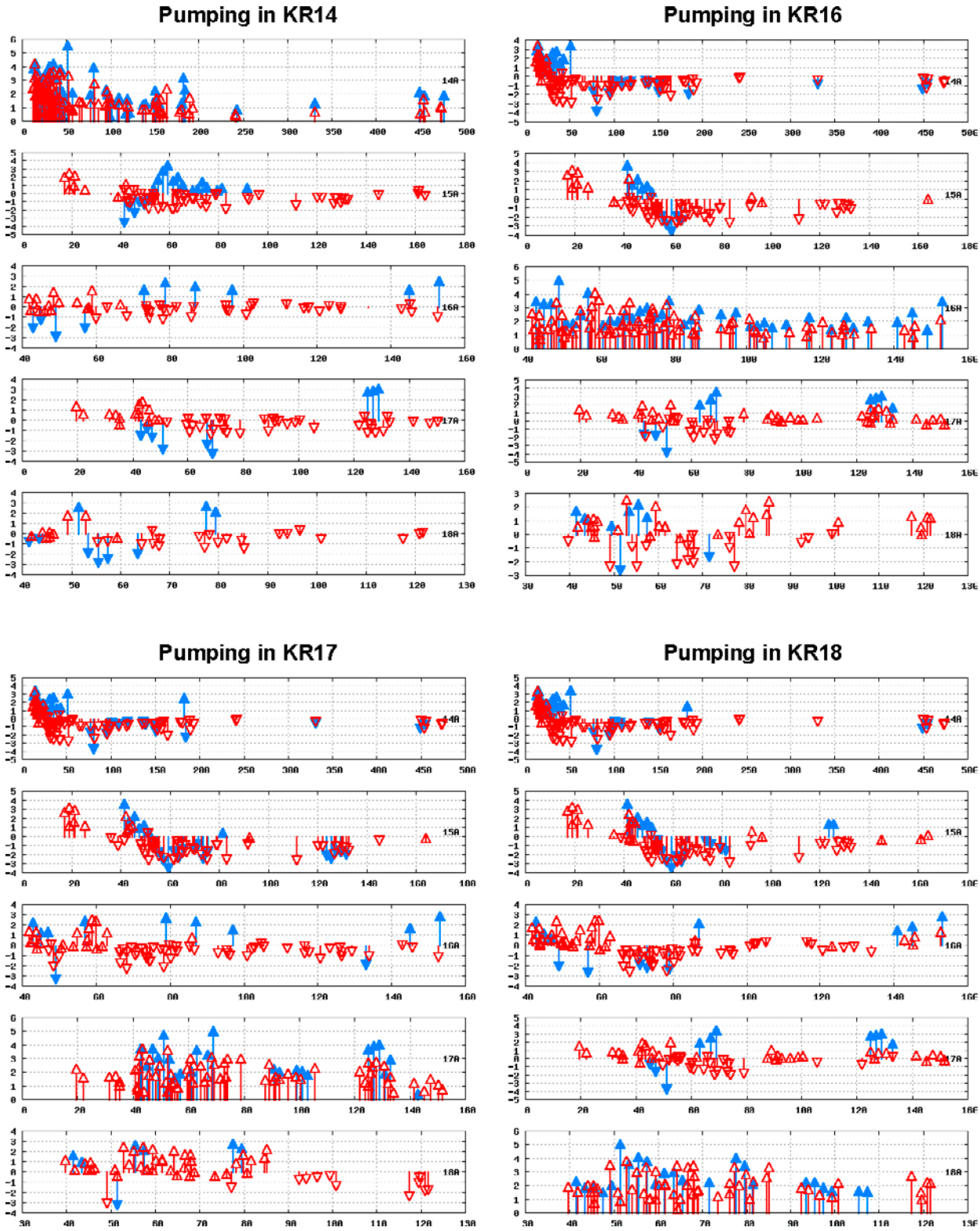

Figure 4-10. *Simulation Test case T1. Fracture flow along borehole depth.*

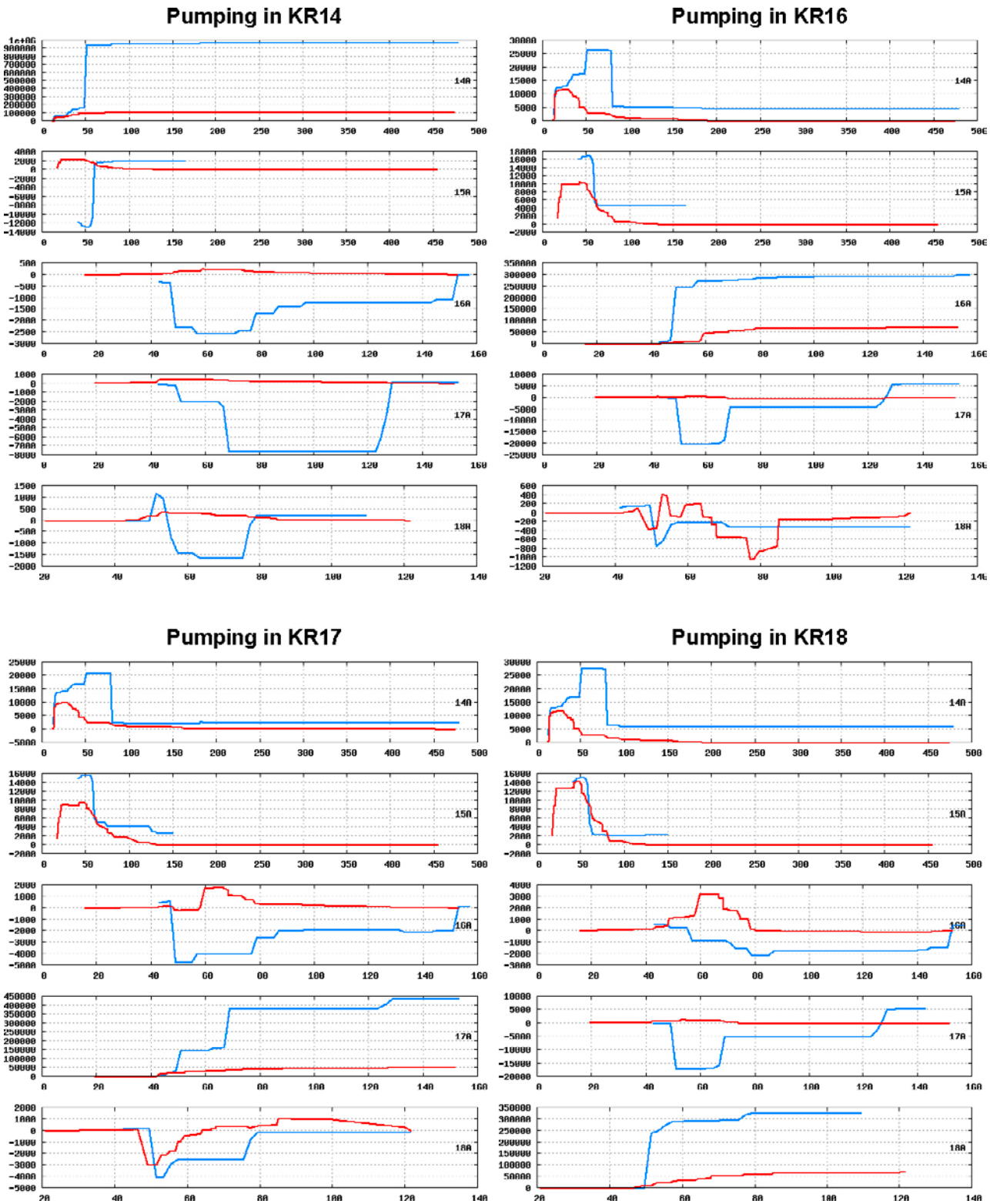

Figure 4-11. *Simulation Test case T1. Cumulative fracture flow along borehole depth. The vertical axis is linear.*

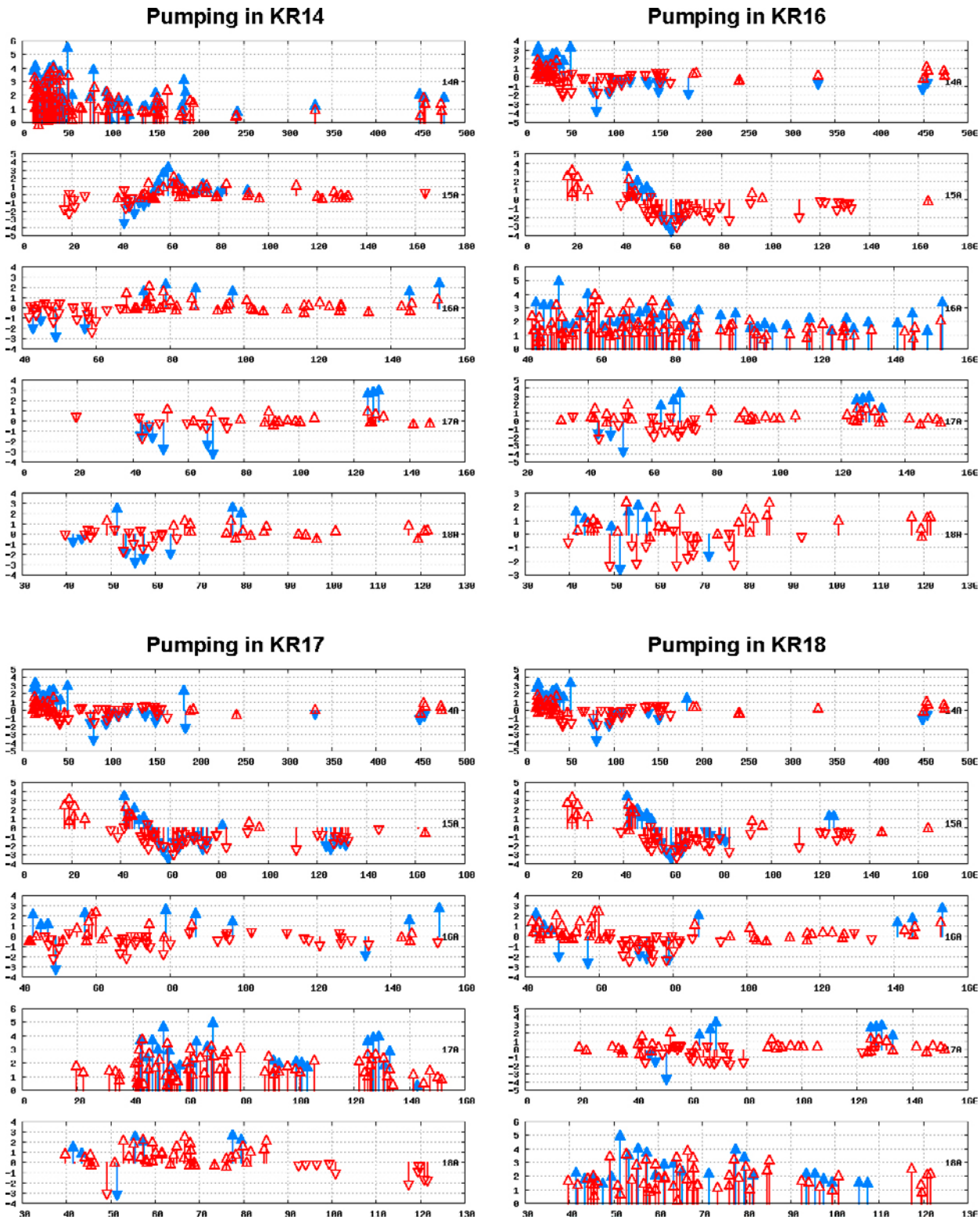

Figure 4-12. *Simulation Test case T2. Fracture flow along borehole depth.*

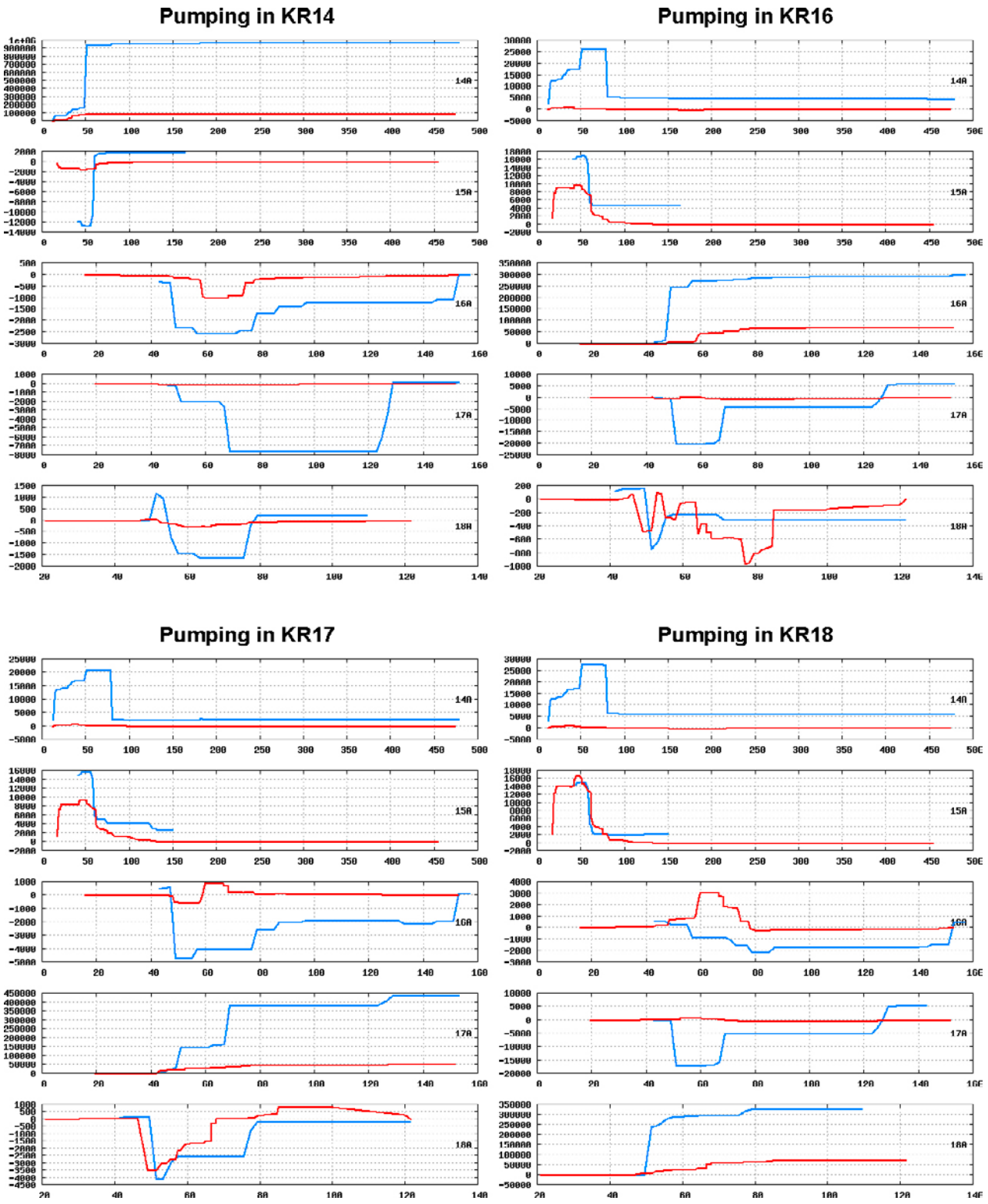

Figure 4-13. *Simulation Test case T2. Cumulative fracture flow along borehole depth. The vertical axis is linear.*

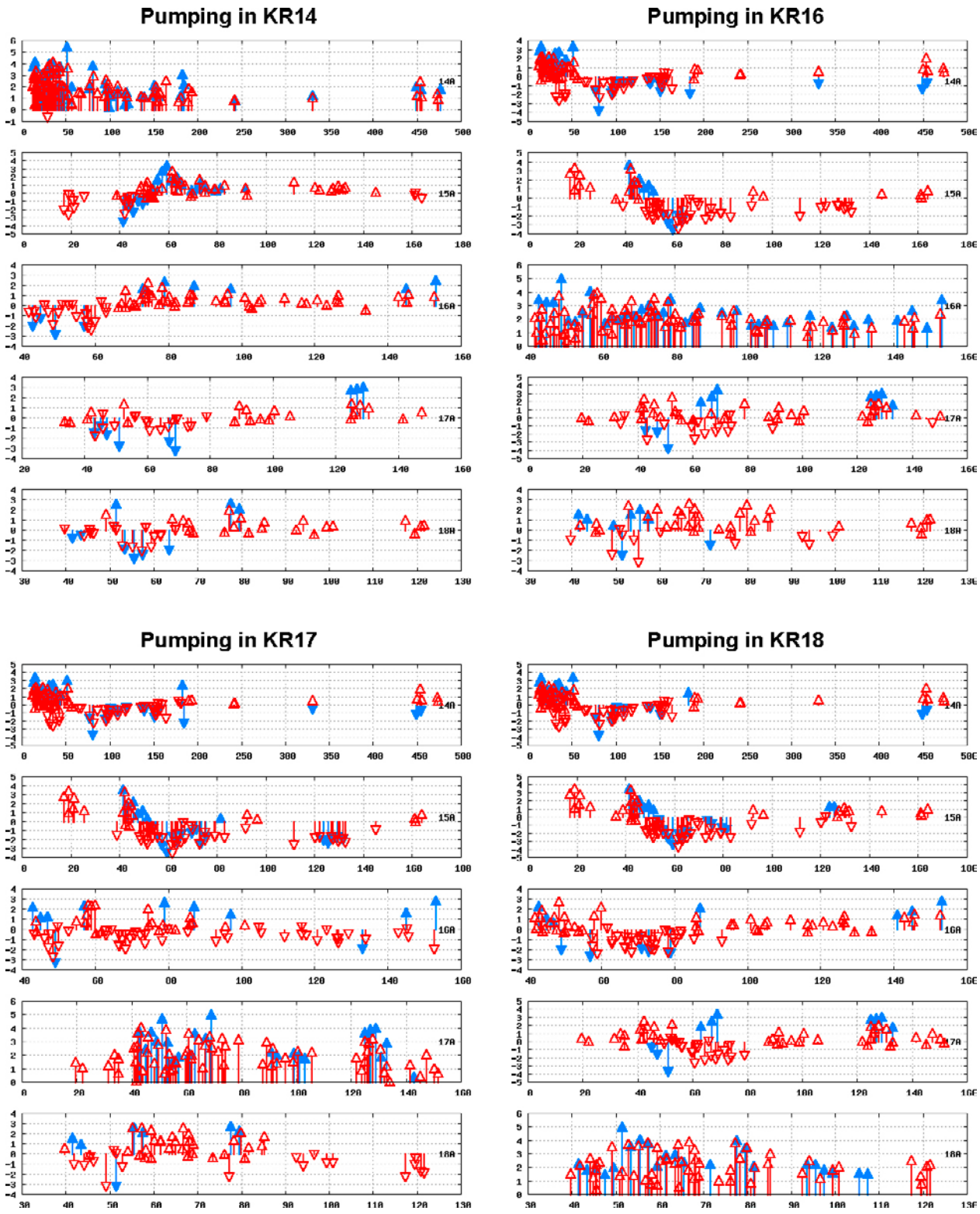

Figure 4-14. *Simulation case B "Improved case". Fracture flow along borehole depth.*

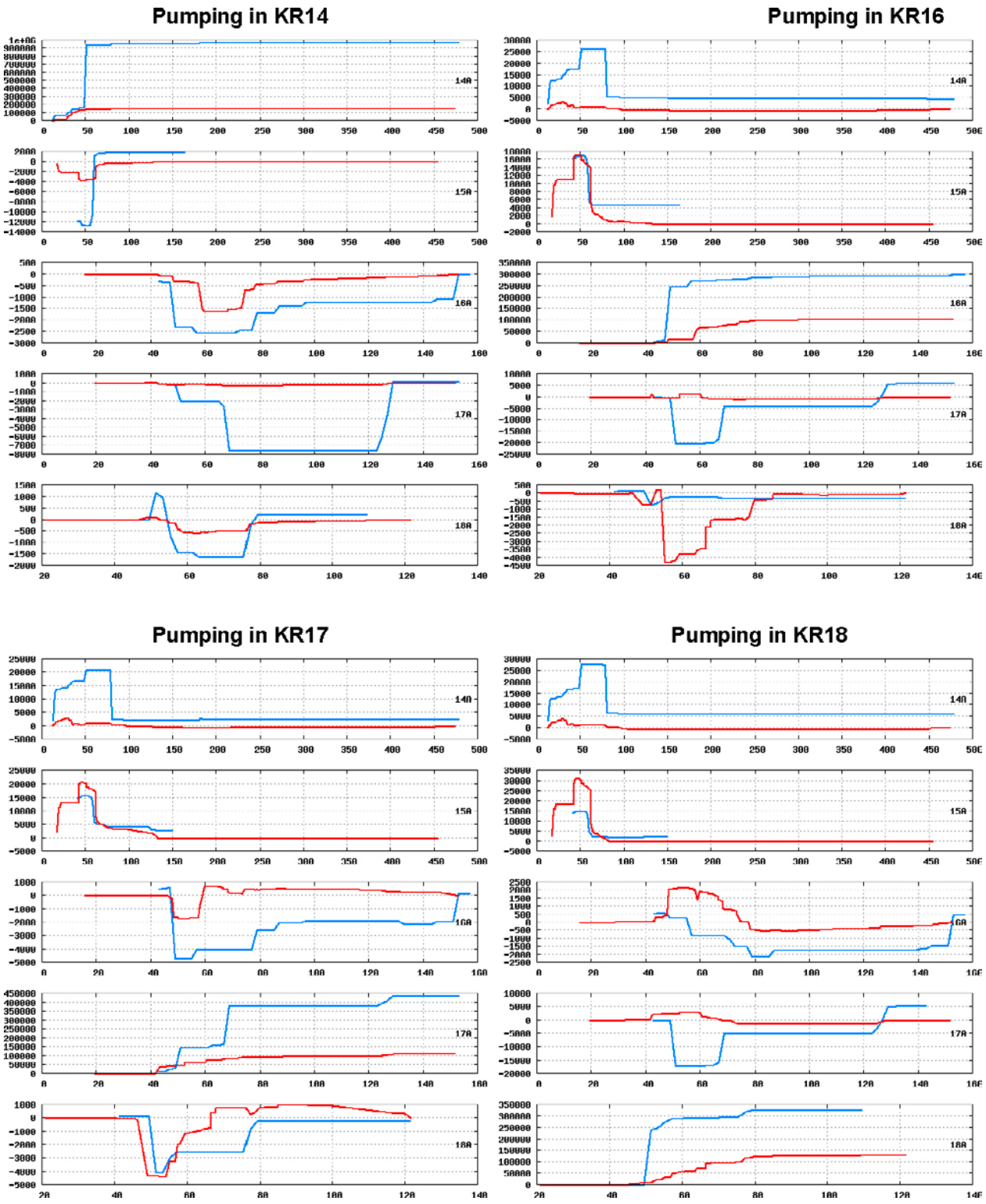

Figure 4-15. *Simulation case B "Improved case". Cumulative fracture flow along borehole depth. The vertical axis is linear.*

4.4.3 Transport modelling

Transport modelling simulations representing advective travel times of water are performed for the improved case B configuration. The four principle directions (North–South, East–West) are analysed (Figure 4-16) by tracking particles across the lateral boundaries of the domain. In general, only two principle directions are necessary to determine travel time statistics, provided a sufficient number of particles are used. However, by injecting a constant number of particles and comparing injection modes (flux and resident injection), it may be possible to determine indications of anisotropy in the fracture network.

Generic long-term flow boundary conditions are adopted, by assigning a moderate hydraulic gradient (of 0.01 m/m) along each of the principle directions with no-flow boundaries on the perpendicular lateral sides. Then for each of the four cases, several particles (1,000) are injected on the corresponding upstream boundary over the entire lateral surface. Both the flux and resident injection modes are employed, such that 1,000 particles are injected for each mode. Here, flux injection means injection locations are selected with a probability proportional to the flow rates of the fractures intersecting the boundary. Thus fractures with higher flow have a greater probability of having more particles injected. Resident injection means particle injection locations are uniformly selected amongst fractures intersection the boundary. Particles are then allowed to follow the advective flow of water through the domain, and the cumulative travel time τ [T], the transport retention parameter β [L/T], as well as vertical dispersion is calculated.

The advective travel time, which here includes dispersion due to network heterogeneity, is defined in a Lagrangian (trajectory) formulation as

$$\tau = \int_r \frac{l}{v} dr$$

where the integral is taken over the pathway trajectory r, consisting of length $l = l(r)$ and velocity $v = v(r)$. In general, transport of contaminants including radionuclides are expected to be slowed down with respect to advective-dispersive transport due to interactions with the rock matrix such as diffusion and sorption, collectively denoted as retention mechanisms. Previously it has been shown (Cvetkovic et al. 1998) that retention in fractured media can be conveniently parameterised by the quantity β, denoted as the *hydrodynamic control of retention*, defined as

$$\beta = \int_r \frac{l}{vb} dr$$

where the integral is taken over the particle pathway trajectory r, accounting for fracture half-aperture $b = b(r)$. For transport in a DFN, the above integrals are replaced by summation over discrete steps, where each step is defined either on the scale of the numerical grid or approximated over segments connecting fracture intersections. Here a combination of both is used, where fractures and intersections are defined over the tessellated fracture network, and at this scale each tessellated fracture is assigned with homogenous properties (transmissivity and hence aperture).

Results for cumulative total transport time τ (yr) divided by the hydraulic gradient (0.01 m/m) are shown in Figure 4-17 for the four principle directions and the two injection modes. For the flux injection mode, the distribution of arrival times is slightly different between North–South and East–West, such that the North–South direction has slightly lower times, indicating slightly faster velocities. For resident injection, there is an apparent anisotropy between N–S and S–N, as well as between E–W and W–E, which indicates additional particles are needed in order to obtain converged distributions. However, the apparent differences in the distributions indicate there may be some anisotropy in the fracture network. In general, analysis of resident injection requires a significantly larger amount of particles to obtain converged distributions, since this injection mode is more sensitive to lower fluxes (Frampton and Cvetkovic 2009).

The results for the hydrodynamic control of retention parameter β (yr/m) are shown in Figure 4-18 for the four principle directions and the two injection modes. Since the span and overall shape of the β distributions are very similar to the τ distributions, except for the parameter values, this indicates that variation in transmissivity (ie aperture) in the fracture network, as experience by particle trajectories, is relatively modest.

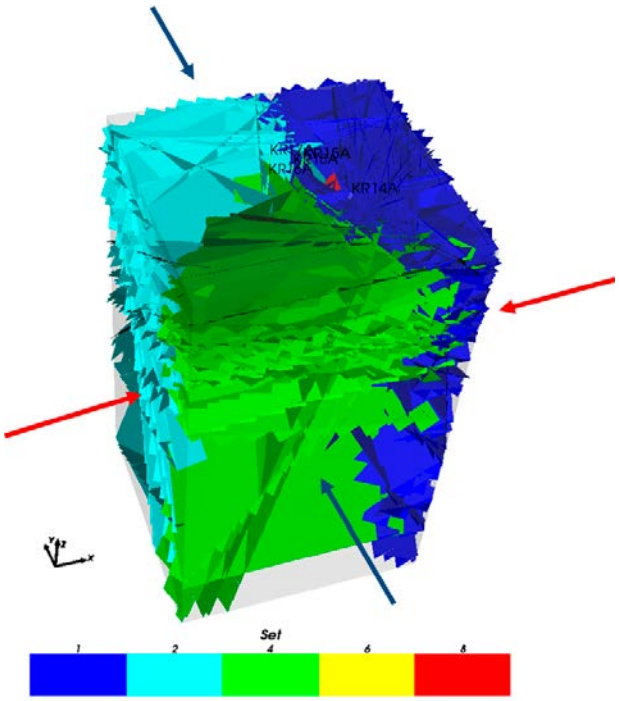

Figure 4-16. *The four principle directions (North–South and East–West) analysed with particle tracking. Generic long-term boundary conditions are adopted, representing a weak hydraulic gradient along each of the principle directions. Then for each of the four cases, several particles (1,000) are injected on the corresponding upstream boundary over that entire lateral surface using both the flux and resident injection modes. Particles are then allowed to traverse the domain, and the cumulative travel time tau, the cumulative transport retention characterisation parameter beta, as well as vertical dispersion is calculated.*

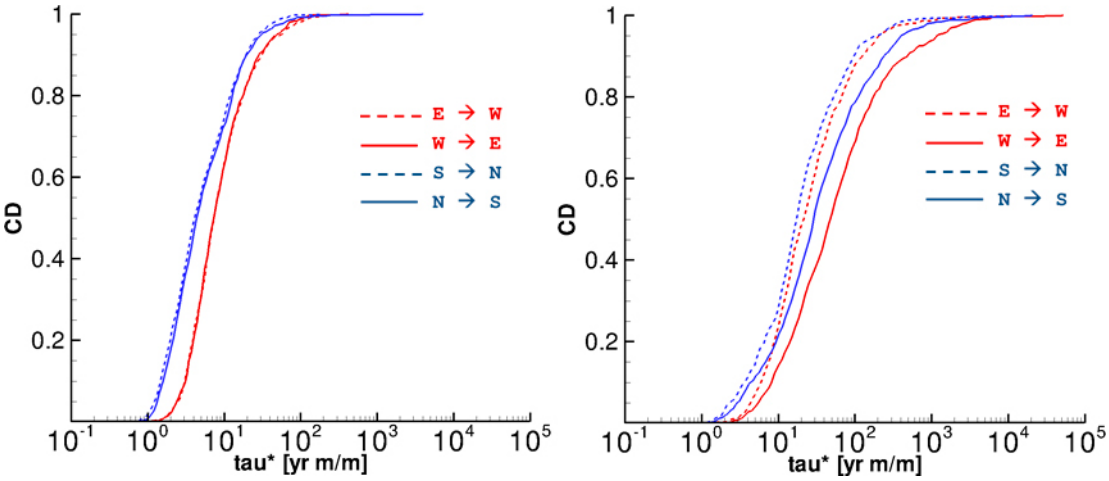

Figure 4-17. *Cumulative distribution of total particle travel time τ normalised by the value of the hydraulic gradient for each of the four principle directions. Left: Flux injection mode. Right: Resident injection mode.*

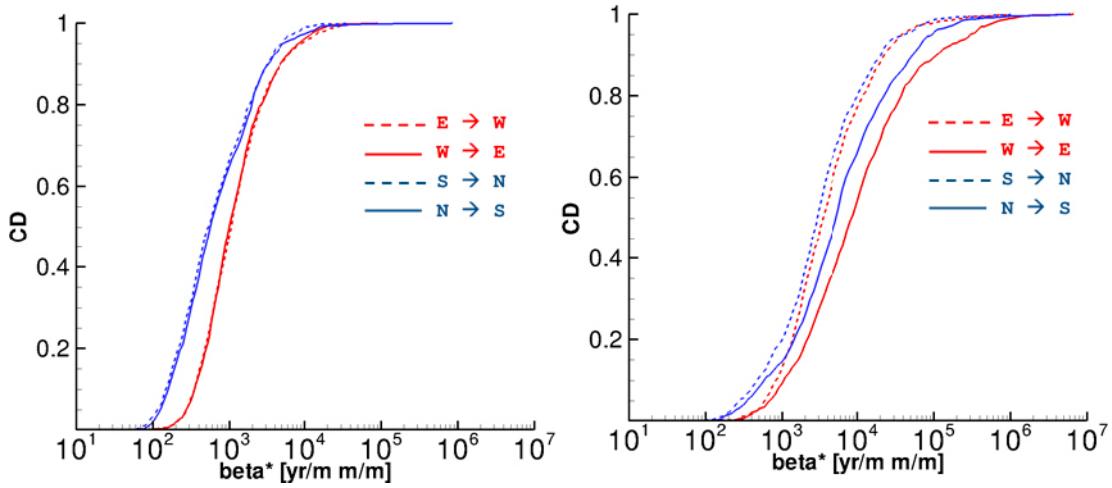

Figure 4-18. *Cumulative distribution of transport retention parameter β normalised by the hydraulic gradient. Left: Flux injection mode. Right: Resident injection mode.*

Particle travel distances, ie the total trajectory lengths, are shown in Figure 4-19 for the four directions and two injection modes. Most particles experience a travel distance of 400–500 m, which is about 30–60% greater than the lateral extent of the domain (300 m). A trajectory distance of 2 to 3 times greater than the lateral extent of the domain is experienced by very few (less than 10%) of the particles. Slightly greater distances are experienced in the E–W direction than in the N–S direction.

Perhaps of greater interest is the vertical displacement experienced by particles (Figure 4-20). Here, this is defined as the displacement along the z-axis from the starting location on one of the lateral inflow planes to the exit location on the corresponding lateral outflow plane. Injection can in principle be along any position on the inflow plane; however injection locations are likely to be more widespread for the resident injection mode. This is also expected to create more vertical movement, as particles have a bias towards high flow pathways at all intersections occurring after injection. This behaviour is evident in Figure 4-20, where the distribution histogram of vertical displacement for the resident injection mode (right) is extended, smoother, and has fewer pronounced peaks than flux injection modes (left). Interestingly, for flux injection, there are two distinguished peaks for the E–W directions, but none for the N–S directions. The peaks for the E–W directions occur close to 0 m and 100 m vertical displacement. This indicates one dominant flow pathway exists which is relatively horizontal, and another which is has a net horizontal displacement of about 100 m. Note these pathways may consist of one or several fractures.

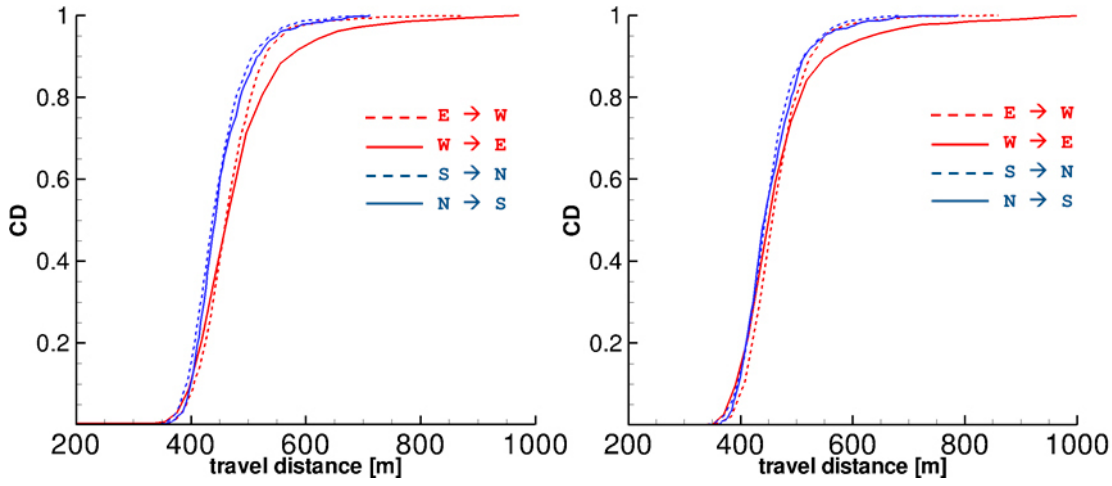

Figure 4-19. *Travel distance normalised by domain size. Left: Flux injection mode. Right: Resident injection mode.*

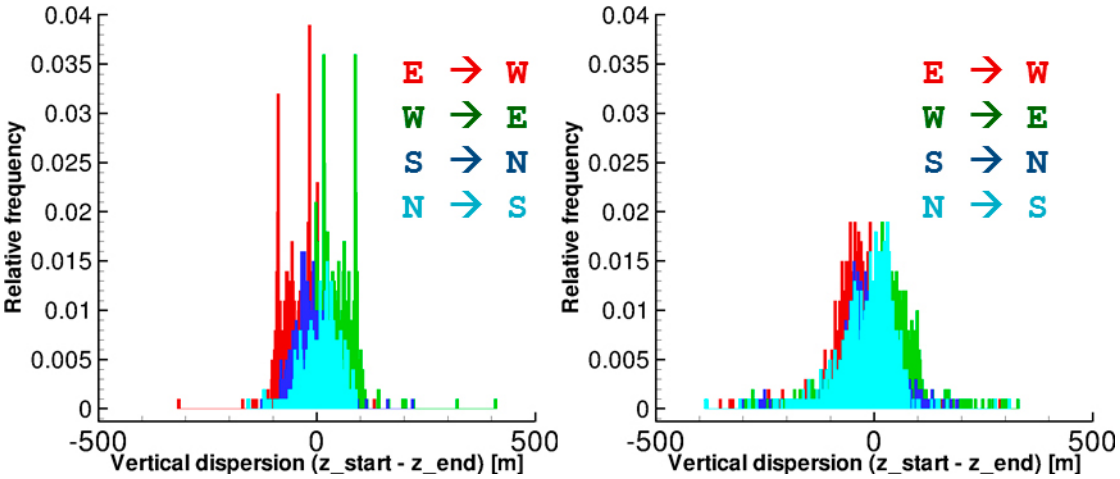

Figure 4-20. *Vertical displacement. Left: Flux injection mode. Right: Resident injection mode.*

4.5 Discussion and conclusions

4.5.1 Discussion of results

Traditional hydrological measurements and model conditioning generally involve using pressure head data, which is a scalar quantity. The PFL tool allows for direct, in situ flow measurements involving both flow direction and magnitude, in this sense similar to a vector quantity. A challenge with using this kind of data is it introduces much greater complexity in field data, and may therefore require new approaches for making efficient use of PFL measurements in groundwater modelling.

Analysis of PFL flows obtained from the KR14–KR18 cross-hole interference test clearly show the discrete nature of flow in sparsely fractured crystalline rock, and also its complexity in terms of greatly varying flow magnitudes, and transitions in flow directions entering/leaving boreholes along its extent. In general flow patterns exhibit a transition in terms of flow direction at around 50 m depth in boreholes. Directions greatly depend on which borehole is being pumped, and can easily be reversed between pumping in different boreholes.

A new approach for incorporating fractures observed in boreholes is introduced, denoted as a compartmentalized fracture growth model. For this, extensive use of PFL flow data is made to construct a simple yet functional DFN model for the KR14–KR18 region, applicable for the cross-hole interference pumping tests conducted. Its main feature is it enables direct comparisons between modelled and field measured flow values, both in terms of flow magnitude and direction, and at the precise locations of interest, that is, where field measurable are obtainable (fracture intersections with boreholes). The fracture growth approach is evaluated and shown to be a useful approach at least for local-scaled sparsely fractured crystalline rock, comprising scales up to about 100 m in length (between boreholes), and several hundreds of meters in depth, and for a system containing multiple boreholes.

The compartmentalized fracture growth model is a simplistic yet functional DFN approach which is capable of using PFL-identified fractures to generate a fracture network for the KR14–KR18 region. It works relatively well and makes it possible to directly compare PFL flow data with simulated flow values. This enables the applicability of the DFN model to be determined, and by varying conceptual details and various parameters of the model, a simplified conditioning approach is made possible. The improved or ‘conditioned’ model is based on a somewhat subjective analysis of flow directions and magnitudes. Clearly a formal conditioning method or scoring scheme would improve the analysis. Nevertheless, the main re-configuration required to obtain improved matches in flow directions seems to be a no-flow top boundary condition.

The no-flow boundary condition on the top of the domain indicates the dominant flow in this localized region seems to be entering the system from the lateral sides of the domain, rather than from the

upper surface; that is, the main flow pathways seem to be dominated by subsurface recharge rather than surface recharge. It should be noted that the surface of the domain (300 m × 300 m) has a rather smooth surface topography and does not in any way encapsulate a catchment or sub-catchment, hence subsurface recharge is likely to occur. The latter is simplified in the model configuration, as all lateral sides have a constant and equal head value (0 m), however the lateral sides are more realistically expected to have head values which may be depth dependent and, perhaps more importantly, depend on the large scale fracture network. Hence, an interesting result observed here is that subsurface recharge along the lateral sides of the domain seems to exhibit a dominant or controlling factor, which may likely be due to the observed sub-horizontal hydraulic zones intersecting the upper part of the region.

Clearly, there is a need for developing methods for comparison of this type of binary vector flow data combined with multiple cross-borehole interference tests. Improvements to the current method of presenting results are needed. In particular, it would be desirable to introduced quantification of the degree of agreement between simulated and measured data in order to simplify comparisons. One untested but possible approach could be to introduce soft conditioning, by comparing statistical agreement of distributions of simulated flow with measured flows, which has previously been attempted by adopting the Kolmogorov-Smirnov and Kuiper tests (Kolmogorov 1933, Kuiper 1962, Press et al. 1992) tests for single-borehole pump tests with PFL data (Frampton and Cvetkovic 2010). For cross-hole pump tests where responses are measured, it would be necessary to distinguish flow directions, for example constructing two distributions, one based on inflows and the other on outflows. A disadvantage however is the sample size of flow measurements may not be well represented if the sample size is too small, which may in particular be the case for of sparsely fractured rock environments.

Comments on the use of the PFL device.

It should be noted the measurement limits of the PFL device impose restrictions on the number of fractures identified as ‘flowing features’, which in turn will limit the number of simulated fractures. Whereas this is mainly a technical limitation, since the approach could readily incorporate more or less fractures as needed, it may be expected to restrict the predictive capability of the approach, since potential (unmeasured) low-flow features are disregarded. However, low-flow features may be assumed not to have a significant impact on large-scale advective transport, as transport is generally assumed to follow dominant flow pathways. The limitation may lie mainly in short-term or near-canister scale predictions of transport, which may have a greater impact on the resident injection mode. Also, retention characteristics, such as the quantification of β, may be restricted as retention may be more sensitive to small-scale and low-flow features (Cvetkovic and Frampton 2010). Nevertheless, it should be noted that the low-flow measurable features are included, and are given equal (geometric) importance as large-flow features. That is, these features are active and part of the network scale model, and will have sizes comparable to large flowing features, so may add an important component of low-flow predictions and retention quantities. This may be of significance when accounting for retention.

Furthermore, it should be noted that transmissivity obtained from the PFL device is based on homogenization assumptions, which may in general not be applicable to fractured media, in particular sparsely fractured rock. Previous studies have indicated that PFL inferred transmissivities may be lower than transmissivity measured by other means (Pöllänen and Rouhiainen 2001, Rouhiainen and Sokolnicki 2005). For example, by comparing HTU and PFL transmissivities in Figure 4-21, the tail of the cumulative distribution shows the highest densities are almost an-order of magnitude greater for HTU transmissivities than for PFL transmissivities. (Low transmissivities are under-represented by the PFL, which is mainly due to the lower measurement limit of the PFL device.)

Comments on transport simulation results.

In terms of transport, the system clearly exhibits flow anisotropy between the North–South and East–West directions. It would be of interest to compare measures of anisotropy obtained from this approach, which includes a network based on PFL flowing fractures combined with their geometric orientations, with a statistical hydro-DFN model of this region of Olkiluoto.

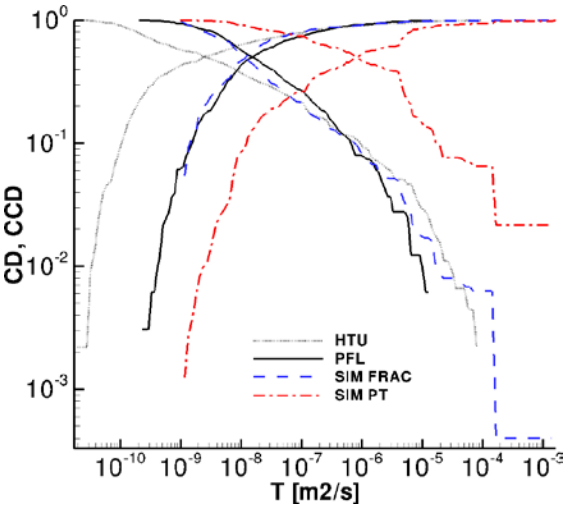

Figure 4-21. *Cumulative and complement of the cumulative distribution of fracture transmissivities obtained from PFL flow logs (solid black) and from HTU tests (thin black). (HTU transmissivity data is not adopted in this study.) Also showing the distribution of transmissivities assigned to fractures (dashed blue), which follows the PFL measured data, and the transmissivities of fractures traversed by particle tracking in flux injection mode (dashed-dot red). Some simulated fractures have higher transmissivity than the values assigned by PFL after conditioning.*

For these simulations, median advective transport times across the 300 m-scaled domain and under the flux injection mode, representing injection in dominant flow pathways, are of the order of 10 yr per unit hydraulic gradient (1 m/m), and median values of the hydrodynamic control of retention are of the order to 10,000 yr/m per unit hydraulic gradient. For the resident injection mode, representing random injection with uniform spatial probability, median advective transport times are of the order to 100 yr per unit hydraulic gradient, and median values of the hydrodynamic control of retention are of the order to 10,000 yr/m per unit hydraulic gradient.

Based on median values of transport time (cf. Figure 4-17), the flux injection mode corresponds to a median Lagrangian advective-dispersive velocity of about 40 m/yr per unit hydraulic gradient (assuming a transport distance 50% greater than the lateral extent of the domain, cf. Figure 4-19). The corresponding resident injection mode velocity is 4 m/yr. Hence, adopting a weak, long-term gradient of say 10^{-4} m/m, velocities of the order of 4×10^{-3} m/yr and 4×10^{-4} m/yr may be expected.

These values could be used as comparison to other models of Olkiluoto and values obtained from other similar sparsely fractured sites.

4.5.2 Main conclusions

The main conclusions based on the analysis of PFL flows, simulation results and discussion of results are listed in the following.

- PFL data provides binary vector quantities, which introduces additional complexity, but also reveals additional features of the hydrogeological system which would not be distinguishable solely with pressure head information.
- Analysis of PFL flow data for extensive data sets such as the KR14–KR18 cross-hole interference tests is made possible by using logarithmic flow plots which include flow direction as positive or negative values. This is useful for modelling and comparison between simulated and field flows since both flow magnitude and direction can be accounted for.
- Multiple forcing of the system yields significantly more information in terms of constraining a model configuration than if pumping in a single borehole only were considered.

- In general flow patterns exhibit a transition in terms of flow direction at around 50 m depth in boreholes. Directions greatly depend on which borehole is being pumped, and can easily be reversed between pumping in two different boreholes.
- In order to make direct comparisons of PFL flows with simulated flows, accurate locations of fractures in the hydrogeological model are needed. The proposed fracture growth model enables this to be achieved for DFN modelling.
- The compartmentalized fracture growth model is determined to be a useful approach which can make extensive use of PFL flow data. It is also shown that conceptual aspects of the DFN model can to some extent be constrained, even by simple conditioning against PFL data.
- Multiple forcing of the system combined with the fracture growth model allows for direct comparison of field measurables, and is shown to be a viable method to provide insight into the behaviour of underlying features of the system, in particular concerning conceptual aspects of the system.
- Thus the fracture growth model is evaluated and shown to be a useful approach at least for local-scaled sparsely fractured crystalline rock, comprising scales up to about 100 m in length (between boreholes), and several hundreds of meters in depth, and for a system containing multiple boreholes.
- As such, the compartmentalized fracture growth model can be seen as one way in bridging the gap between stochastic modelling of background fractures and deterministic modelling of hydraulic zones.
- Predictions on advective-dispersive transport, mainly in terms of transport times based on normalised median-value quantities, indicate the simulated system exhibits relatively slow transport velocities.

4.5.3 Evaluation and lessons learned

The developed fracture growth model is simple and essentially based on a minimalistic approach at configuring and constraining a discrete fractured network based on available hydrogeological data. For example, only fractures with PFL measurable flows are used, and are thereafter evaluated against PFL flows at the locations of fractures intersecting boreholes. The main unknown parameters are fracture sizes, which in turn are constrained by the distance between neighbouring boreholes. Internal fracture heterogeneity is also a significant unknown, as the PFL inferred transmissivity is based on using homogenization assumptions, which are likely not fully applicable even for this system consisting of rather sparsely fractured rock.

Here the approach is adopted in a simplified manner, but even so shown to be useful in being able to discard certain aspects of possible simulation configurations and increase the confidence in others. Also, it is shown to be a useful tool in understanding fundamental features of the system, such as the main flow pathways in this localized region seem to be dominated by subsurface recharge rather than surface recharge.

The main drawback with the approach is relatively extensive data sets are required, in terms of multiple boreholes and forcing of the system. Also, features may exist and not be accounted for if not identified by the PFL device, for example due to measurement limits. In particular, very low flows may not be measured, and extremely high flows may be truncated by the upper measurement limit. The lower limit may be of significance for interpreting model performance in terms of retention of transport mechanisms, as then even small flows may be of significance.

Several improvements to the approach would be desirable. In particular, the technical implementation of the fracture growth model used in this analysis is based on fixed geometrical domains surrounding boreholes. As such, it is based on a radial length scale from the borehole locations. It would be preferable to have a more physically-based implementation, such as by extending fractures until their first intersection with neighbouring fractures, i.e. regardless of a fixed radial distance. Also, if fractures are dated by lithology etc, it would be possible to introduce fracture hierarchies, for example by allow younger fractures to truncate at older fractures.

Also, more advanced means of introducing fracture heterogeneity, and especially exerting control over fracture intersections would be useful to further analyse the system in terms of flow directions and flow continuity between boreholes. Here, additional information of the system could also be adopted. For example, incorporating hydraulic testing with packed-off boreholes should provide more detailed information on internal compartmentalization of the model, especially along the vertical extent of the domain.

Further, as a major challenge for inverse modelling and conditioning, improved conditioning and evaluation approaches for hydrogeological vector quantities are needed. Here a manual, trial-based approach is used, where the main focus is on reconfiguring conceptual aspects of the model. Also, comparisons with field data are conducted manually to determine if the model is improved or not. If formal testing or scoring methods are developed, this may enable more efficient and accurate comparisons, enabling an increased number of possible configurations to be tested.

5 Task 7C

5.1 Modelling Approach

5.1.1 Overall approach

The overall aim is to improve the understanding of flow in heterogeneous low-transmissive fractures. The approach adopted is to attempt to constrain parameters which can be used to describe heterogeneity in a fracture plane by comparing simulated flows with field-measured flows.

Specifically, one main objective is to attempt to conduct a hydrogeological characterisation of a single low-transmissive fracture which intersects a vertical ventilation shaft in the Onkalo facility on Olkiluoto Island. Here, the hydrogeological characterisation involves identifying textures and constraining parameters which describe heterogeneity. This is achieved by visually comparing flow distributions obtained from field measurements with corresponding flow distributions obtained from simulations. The simulation cases which are not consistent with field data are determined to be less likely representations of fracture heterogeneity. Thereby, some constraints on the description and parameterisation of fracture heterogeneity may be achieved. That is, one main objective is to obtain constraints on the description and parameterisation of heterogeneity for single, low-transmissive fractures in sparsely fractured crystalline rock, which intersects a relatively large circular shaft with multiple inflow points measured around its circumference.

The heterogeneity parameterisation used is a combination of types of textures and the variability in transmissivity within textures. Also, a sensitivity on parameterisation of transmissivity is considered.

5.1.2 Data usage and interpretation

The main focus has been on using flow measurements acquired from a ventilation shaft, denoted as the Nappy experiments. The Nappy experiments consisted of measuring the inflow for selected fracture traces along the shaft circumference, using absorbing material (disposable diapers) with an approximate 0.2 m support scale, and water was allowed to be absorbed for a time period of 1 minute (Vidstrand et al. 2015). Three fractures in the ventilation shaft KU2 were measured. For the work conducted within Task 7C, measurements from only one of these fractures are considered.

The fracture considered is denoted as Fracture1 in shaft KU2, or FR1-KU2. Visual inspection identifies some heterogeneity in inflow from the fracture trace along the shaft wall (Figure 5-1), where regions are identified as damp, wet, dry (not labelled), and possibly disturbed by cement dust from construction work.

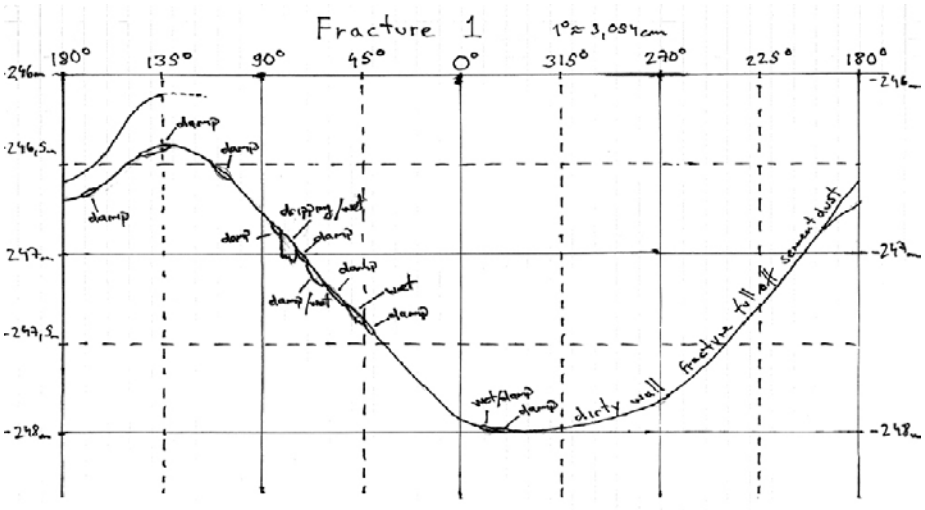

Figure 5-1. *Showing fracture KU2 at its intersection with the shaft, and the observed wet, damp and dry regions. Also showing the regions where cement dust may have filled parts of the fracture void space, thereby potentially reducing flow into the shaft in those regions.*

Prior to the construction of the shaft there have been several boreholes drilled within the region of the shaft circumference (Figure 5-2). These consist of one surface borehole (KR38) and five pilot boreholes (PP122–PP128), all of which are flow-logged with the PFL instrument (Table 5-1). From all these measurements, the geometric mean transmissivity of this fracture is estimated to be about $T = 2.8 \times 10^{-9}$ m^2/s, that is, of the order of magnitude of $T \sim 10^{-9}$ m^2/s, and with some heterogeneity at the scale of the shaft circumference, which is about 3.5 m in diameter. However, it should be noted that PFL flows and hence transmissivities are assumed to have a relatively large-scaled influence zone, and thus represent effective values (Pöllänen and Rouhiainen 2001, Rouhiainen and Sokolnicki 2005).

Flow measurements obtained from the Nappy experiments (Table 5-2) indicate most of the inflow occurs as three peaks in the (corrected bearing) range 270°–320°, with a minor fourth peak in the range 10°–20° (Figure 5-3). The total inflow is about 35 ml/min, and about half of this (17 ml/min) occurs in the range 270°–285°, and about 90% (32 ml/min) in the range 270°–320°.

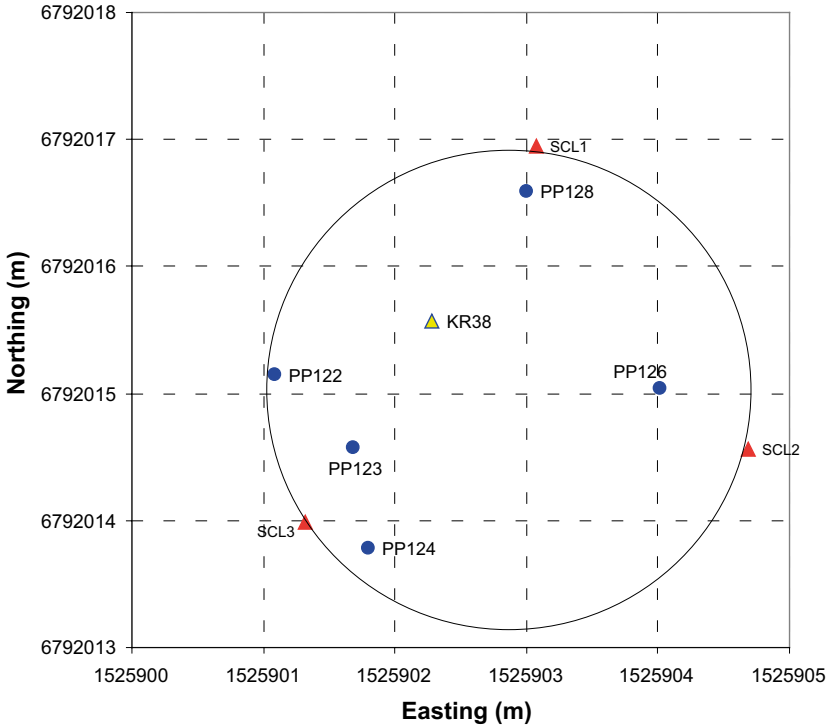

Figure 5-2. *The location of the shaft at the level of intersection with fracture KU2, using the Swedish RT90 coordinate system. Also showing the locations of boreholes drilled prior to shaft sinking. Pilot boreholes are denoted as PP, and the surface core-drilled borehole is denoted as KR. The plane of intersection corresponds to a low transmissive fracture denoted as KU2, located at depth z = –247 m. The shaft is about 3.5 m in diameter.*

Table 5-1. Flow and inferred transmissivity obtained from PFL measurements in surface borehole KR38 and five pilot boreholes at the location of fracture KU2 prior to shaft sinking.

Borehole	Depth (m.a.s.l.)	Drawdown (m)	Flow (ml/h)	Transmissivity (m^2/s)
KR38				1.2E–08
PP124	–247.49	187.09	2,870	4.2E–09
PP123	–247.49	187.09	961	1.4E–09
PP122	–247.39	187.09	996	1.5E–09
PP126	–248.69	187.09	2,930	4.3E–09
PP128	–248.59	187.09	761	1.1E–09
Geometric mean				2.8E–09

Table 5-2. Field data obtained from the 'Nappy experiments', showing measured inflow seepage rates across the internal circumference of the shaft wall at the location of the fracture intersection. Note the resolution of each measurement is about 4°, which corresponds to about 0.2 m. Each measurement was conducted over a time period of 1 minute.

Fracture Flow (ml/min)	Mapped Level (m.a.s.l.)	Mapped Bearing (degrees)	Corrected Level (m.a.s.l.)	Corrected Bearing (degrees)
1.78	–248.00	349°–346°	–249.09	11°–14°
0.50	–248.00	346°–342°	–249.09	14°–18°
0.20	–248.00	342°–338°	–249.09	18°–22°
0.15	–246.70	170°–166°	–247.79	190°–194°
0.20	–246.45	143°–139°	–247.54	217°–221°
0.30	–246.40	139°–135°	–247.49	221°–225°
0.35	–246.40	135°–131°	–247.49	225°–229°
0.35	–246.55	110°–107°	–247.64	250°–253°
1.00	–246.85	86°–83°	–247.94	274°–277°
7.35	–246.90	83°–79°	–247.99	277°–281°
8.20	–246.95	79°–75°	–248.04	281°–285°
0.30	–247.00	74°–70°	–248.09	286°–290°
2.50	–247.05	70°–66°	–248.14	290°–294°
2.00	–247.10	66°–62°	–248.19	294°–298°
0.25	–247.15	62°–58°	–248.24	298°–302°
0.55	–247.20	58°–55°	–248.29	302°–305°
0.50	–247.30	55°–51°	–248.39	305°–309°
3.10	–247.30	51°–48°	–248.39	309°–312°
4.40	–247.40	48°–45°	–248.49	312°–315°
0.90	–247.40	45°–42°	–248.49	315°–318°
0.35	–247.45	42°–39°	–248.54	318°–321°

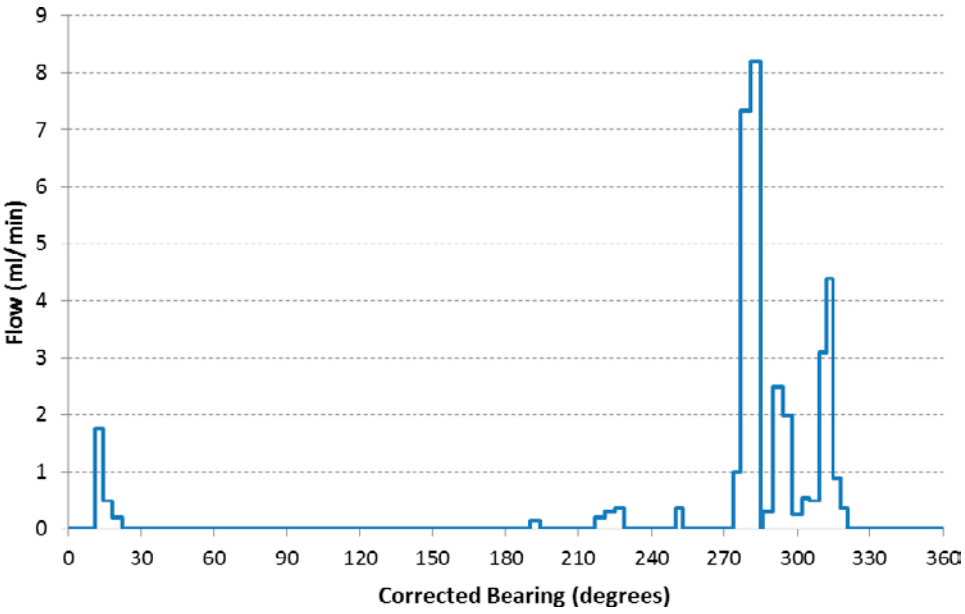

Figure 5-3. *Fracture inflow in FR1-KU2 along shaft circumference obtained from the Nappy experiments (cf. Table 5-2). Most of the inflow occurs along the western side, in the range 270°–320°.*

5.2 Conceptual Model

5.2.1 Main assumptions and simplifications

The main underlying assumption for the conceptual model is that fractures are expected to have rough surfaces and therefore have variability in hydraulic properties (transmissivity, hydraulic conductivity or aperture). The general assumption of variability is supported from field data obtained from the Olkiluoto site characterisation programme, mainly based on observed variability in transmissivity obtained from in situ PFL measurements. There is also a commonly accepted notion that fractures have significant internal heterogeneity, based on general experience, as for example gained from the Äspö TRUE experiments (Dershowitz et al. 2003, Cvetkovic et al. 2007).

As previously noted, even though there is only minor variability based on transmissivity obtained from the PFL in the shaft region (Table 5-1), this can be expected since the instrument measures larger scale effective transmissivities.

In order to study the effects of fracture heterogeneity, suitable models for heterogeneity structures are required. In this work, three correlation structures are considered, following the approach used by Zinn and Harvey (2003) and represented as

- an assigned isotropic Gaussian variogram texture, denoted as a Multi-Gaussian (MG) field;
- a non-Gaussian texture with connected low permeable zones, denoted as a Disconnected (DN) field; and
- a non-Gaussian texture with connected high permeable zones, denoted as a Connected (CN) field (an inverse to the DN field).

Furthermore, each texture (field) is described by assigning a variability class, which is described by the variance of the natural logarithm of transmissivity. If the natural logarithm of transmissivity is $Y = \mathrm{Ln}(T)$, then values selected for $\mathrm{Var}(Y) = 1$, 4, and 8, which correspond to low, moderate, and high variability in transmissivity respectively. Note also the Disconnected and Connected fields are complementary to each other.

Water flow q (L/T) is obtained from the hydraulic head gradients dh/dx and dh/dy by assigning a power-law parameterisation for aperture b (L),

$$q_x = c_{0n}\left(b^{m-1}(x,y)\frac{\partial h}{\partial x}\right) \quad and \quad q_y = c_{0n}\left(b^{m-1}(x,y)\frac{\partial h}{\partial y}\right) \qquad \text{Equation 5-1}$$

where c_0 (L^{2-m}/T) is a constant, with units depending on the power exponent m. Integrating q over the cross-sectional area of flow, which for fractures corresponds to a width w and aperture b, results in volumetric flow Q (L^3/T). The familiar form of Darcy's law is obtained by relating transmissivity to aperture as $T = c_{0m}\, b^m$. This type of formulation is particularly convenient when investigating transport since aperture is accounted for, and the exponent m can be used to define, for example, the cubic or quadratic flow laws. However, the current analysis is focused on flow and flow variability rather than transport.

The numerical value of c_0 is related to effective hydraulic properties (transmissivity) of the media, and heterogeneity is implemented by varying the numerical value of aperture b. A sensitivity on parameterisation of transmissivity from field data is made through decreasing the effective transmissity by 2/3 (see parameter descriptions below).

A correlation length assumption is required, which is in this work set to 0.5 m.

The combination of three textures, three modes of variability and two transmissivity parameterisation sensitivity cases results in 18 simulation cases for a given fracture. In addition, both single and multiple realisations are conducted. Comparison with the field-measured flow rates are only done for arbitrarily selected realisations. Empirical probability distributions (histograms) and sample statistics are provided based on the sample ensemble of realisations.

5.2.2 Geometrical description

A single planar two-dimensional fracture is considered, represented as a square with side length 32 m (Figure 5-4). The effective (mean) fracture transmissivity is set to 4.2×10^{-9} m^2/s for the base case. Several configurations are adopted for representing the internal fracture variability in terms hydraulic properties (aperture and hence transmissivity). A circular shaft is imposed in the centre with radius 1.75 m from the origin, and is assigned a prescribed hydraulic head as an internal boundary condition (see Section 5.2.4).

5.2.3 Processes considered

Fluid properties are that of fresh water with constant density. Steady-state conditions are assumed throughout, that is, the initial transient responses during pumping of boreholes are ignored. Thus possible processes such as saltwater intrusion and density-dependent effects in the fracture plane are not considered.

Here, internal fracture variability is explicitly accounted for based on assumed structural models of heterogeneity.

Possible sealing effects due to the cement dust on the shaft wall and acting as a grouting material in the fracture in the immediate proximity to the shaft are only briefly considered in an extension to the main study (Section 5.4.6 below). The visible occurrence of cement dust is due to construction work and grouting activities performed above the current location in the shaft, and may inadvertently play a role as infill material sealing the fracture close to the shaft wall. This may cause the natural inflow distribution to be altered and as such may bias the measurements. It should be noted that no measured inflow occurs for the sections of the fracture circumference where cement dust is visible on the shaft wall.

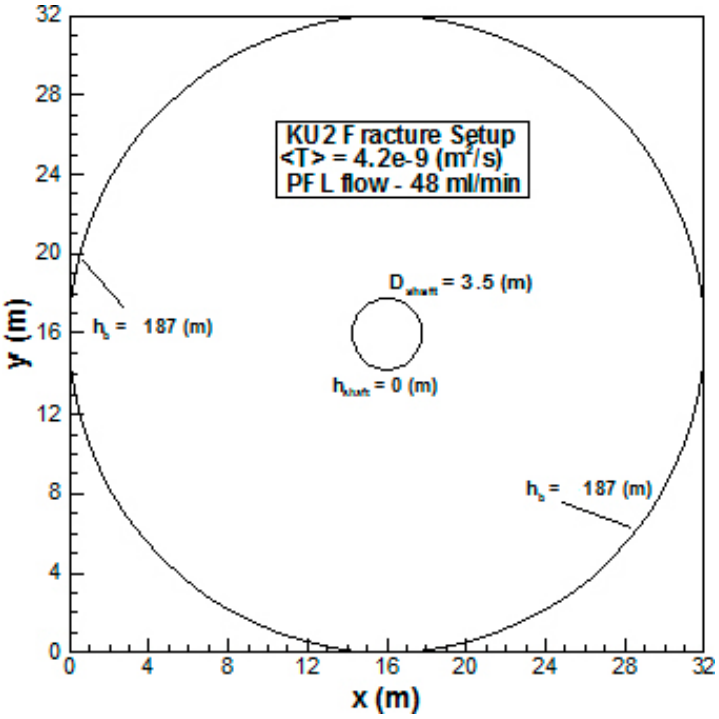

Figure 5-4. *Illustration of the computational setup for the fracture KU2. Showing the fracture surface with assigned mean transmissivity of 4.2×10^{-9} m^2/s. The open shaft is assigned a constant head value of h = 0 m representing atmospheric conditions, with an internal diameter of 3.5 m (small circle). The outer constant pressure boundary is assigned a head value h = 187 m at a radius of 16 m from the centre (large circle).*

5.2.4 Boundary and initial conditions

Boundary conditions are assigned as follows. A radial pressure gradient is imposed between the shaft centre and the outer rim of the fracture. A head value of 187 m is assigned at a radial distance of 16 m from the origin, which represents the outer boundary of the fracture. A head of 0 m is imposed at a radial distance of 1.75 m from the origin, which corresponds to the shaft wall.

As steady-state conditions are assumed, no initial conditions are needed.

5.3 Model Implementation

5.3.1 Numerical model

In this section, an adaptive multi-resolution Fup methodology suitable for many groundwater flow and transport problems is used and will be briefly presented in the following sections. A detailed description is given in the related papers (Gotovac et al. 2007, 2009a, b).

Fup transformations

Fup transformations are versatile tools for the description of heterogeneity, pumping or recharge, as well as all other flow and transport variables that consist of different spatial and/or temporal scales. Firstly, we present here the *Fup Collocation Transform* (FCT), which is an efficient numerical tool for describing various types of data, signals and functions using a linear combination of the Fup basis functions (Gotovac et al. 2007). The main feature of the FCT is that specific frequencies and corresponding Fup coefficients are associated with a particular resolution level and spatial location, which is not possible in the classic discrete Fourier transform. The zero level is the starting (coarsest) level, which is always present in the grid (Figure 5-6). The FCT satisfies function values at all collocation points and related derivatives at boundary collocation points. The key step in the FCT is the transfer from the current level to the next level. The residual between the true function and the previous level approximation is checked and the points with a residual below the prescribed threshold are dropped from the grid. This procedure presents an a-priori adaptive criterion for defining the new collocation points at the next level. For the first and each subsequent level, the collocation algorithm should only satisfy the residual between the true function and its approximation from the previous levels. In other words, all Fup coefficients from previous levels are "frozen" and only Fup coefficients at the current level should be found. Higher levels include only higher frequencies and provide a more detailed description of the chosen function.

The multi-resolution 2-D FCT of the function *u(x,y)* can be presented as

$$u^J(x,y) = \sum_{j=0}^{J} \sum_{k,l \in Z^j} d_{k,l}^j \varphi_{k,l}^j(x,y) \qquad \text{(Eq. 5-2)}$$

where J is an arbitrary chosen maximum level, Z^j is the irregular grid at each level, which contains only the significant collocation points and Fup basis functions needed for the Fup presentation in (Eq 5-2) with the desired accuracy defined by the threshold ε, $d_{k,l}^j$ are Fup coefficients, $\varphi_{k,l}^j$ are Fup basis functions and k and l represent the indexes of collocation points at the current level for the x and y directions, respectively. The zero level is defined by a chosen resolution level j_{minx} for the x-direction and by j_{miny} for the y-direction. Generally, a sparse linear system of equations can be obtained at each level j

$$\sum_{k,l \in Z^j} d_{k,l}^j \varphi_{k,l}^j(x_p^j, y_q^j) = \Delta_j(x_p^j, y_q^j), \qquad \text{(Eq. 5-3)}$$
$$p,q \in Z^j : 0 \le p \le 2^{j_{\min x}+j}, 0 \le q \le 2^{j_{\min y}+j}$$

$$\sum_{k,l \in Z^j} d_{k,l}^j \varphi_{k,l}^{j\,(m_x,m_y)}(x_p^j, y_q^j) = \Delta_j^{(m_x,m_y)}(x_p^j, y_q^j), \qquad \text{(Eq. 5-4)}$$
$$p,q \in Z^j : (p = 0 \ or \ p = 2^{j_{\min x}+j}$$
$$or \ q = 0 \ or \ q = 2^{j_{\min y}+j})$$
$$and \quad (m_x > 0 \ or \ m_y > 0)$$

where m_x and m_y are the orders of the derivative in the x and y directions, respectively. The system (Eq. 5.3–5.4) presents conditions for satisfying function values within the domain (Eq. 5-3) and partial derivatives at the boundary points (Eq. 5-4). The residual vector on the right side presents the residual between the real function and its approximation, including all previous levels.

The main drawback of the FCT is the solving of the sparse linear system of equations at each level (Eq. 5-3–5-4). The *Fup Regularized Transform* (FRT) has the same purpose and uses the exact same adaptive strategy as the FCT, but directly connects function or data values with Fup coefficients (without solving the system Eq. 5-3–5-4), using at each collocation point the local equivalence between the Fup and a polynomial approximation (Gotovac et al. 2009a). Therefore, FRT exactly describes polynomials up to the Fup order. FCT requires a slightly less number of collocation points than FRT for a general function. One possible application of the FCT and FRT is presented on Figure 5-4 in order to describe complex heterogeneous log-transmissivity field.

Adaptive Fup Collocation Method

The *Adaptive Fup Collocation Method* (AFCM) suitable for solving an initial-boundary value problem can be divided into the three main parts:

- Spatial grid adaptation.
- Calculation of spatial derivatives.
- Time integration.

The spatial adaptive procedure is performed after each time step according to the presented FCT and the corresponding adaptive strategy. This procedure dynamically changes the grid and significantly reduces computational cost. A solution from the initial conditions or previous time step is described by FCT. All FCT points are called basic points since they create the basic grid. Apart from basic points (which are related to the FCT a-priori adaptive criterion), additional points are needed for consistent approximation of the system dynamics (temporal solution changes) during the calculated adaptive time step, Δt. Basic and additional points create the total grid needed for the description of the system dynamics from time T to time $T + \Delta t$. The basic hypothesis behind the algorithm (during the time step Δt) is that the solution does not "move" outside the border of the adapted non–uniform grid. Finally, the total grid needs to be transformed into an effective grid suitable for time integration.

Time integration is obtained by solving a system of differential-algebraic equations where time-dependent partial differential equations describe the time evolution of the solution, while the algebraic equations present the boundary conditions (Dirichlet, Neumann or Chauchy mixed type).

The particular possible application of the AFCM (Gotovac et al. 2009a, b) solves the flow problem (Eq. 5-1) with only Fup basis functions at each level using the collocation framework and an adaptive strategy similar to the FCT in the following way

$$\sum_{k,l\in Z^j} d_{k,l}^j \left(\frac{\partial^2 \varphi_{k,l}^j\left(x_p^j, y_q^j\right)}{\partial x^2} + \frac{\partial^2 \varphi_{k,l}^j\left(x_p^j, y_q^j\right)}{\partial y^2} \right) +$$
$$\frac{\partial Y\left(x_p^j, y_q^j\right)}{\partial x} \left(\sum_{k,l\in Z^j} d_{k,l}^j \frac{\partial \varphi_{k,l}^j\left(x_p^j, y_q^j\right)}{\partial x} \right) +$$
$$\frac{\partial Y\left(x_p^j, y_q^j\right)}{\partial y} \left(\sum_{k,l\in Z^j} d_{k,l}^j \frac{\partial \varphi_{k,l}^j\left(x_p^j, y_q^j\right)}{\partial y} \right) = \quad \text{(Eq. 5-5)}$$
$$\Delta_j\left(x_p^j, y_q^j\right): 0 \le p \le 2^{j_{\min x}+j},$$
$$0 \le q \le 2^{j_{\min y}+j}, p, q \in Z^j$$

$$\sum_{k,l\in Z^j} d_{k,l}^j \varphi_{k,l}^j(x_p^j, y_q^j) = \Delta_j^{(n_x,n_y)}(x_p^j, y_q^j) : \quad \text{(Eq. 5-6)}$$
$$(p = 0 \ \ or \ \ p = 2^{j_{\min x}+j}, p, q \in Z^j)$$

$$\sum_{k,l\in Z^j} d_{k,l}^j \frac{\partial \varphi_{k,l}^j(x_p^j, y_q^j)}{\partial y} = \Delta_j^{(n_x,n_y)}(x_p^j, y_q^j) : \quad \text{(Eq. 5-7)}$$

$$(q = 0 \ \ or \ q = 2^{j_{\min y}+j}, p, q \in Z^j)$$

for a given FRT approximation of the log-conductivity field *Y*. Each non-zero level solves only the residual of the flow equation and corresponding boundary conditions from all previous levels ("frozen" Fup coefficients) and gives particular head corrections (Fup coefficients at the current level). The adaptive criterion adds new collocation points in the next level only in the zones where the head correction is greater than the prescribed threshold.

Adaptive Fup Monte-Carlo Method

The *Adaptive Fup Monte Carlo Method* (AFMCM) (Gotovac et al. 2009a, b) follows the Eulerian-Lagrangian formulation, separates the flow from the transport problem. The flow chart of the AFMCM, which represents a general framework for flow and transport in heterogeneous porous media is presented in Figures 5-5 and 5-6.

AFMCM uses the random field generator HYDRO_GEN (Bellin and Rubin 1996) for step 1 due to its accuracy and generality. Log-conductivity approximation (step 2) is solved by FRT, reproducing very accurately prescribed ensemble statistics (Figure 5-7). Step 3 uses an AFCM for the differential flow equation (3) in order to get an accurate and continuous velocity field in each realization. The positions of particles and related travel times are calculated with a new particle-tracking strategy (step 4) using the high-order Runge-Kutta-Verner (8-5:6) time integration scheme and FRT. In that way, travel time and transverse displacement fields are described as continuous functions with prescribed accuracy. Finally, it is possible to extract an unlimited or desired number of particles from these solutions in order to eliminate statistical fluctuations in ensemble statistics. Ensemble statistics are described in a multi-resolution way (Eq. 5-2) as all other mentioned fields in each realization (step 6). All mentioned MC methodology steps are detailed in Gotovac et al. (2009b).

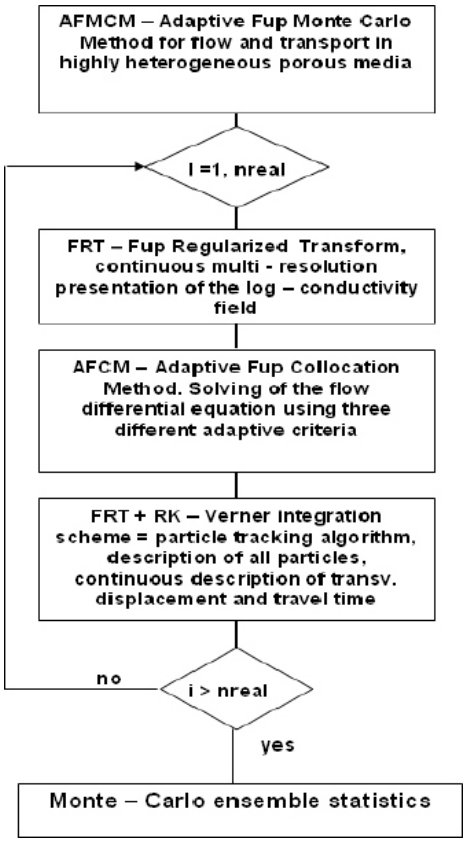

Figure 5-5. *Flow chart of the AFMCM (Gotovac et al. 2009a, b).*

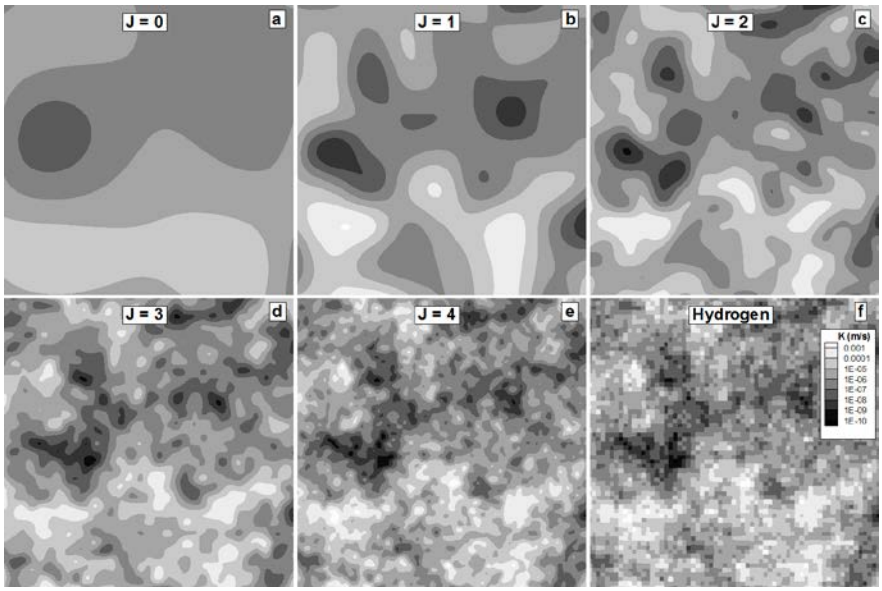

Figure 5-6. *Heterogeneity field described with analytical basis functions to arbitrary degree, which allows for accurate solution of the flow field and pathways. From Gotovac (2009).*

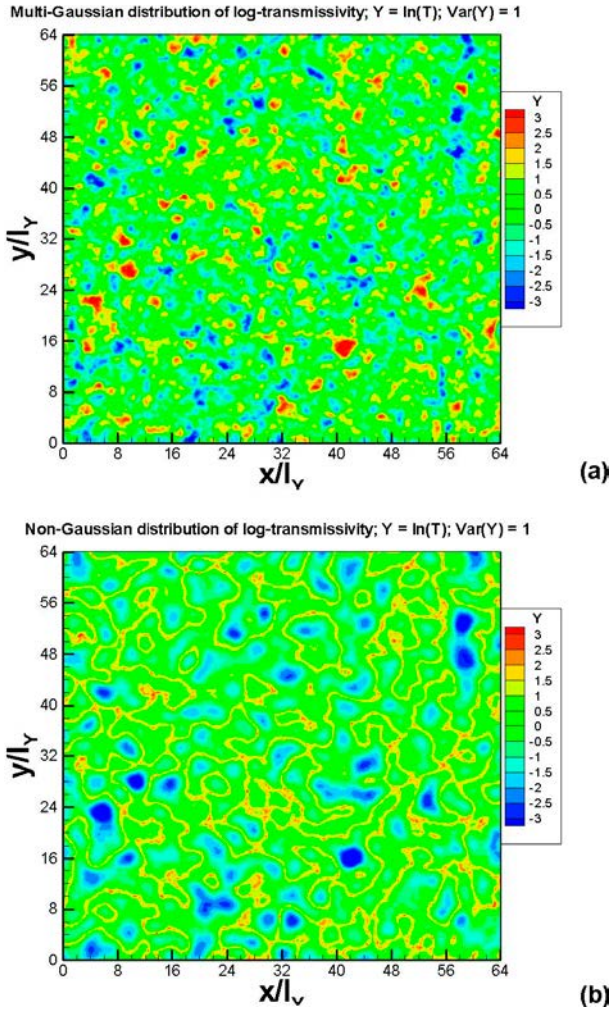

Figure 5-7. *Micro-structural models used to obtain various porous media textures, which in turn are used to represent internal heterogeneity of the fracture surface. Coloured by Y = ln(T) where red indicates a high transmissivity value and blue indicates a low transmissivity value. (a) Multi-Gaussian field with Var(Y) = 1. (b) Non-Gaussian field with Var(Y) = 1 and correlation between high transmissivity values, denoted as a 'connected' texture.*

5.3.2 Parameters

The parameters used in this study are related to the descriptions of fracture heterogeneity. These are listed as follows (cf. Figure 5-7):

- Texture type: Multi-Gaussian (MG), Connected (CN), Disconnected (DN).
- Variability in log-transmissivity $Y = \mathrm{Ln}(T)$: $\mathrm{Var}(Y) = 1, 4, 8$.
- Transmissivity parameterisation sensitivity; base case mean T from data (denoted as $n = 2$), and decreased mean T by 2/3 (denoted as $n = 3$).
- Correlation length (constant): 0.5 m.

5.3.3 Model conditioning and calibration

No formal conditioning or calibration procedure is adopted. Instead, the procedure adopted is to conduct a sensitivity analysis of the influence of heterogeneity models combined with parameterisation of variability in transmissivity, that is to study the influence of structure and variability in fracture heterogeneity, with respect to flow variability along the shaft wall, inferred from comparisons between field experiments and numerical simulations.

For single realisations, the flow distribution entering the shaft from the fracture obtained from simulations is compared with the distribution of field measured inflows. For multiple realisations, statistics of the simulated field measured flow distributions are presented.

5.4 Results

The main results are presented in terms of flow entering the shaft. These are first shown for single realisations which are compared with the field measured inflows obtained from the Nappy experiments. Here, the comparisons are conducted with arbitrarily selected realisations, and provide a rough visual impression of how the inflow distribution tend to behave. The comparisons of simulated inflows should not be expected to match the locations of field measured inflows. Instead, the overall shape of the inflow distribution, with magnitude and frequency of inflow peaks, as well as the total inflow, may be compared with the measurements. For multiple realisations, the full empirical probability distributions of simulated inflows are provided. Here, the respective simulation cases are compared with each other.

In addition, illustrations of the hydraulic head field and flow pathways are provided. Also, the distribution of transport parameters and resulting correlation lengths obtained from simulations are shown for selected simulation cases.

5.4.1 Pressure fields and pathways

For a homogenous fracture (not shown), the hydraulic head field for the selected configuration of boundary conditions (cf. Section 5.2.4 and Figure 5-4) would result in smooth, logarithmically-spaced concentric circles, forming a typical cone of depression. For the case of low variability, i.e. $\mathrm{Var}(Y) = 1$, the resulting head field is similar, however forming slightly irregular and semi-concentric circles, due to the minor heterogeneity (Figure 5-8a). For high variability, i.e. $\mathrm{Var}(Y) = 8$, the head field is significantly altered due to the heterogeneity (Figure 5-8b). Similar images are obtained regardless of texture, i.e. also for the Connected and Disconnected fields (not shown).

In order to visualise flow pathways, particle tracking is adopted. Here, particles are injected evenly around the circumference of the fracture, i.e. along the location of the outer constant head boundary, and are terminated upon arrival at the shaft, i.e. the inner circle and inner constant head boundary. Thus the streamline flow density is proportional to the plotted line density (Figure 5-9). The low variability case results in relatively evenly distributed streamline densities and smooth pathways (Figure 5-9a), whereas the high variability case results in relatively tortuous pathways (Figure 5-9b). For this realisation, the high variability case results in about four dominant pathways. Similar images are obtained regardless of texture, i.e. also for the Connected and Disconnected fields (not shown).

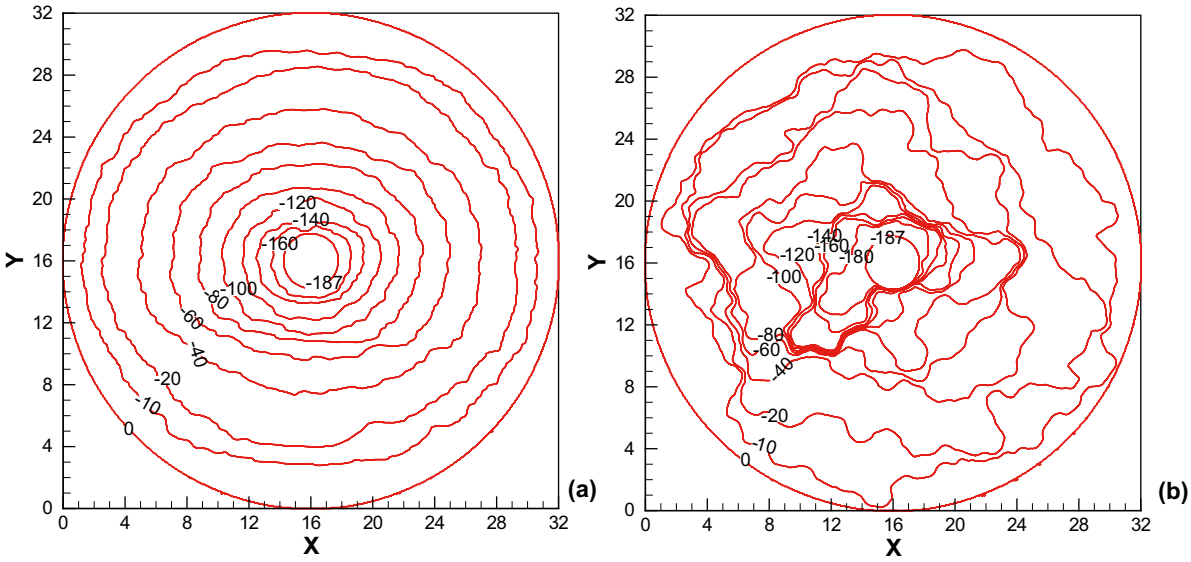

Figure 5-8. *Showing contours of equal head values for the resulting head distribution in the fracture plane for the case of a Multi-Gaussian texture with (a) Var(Y) = 1 and (b) Var(Y) = 8. The inner circle represents the shaft and the outer circle represents the location of the constant head boundary.*

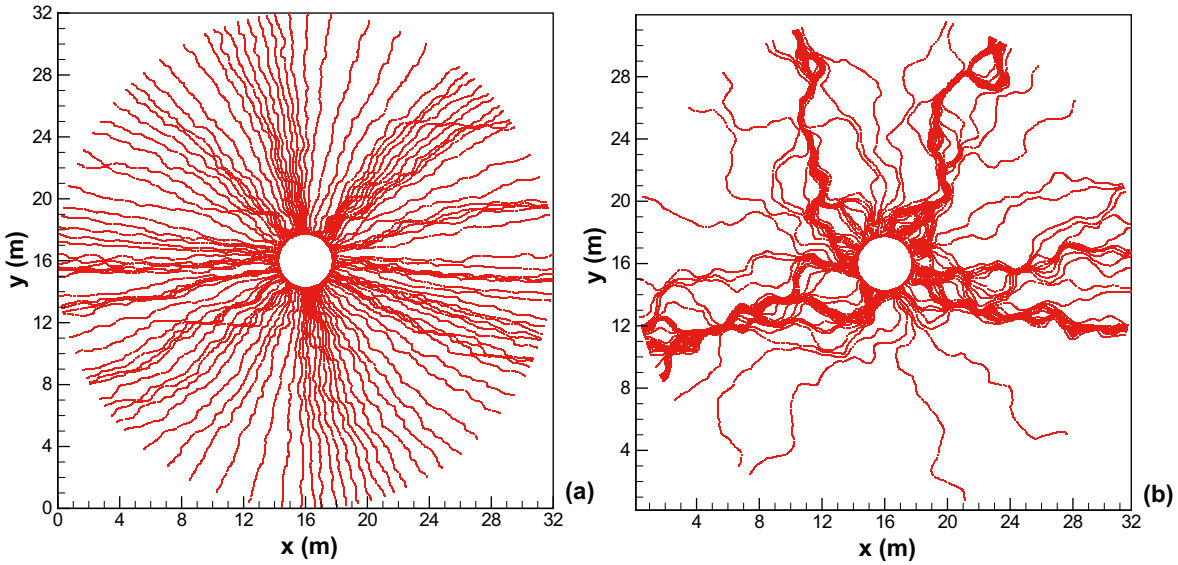

Figure 5-9. *Showing resulting streamline distribution in the fracture plane for the case of a Multi-Gaussian texture with (a) Var(Y) = 1 and (b) Var(Y) = 8. The streamline density is proportional to the plotted line density. Particles are injected along the location of the constant head boundary and are terminated upon arrival at the shaft (inner circle).*

5.4.2 Inflow distributions for single realisations

The resulting inflow distributions along the shaft circumference for several simulation cases and arbitrarily selected single realisations are shown in Figure 5-10, Figure 5-11, and Figure 5-12. For the case of a Multi-Gaussian texture (Figure 5-10), only the case of high variability (Var(Y) = 8) can create sufficiently high inflow peaks, however does not seem to capture the variability in terms of multiple-peaks sufficiently well, and generally over-estimates the total measurable inflow. The lower variability cases (Var(Y) = 1 and 4) have a relatively smooth distribution of inflows, and generally over-estimate total measurable inflow.

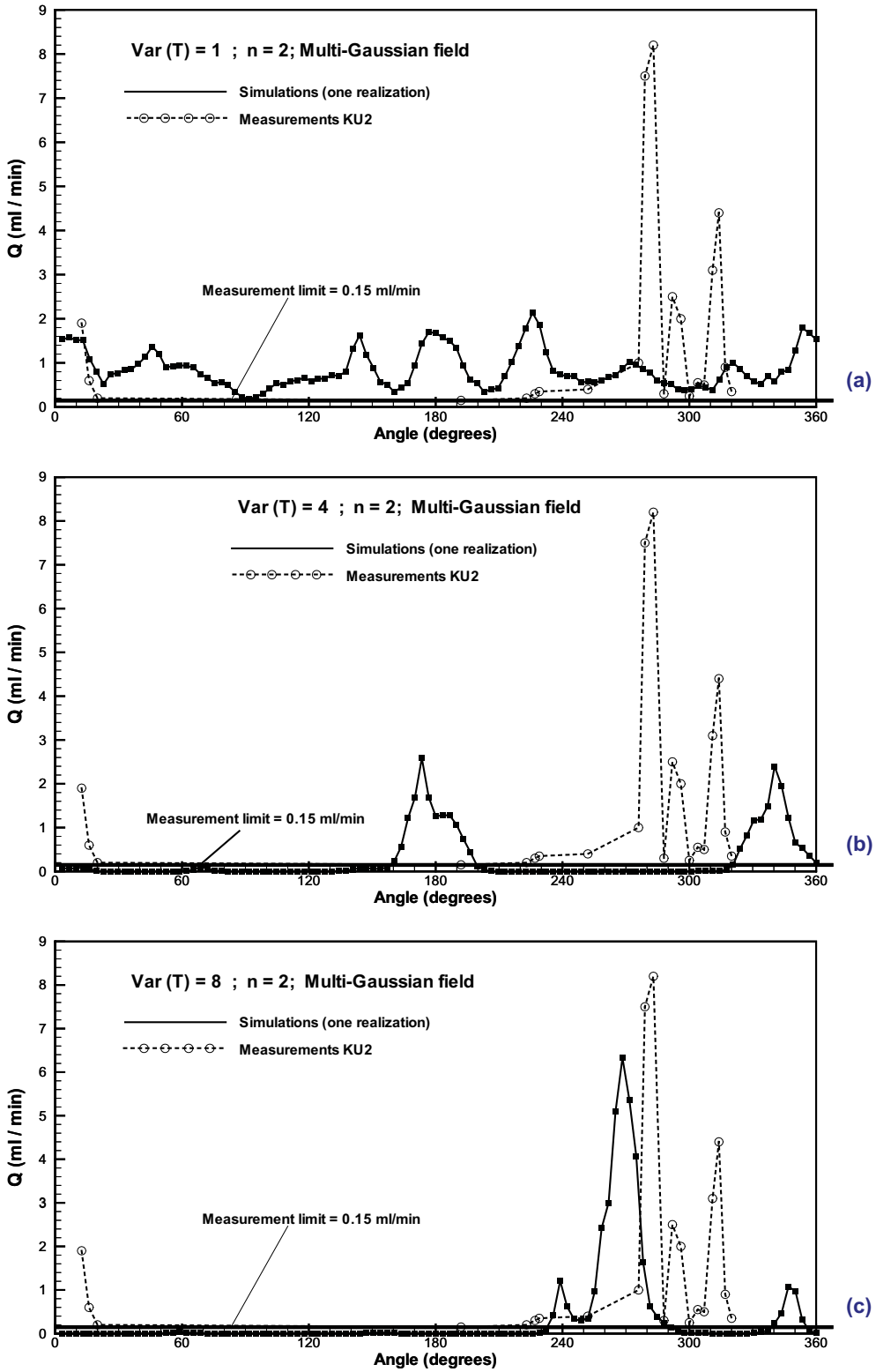

Figure 5-10. *The flow distribution around the shaft for the base case. Comparing field measured data (dotted line with open circles) with simulation results (solid line) for the case of a Multi-Gaussian texture and with (a) low variability Var(Y) = 1, (b) moderate variability Var(Y) = 4, and (c) high variability Var(Y) = 8. The measurement limit for flow is shown as a solid horizontal line.*

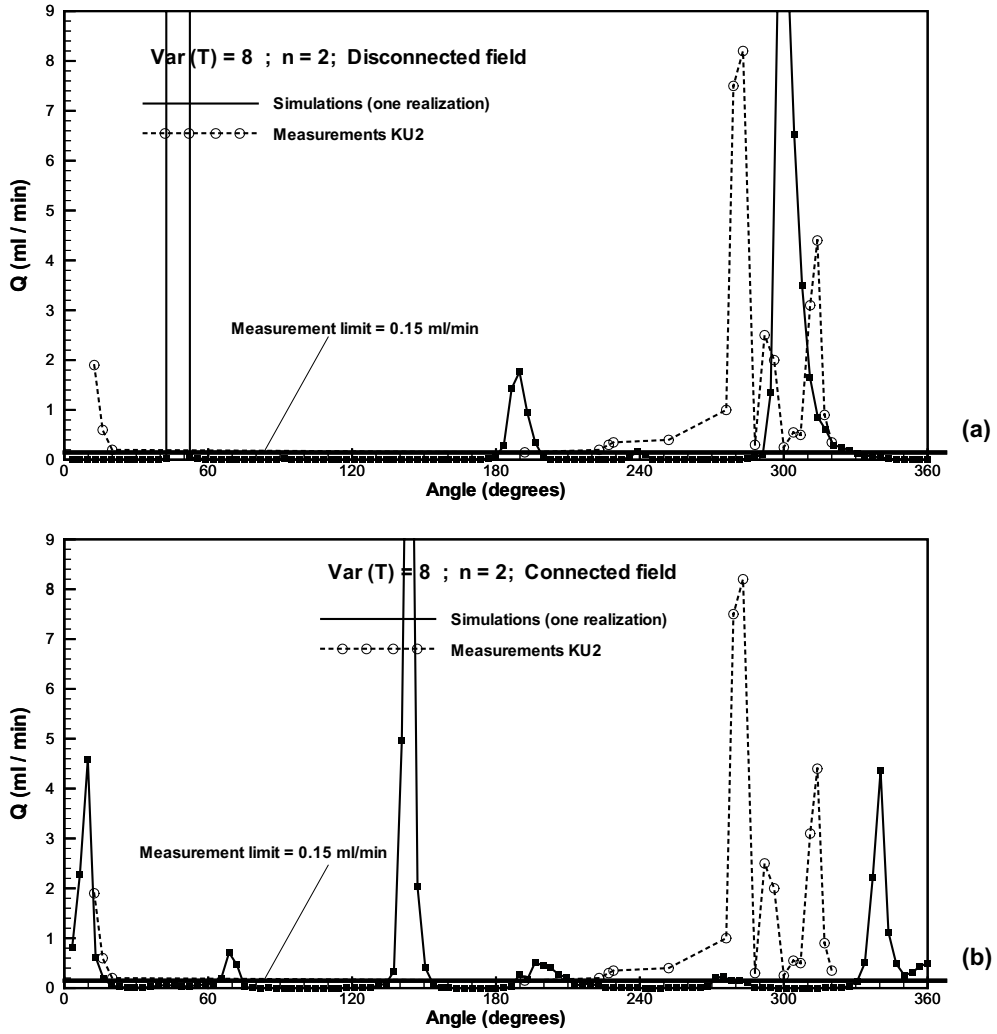

Figure 5-11. *The flow distribution around the shaft for the base case. Comparing field measured data (dotted line with open circles) with simulation results (solid line) and with high variability Var(Y) = 8, for the case of a (a) Disconnected texture and a (b) Connected texture.*

The case of a Disconnected and a Connected texture with high variability (Figure 5-11a and Figure 5-11b respectively) have distinct sharp peaks, consistent with the shaft inflow measurements. The Disconnected case results in a few number of very distinct peaks. The Connected case also results in a few large-inflow peaks, but seems to have a slightly greater number of small-inflow peaks.

The sensitivity case with decreased effective transmissivity (n = 3) with high variability (Var(Y) = 8) for all the three textures are shown in Figure 5-12. Since these are single realisations, differences are not discernable. The Multi-Gaussian texture has a few large inflow peaks, but may not have sufficient small-inflow variability. The Disconnected texture has several inflow peaks, and the small-inflow peaks are greater in flow magnitude and distribution. The Connected texture however maintains several distinct peaks, a few large inflows as well as several minor inflows.

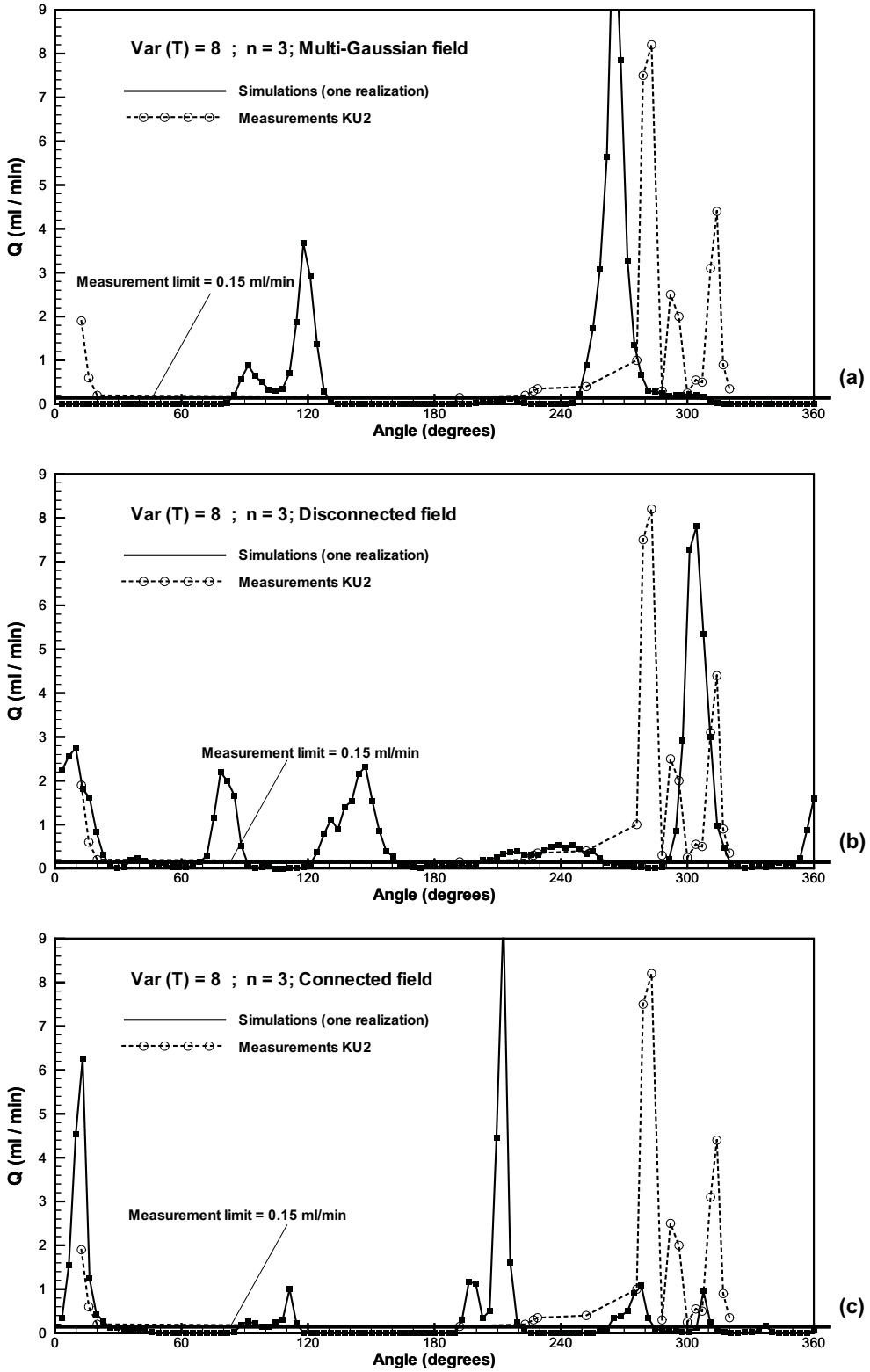

Figure 5-12. *The flow distribution around the shaft for the lower T sensitivity case. Comparing field measured data (dotted line with open circles) with simulation results (solid line) and with high variability Var(Y) = 8, for the case of (a) a Multi-Gaussian texture, (b) a Disconnected texture and (c) a Connected texture.*

5.4.3 Inflow distributions for multiple realisations

Multiple realisations of each case are also conducted and presented in terms of the resulting empirical probability distribution (histogram) of inflow to the shaft (Figure 5-13). As the field measured flows are insufficient to plot a reasonable histogram, only the lower measurement limit is shown (vertical line).

The case of a Multi-Gaussian texture assuming the field-inferred transmissivity (i.e. base case mean T; $n = 2$) for all three variability cases is shown in Figure 5-13a. Generally, as variability Var(Y) increases, the distribution of flows becomes more distinct, with a greater density of small flows.

The behaviour is similar for the lower transmissivity sensitivity case ($n = 3$) (Figure 5-13b), however with a slower transition. For example, there are more pronounced peaks for the base cases than for the lower T cases, which is particularly evident for the low variability case of Var(Y) = 1.

In Figure 5-13c, a comparison of the distribution is made for the three textures, assuming the high variability case. Whereas there is only a minor difference in the distributions, the Disconnected texture has a slightly larger density of low flows, and the Connected texture has a slightly smaller density of low flows (below the measurement limit threshold).

5.4.4 Distributions of transport parameters for multiple realisations

Both travel times and β-parameter (F-factor) values are calculated from particle tracking for each simulation case. Results from multiple realisations are presented in terms of the empirical probability distribution (histogram) of the β-parameter in Figure 5-14. As this is not measured, no comparison with field data is possible.

The case of a Multi-Gaussian texture assuming the quadratic flow law for all three variability cases is shown in Figure 5-14a. Generally, as variability Var(Y) increases, the peak of the distribution of β is shifted to lower values. Similar behaviour is evident for the case of a cubic flow law (Figure 5-14b), however with more pronounced peaks, that is, the densities for corresponding values are greater in magnitude.

In Figure 5-14c, a comparison of the distribution is made for the three textures, assuming the high variability case and quadratic flow law. There is a significant difference in the distribution obtained from the Connected and Disconnected textures, where the Connected texture has a high density of low values, and the Disconnected texture has a very low density of low values. Also, the Disconnected texture results in a relatively uniform distribution over a broad range of β values. The Multi-Gaussian texture also results in a much lower density of small β values compared to the Connected texture, but exhibits a distinguished peak.

5.4.5 Resulting correlation distances for flow

The resulting correlation distances for selected cases are shown in Figure 5-15. All correlation is vanished, i.e. the correlation approaches zero, within about 0.8 m for all cases. The correlation behaviour in terms of flow is similar for all cases. A large-scale ‘dip effect’ is also apparent for larger distances, and with values oscillating about zero. For comparison, a log-normal distribution for correlation is also plotted, which approached zero at a distance of 1 m.

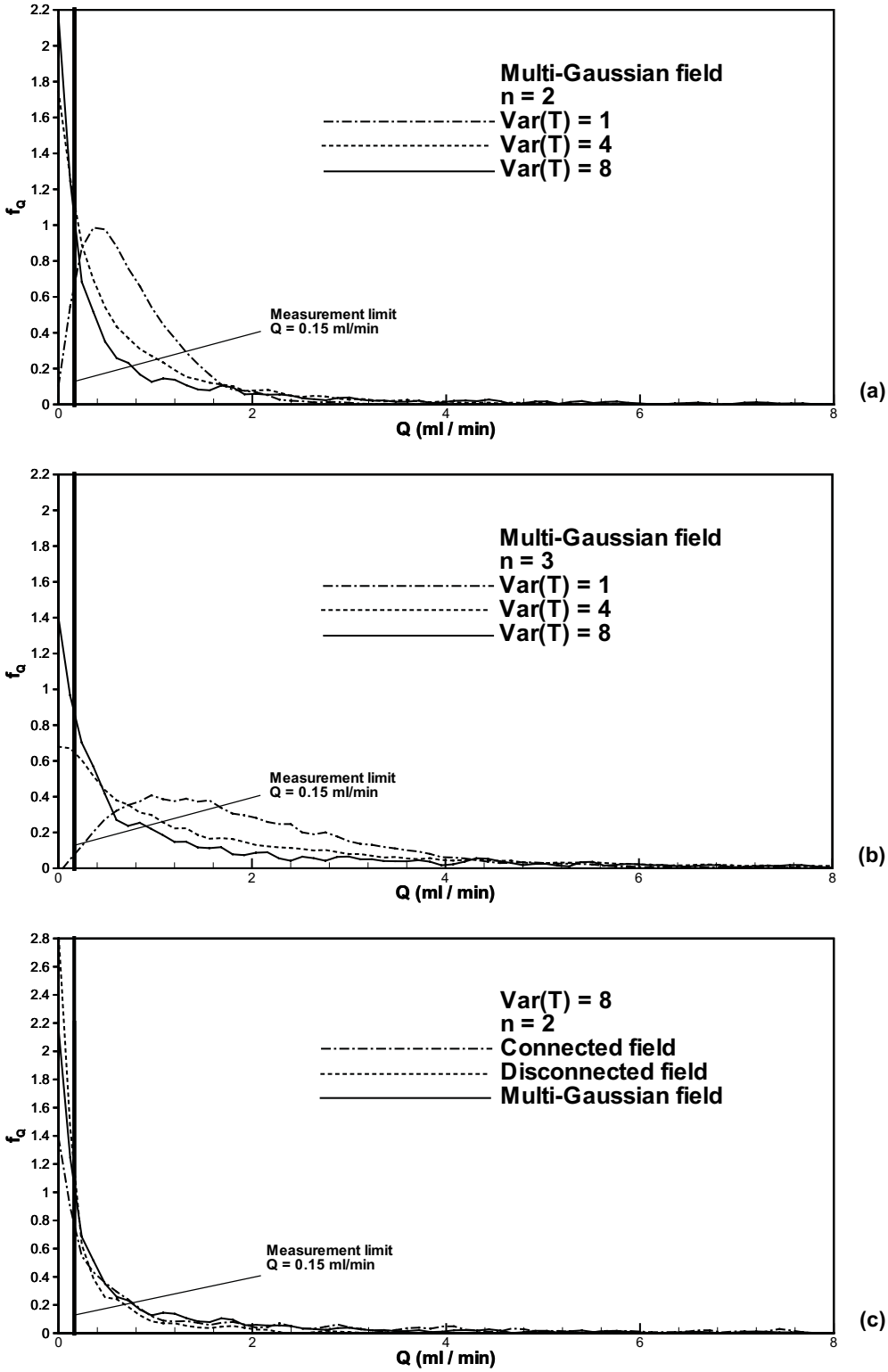

Figure 5-13. *The resulting probability density distribution of flows entering the shaft from multiple realisations of various simulation cases (n = 2 indicates base case T; n = 3 indicates reduced T). The measurement limit of field data is marked as a vertical line. (a) Comparing the three variability cases (Var(Y) = 1, 4, 8) for the Multi-Gaussian texture. (b) Comparing the three variability cases (Var(Y) = 1, 4, 8) for the Muli-Gaussian texture. (c) Comparing the three textures (CN, DC, MG) for the high variability (Var(Y) = 8).*

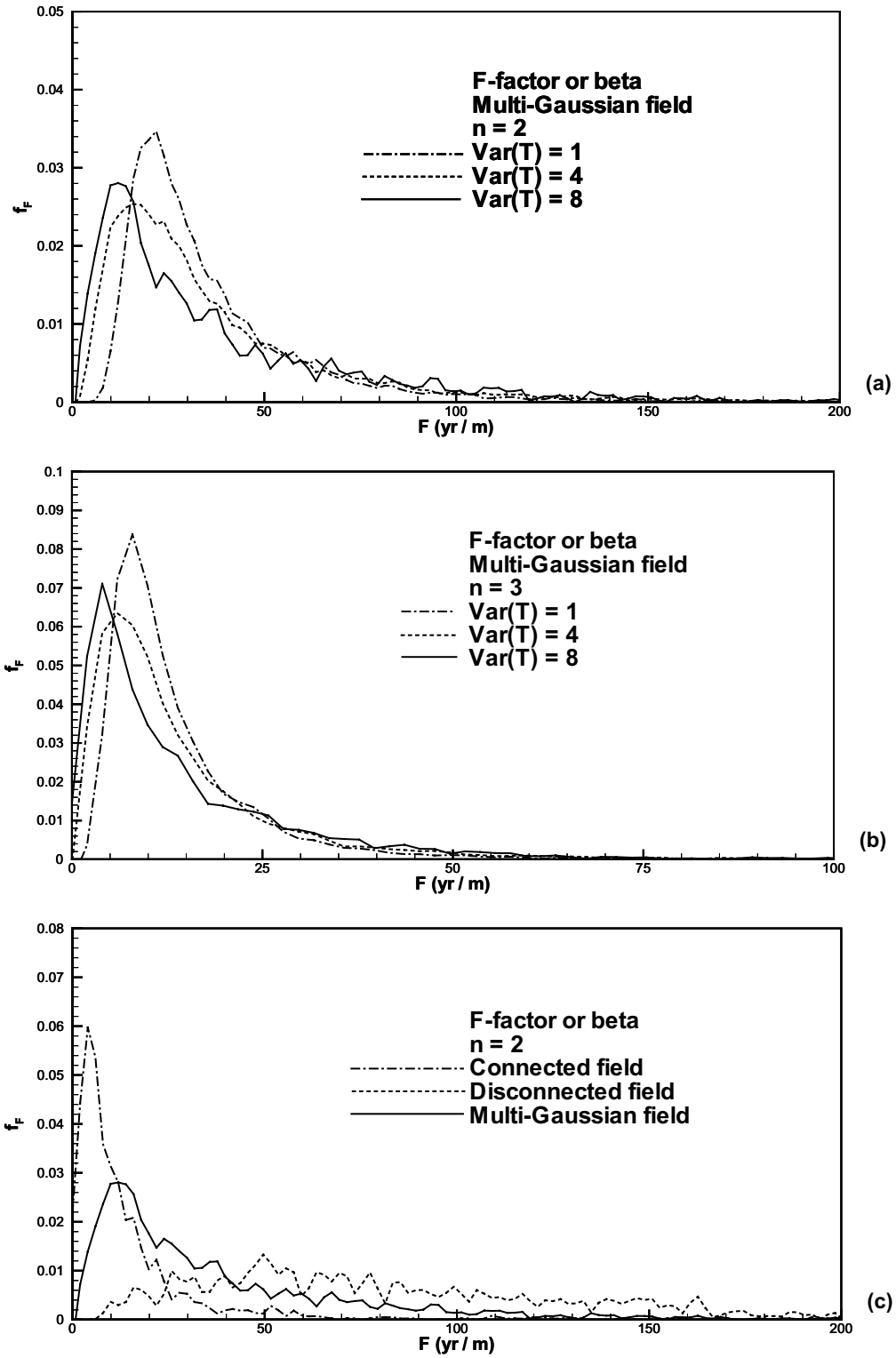

Figure 5-14. *The resulting probability density distribution of β parameter (F-factor) values obtained from particle streamlines from multiple realisations of various simulation cases. (No field data available.) (a) Comparing the three variability cases (Var(Y) = 1, 4, 8) for the Multi-Gaussian texture assuming quadratic law flow. (b) Comparing the three variability cases (Var(Y) = 1, 4, 8) for the Muli-Gaussian texture assuming cubic law flow. (c) Comparing the three textures (CN, DC, MG) for the high variability (Var(Y) = 8) case assuming quadratic law flow.*

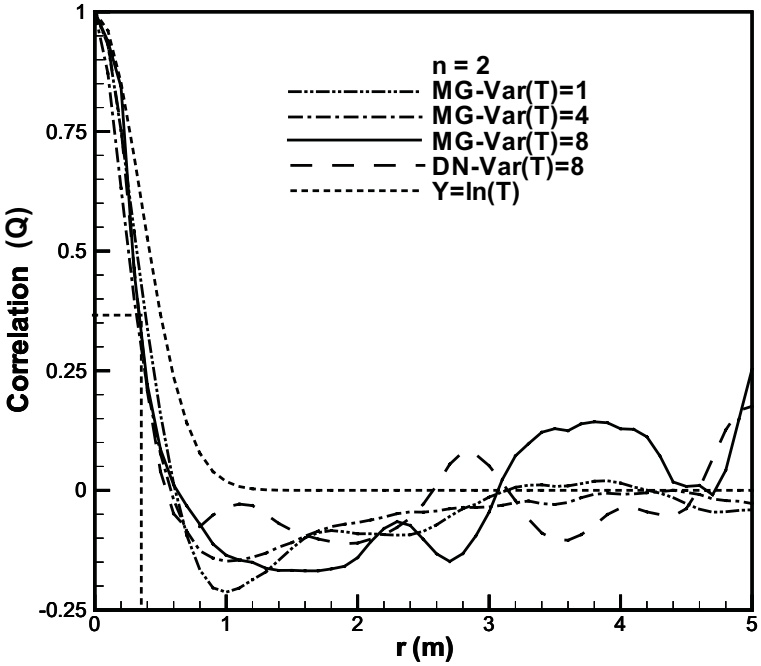

Figure 5-15. *Resulting correlation distances for flow obtained from simulations for the base case mean T. Comparing the Multi-Gaussian textures with Var(Y) = 1, 4, 8, as well as with the Disconnected texture with Var(Y) = 8. Also comparing these against the flow correlation distances obtained from a log-normal distribution Y = ln(T).*

5.4.6 Case with cement dust (descriptive results only)

Descriptive results for additional simulation cases considering the effect of cement dust in the ventilation shaft are presented in this section. The objective of this brief analysis is to evaluate whether the effect of cement dust, which effectively acts as a grouting material reducing inflow into certain sections of the shaft, may be significant in terms of determining fracture heterogeneity properties.

Numerically, the regions of cement dust have been introduced by setting regions of very low conductivity corresponding to the angular segments where cement dust has been observed along the shaft wall at the location of the fracture intersection (cf. Figure 5-1). In all other aspects the simulation domain and configuration settings are as described above (cf. Section 5.2 and Figure 5-4). These simulations impose additional computational challenges since the contrast in conductivity is very large between the cement dust regions (which are assigned a very low conductivity in order to represent a no-flow boundary) and the shaft itself (which is assigned a very high conductivity in order to represent seepage into low pressure atmospheric conditions). With the numerical approach used, these regions require very high refinement in order to obtain accurate solutions for the head and flow fields, and thus require significantly increased computation time and resources.

Example results of the head and flow field are shown for single realisations of the multi-Gaussian texture with $Y = 1$ (Figure 5-16) and $Y = 8$ (Figure 5-17). The flow field in the domain is similar to cases without cement dust other than in the immediate vicinity of the shaft, where inflow is notably restricted to relatively discrete regions of the circumference. Note that whereas flow channelling in the domain is only evident in the $Y = 8$ case, the inflows at the shaft circumference are effectively channelized to small constrained angular segments. The $Y = 8$ case has more such notable inflow regions, corresponding to approximately three segments, whereas the $Y = 1$ case has a wider distribution corresponding to several segments. This is however qualitatively less than the simulation cases without considering effects of cement dust (cf. Figure 5-9).

Also, a comparison with the connected case with $Y = 8$ is shown in Figure 5-18. In this realisation, the local inflows are similar to the MG $Y = 8$ case, but have more notable flow channelling at the full domain scale (not shown).

A more detailed analysis of the inflow distribution for these three selected cases is shown in Figure 5-19. Both $Y = 8$ cases (multi-Gaussian and connected) have one distinct and dominant inflow point. The MG $Y = 1$ case has approximately three distinct inflows, but they are also smaller in terms of flow rate and cover slightly larger angular segments. This can be compared with the corresponding cases without cement dust (cf. Figure 5-10 and Figure 5-11). For both textures, the distribution of inflows is notably more discrete when considering effects of grouting. Also, the MG $Y = 1$ case with grouting behaves in a way similar to approximately MG $Y = 4$ (cf. Figure 5-10b).

The field data has approximately four peaks with flow rates of up to approximately 2, 3, 4 and 8 ml/min (cf. Figure 5-10), which is larger than the inflows obtained from this particular realisation of the MG $Y = 1$ case.

As such, it is clear that the effect of the cement dust as a grouting material may significantly impact possible larger-scaled heterogeneity structures. Even so, variability at the level of $Y = 1$ may be too low to capture field effects, but a plausible range could be restricted to between $Y = 1$ and $Y = 4$, at least for the multi-Gaussian textures. Alternatively, the connected textures with lower variability may offer similar responses. It should however be noted that this brief analysis is based solely on single realisations and only considering a subset of the heterogeneity parameterisation analysed previously in Section 5.2 above.

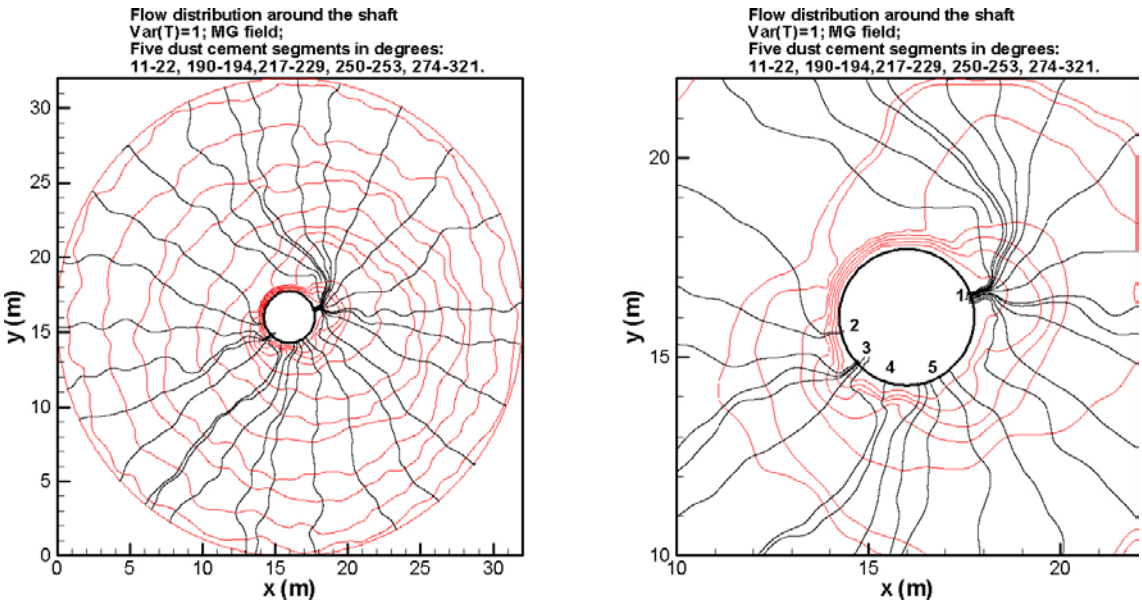

Figure 5-16. *One realisation of the simulated flow field and streamlines for the MG case with Y = 1. Cement dust covers five angular segments of the shaft wall and is implemented as regions with very low conductivity, which effectively restricts the inflow distribution in the vicinity of the shaft wall. Right: Full fracture scale. Left: Detail of the shaft circumference with five main inflow points.*

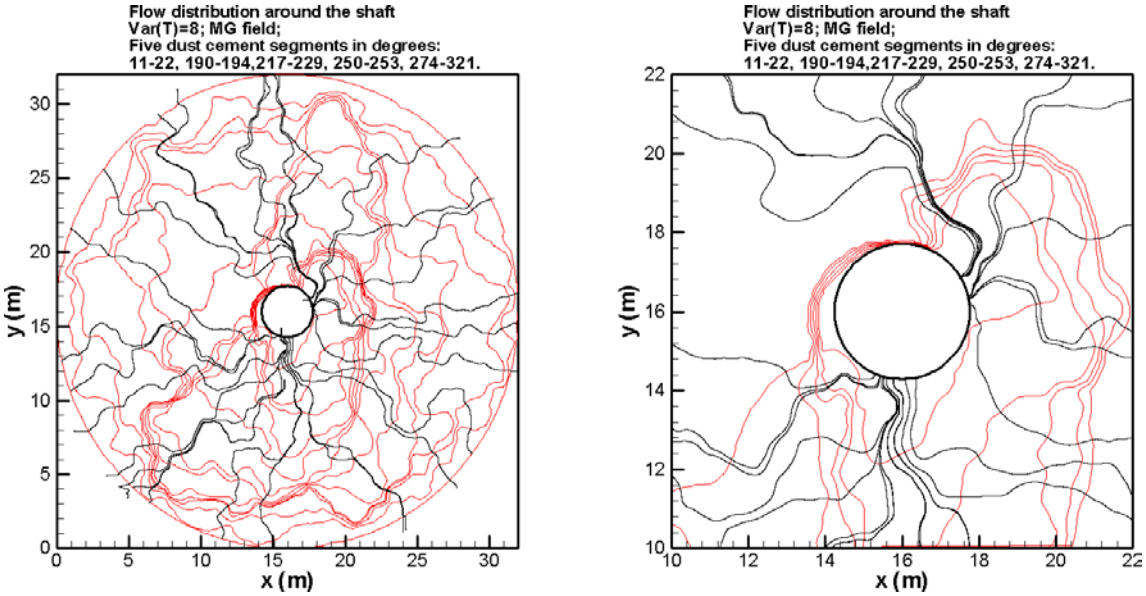

Figure 5-17. *One realisation of the simulated flow field and streamlines for the MG case with Y = 8. Cement dust covers five angular segments of the shaft wall and is implemented as regions with very low conductivity, which effectively restricts the inflow distribution in the vicinity of the shaft wall. Right: Full fracture scale. Left: Detail of the shaft circumference.*

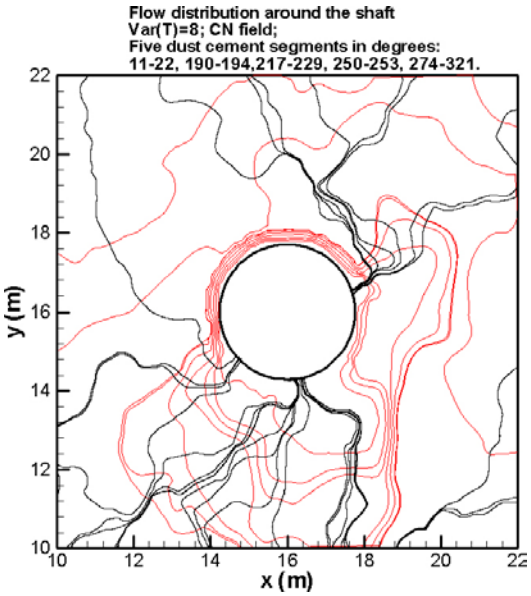

Figure 5-18. *One realisation of the simulated flow field and streamlines for the CN case with Y = 8. Cement dust covers five angular segments of the shaft wall and is implemented as regions with very low conductivity, which effectively restricts the inflow distribution in the vicinity of the shaft wall. (Showing detail of the shaft circumference only.)*

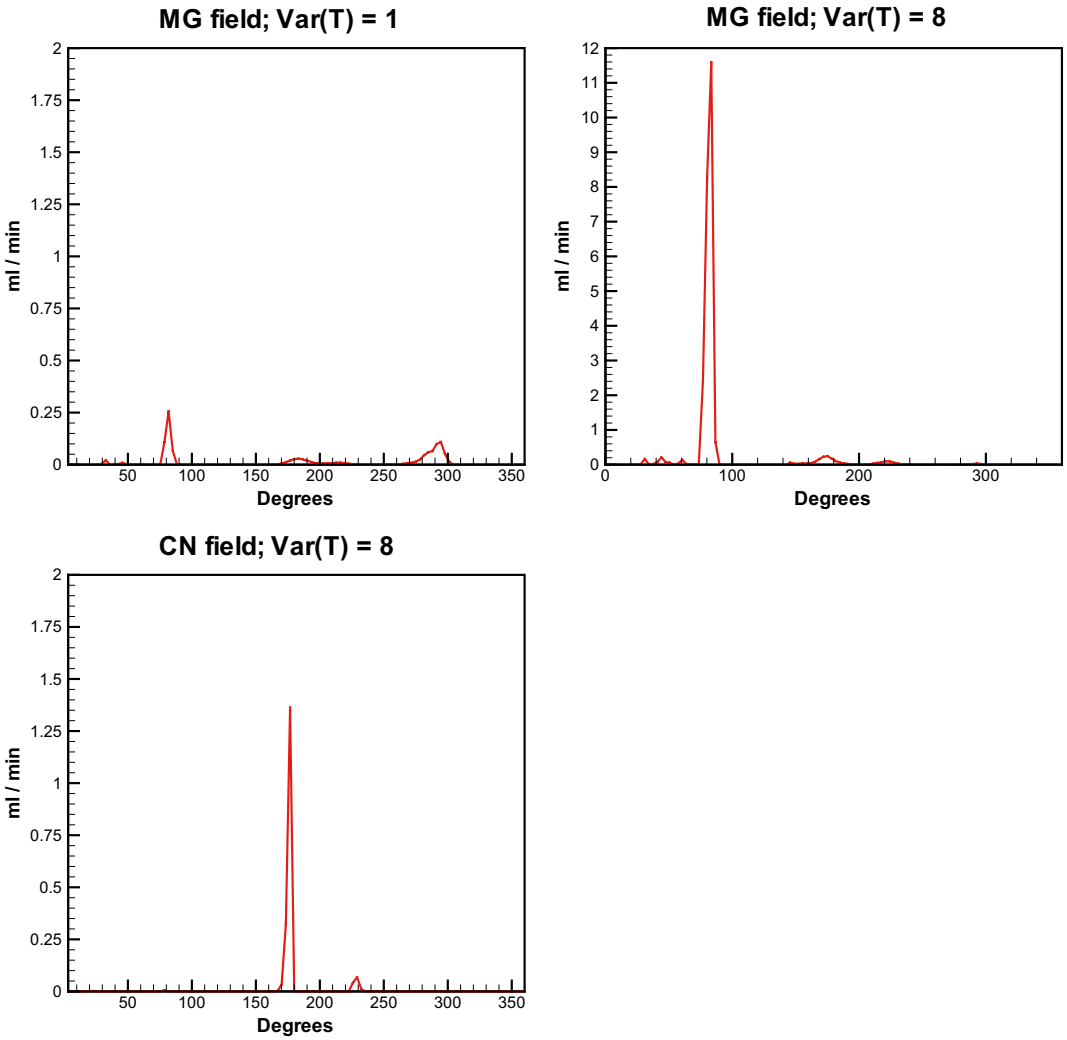

Figure 5-19. *Distribution of flow into the shaft circumference for single realisations of three simulation cases; MG with Y = 1 (upper left), MG with Y = 8 (upper right), and CN with Y = 8 (lower). As the presence of cement dust effectively restricts flow in certain angular segments of the circumference, the inflow distributions are notably discretised (cf. corresponding simulations without cement dust, Figure 5-10 and Figure 5-11).*

5.5 The TS28 case (downscaling simulation)

An additional simulation case combining methods, analysis, field data and simulation results from Tasks 7A, 7B and 7C is considered in this section. The objective is to make use of the multiple cross-hole interference tests and simulations obtained and conducted in Task 7B with single-fracture heterogeneity data analysis and simulation results obtained in Task 7C. This case has been denoted as the TS28 simulation case in the Task 7B description document.

One specific objective considered here is to combine the different methodologies and simulation approaches used in Tasks 7A, 7B and 7C, and by combining these to attempt to model effects of small scale heterogeneity and flow channelling within a larger network. Whereas no direct comparisons with field data are made here, there is a potential possibility of comparing simulation results with information obtainable from improved versions of PFL measurements. In these types of measurements, small-scale directional information of flow across the borehole at the fracture intersection plane can be obtained. Hence an objective of a downscaling simulation would be to obtain flow-directional behaviour which can be compared to or consolidated with field measurements, and an over-arching aim would be to better understand flow channelling behaviour and internal fracture variability. The purpose here however is mainly to demonstrate a possible downscaling approach and its feasibility in simulating flow in small-scale heterogeneous fractures, comprising flow-channelling and resulting in a distribution of flow into a borehole circumference at a specific fracture-borehole intersection.

For the analysis conducted here, the improved simulation configuration obtained in Task 7B, denoted as configuration B, is used (cf. Section 4.4.2). Following task description specifications, the fracture corresponding to the most transmissive feature in borehole KR15 is considered. From PFL field data, this feature is a fracture in the hydraulic zone HZ19C at 59 m depth (Figure 5-20), which corresponds to a discrete fracture at 61 m depth in simulations (Figure 5-21). The flow rate in this feature in this simulation is about five times less than that measured by PFL (Table 5-3); the improved configuration was selected on a basis of obtaining improved matches for both flow directions and flow magnitudes as well as cumulative flows considering responses in all boreholes, hence an exact match in flows should not be expected.

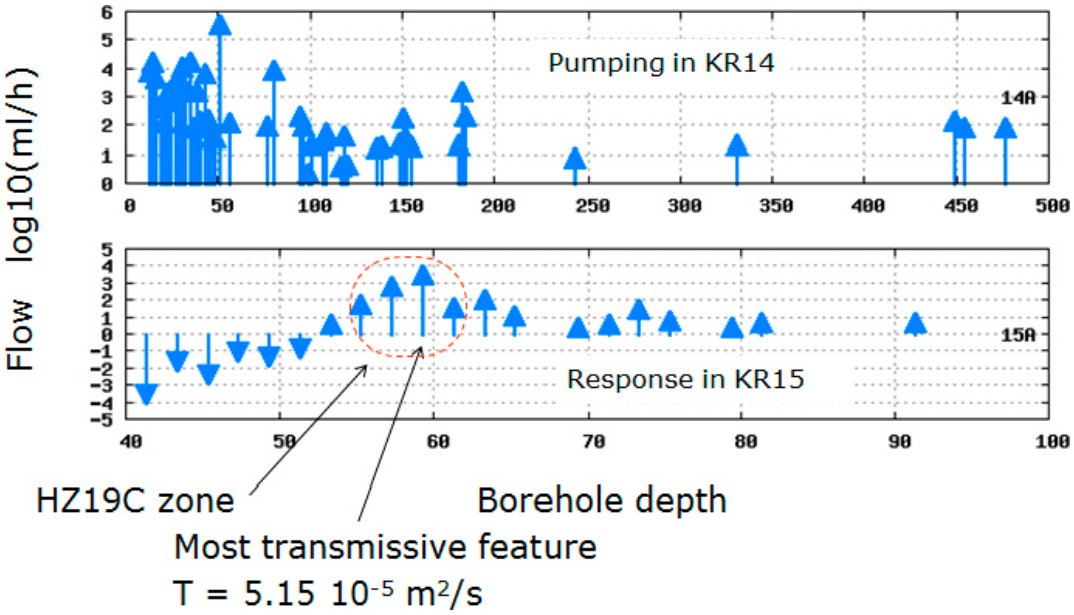

Figure 5-20. *The fracture feature which is the focus of study for the simulation case denoted as TS28. The figure shows PFL measured flow rates in boreholes KR14 and KR15, where KR14 is pumped and responses detected in KR15. The HZ19C zone is the most water-conductive region of borehole KR15 and within this zone there is one fracture in particular which has a high flow rate and hence large transmissivity (of approximately 5.15 × 10^{-5} m^2/s).*

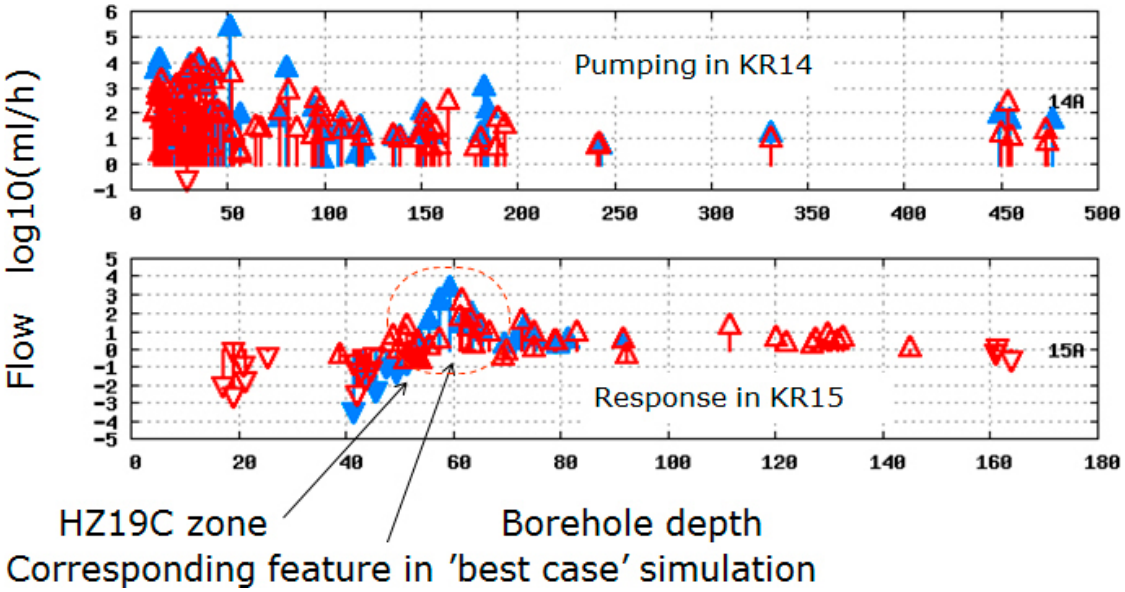

Figure 5-21. *The corresponding simulated fracture flows from the improved configuration B developed in Task 7B (cf. Section 4.4.2).*

Table 5-3. The PFL field measured flow rate for the most transmissive feature in KR15 and the corresponding feature in simulation with simulated flow rate. The simulated flow rate is about 5 times lower than the field measured flow rate.

	PFL field measured	Simulation
Flow rate (ml/h)	11,537	2,130
Flow rate (ml/min)	192.3	35.5
Depth in borehole (m)	59	61

A 10 m by 10 m square sub-region centred by the location of intersection with borehole KR15 of this fracture is considered. The pressure head at points displaced at 1-m intervals along the edges of the square is extracted from the DFN simulation (Figure 5-22). Note the fracture is a homogenous feature with constant transmissivity, hence variations in pressure is due to the network-scale heterogeneity and the pressure field obtained by the large scale boundary conditions as well as pumping in the neighbouring borehole KR14. The highest pressure occurs at the northern-most corner (–4.572681 m) and the lowest along the south-eastern edge (–4.741768 m). However the borehole head in simulation is slightly smaller (–4.741794 m) and hence acts as the point of outflow, or from the plane of reference of the fracture it effectively acts as a sink.

The pressure head along the edges (Figure 5-23) is then used to define the boundaries of a single heterogeneous fracture feature for simulations using the same numerical model and approach as above (cf. Section 5.3.1). In effect, the scenario considered here can be seen as a downscaling simulation, where a discrete fracture network simulation with no internal fracture variability is used to obtain boundary conditions for a small region of a single fracture feature within the domain, and then adopting small scale internal variability at the single fracture scale only.

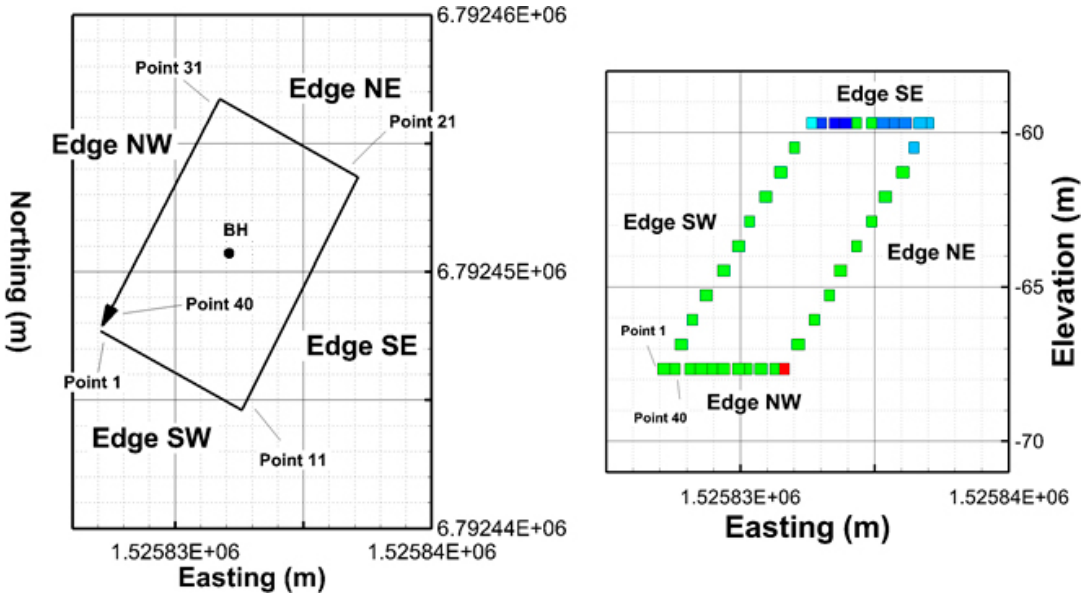

Figure 5-22. *A 10 m × 10 m extract of the fracture considered for the TS28 simulation case, centred by the location of intersection with borehole KR15. Left: Showing the x-y plane view which corresponds to Easting and Northing coordinates. Right: Showing the x-z plane view which corresponds to Easting coordinates and elevation depth. The markers are coloured according to the pressure head at discrete points along the 10 m × 10 m edge with 1-m spacing, where red corresponds to the highest pressure (–4.57 m) and blue to the lowest (–4.74 m), cf. Figure 5-23. The fracture does not appear square due to the angle of projection.*

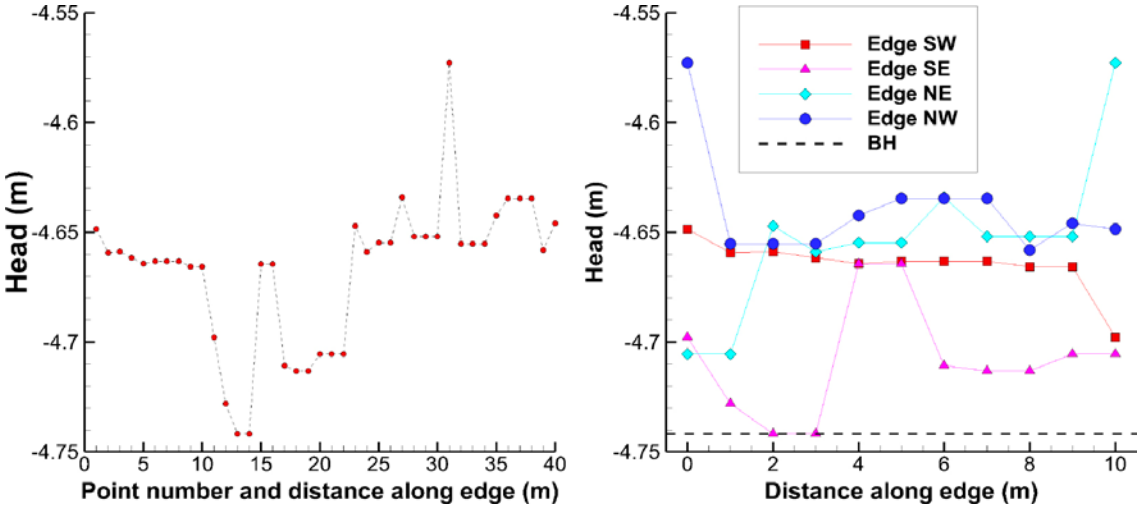

Figure 5-23. *Pressure head (m) along the edges of the 10 m × 10 m section of a homogenous fracture obtained from DFN simulations in Task 7B, which is used as boundary conditions for the heterogeneous fracture in simulation TS28. This fracture corresponding to the most transmissive feature in borehole KR15. Left: The highest pressure (–4.57 m) occurs at the northernmost point (point nr 31) and the lowest (–4.74 m) at along the south-eastern edge (point nrs 13–14). Right: Pressure head (m) along each individual edge. Also showing the drawdown pressure head in borehole KR15 during the KR14 pump test (dashed line); note however the borehole is located at the centre of the fracture. The highest pressure (–4.57 m) occurs at the northernmost point (corner of edges NE and NW) and the lowest (–4.74 m) at 2–3 m along the south-eastern edge.*

Hence for the single-fracture simulations shown in this section, the boundary conditions are prescribed and obtained from large scale DFN simulations. The domain is configured as a two-dimensional square fracture with dimensions 10.24 m by 10.24 m. A borehole of diameter 76 mm is located in the centre of the domain and is prescribed a very high conductivity. The mean effective transmissivity of the fracture is set to 5.15×10^{-5} m^2/s, which is equal to the constant transmissivity value of the original homogeneous fracture, and a spatial correlation is set to 0.08 m in each direction. The following scenarios are considered, adopting a similar procedure and nomenclature as the previous sections above:

- Three heterogeneity structures are considered; Multi-Gaussian (MG), Connected (CN), and Disconnected (DN) textures.
- Two values for the variance in the natural logarithm of transmissivity are considered; Var(Y) = 1 and Var(Y) = 8, where $Y = \ln(T)$.
- Two sensitivity cases for transmissivity parameterisation are considered; a base case adopting the mean fracture T ($n = 2$ with $c_{02} = 1.6\ 10^{-3}$ m^2/s) and a lower T case where the mean fracture T is reduced by 2/3 ($n = 3$ with $c_{03} = 1.07\ 10^{-3}$ m/s).

For each scenario, the flow and velocity fields in the domain are calculated for multiple (100) Monte-Carlo realisations. The grid resolution is 0.02 m by 0.02 m in the domain but is significantly increased (to a scale below 0.01 m) at the borehole location to enable a detailed analysis of the flow distribution around the borehole circumference. Then sample ensemble statistics of the flow of water and velocity distribution of streamlines entering the borehole are obtained for the set of 100 realisations.

Example realisations of the calculated head and flow fields are shown in Figure 5-24 for the multi-Gaussian texture with Var(Y) = 1 and Var(Y) = 8, and in Figure 5-25 for the connected and disconnected textures with Var(Y) = 8. Note the significantly increased flow channelling for the Var(Y) = 8 cases, and the particularly narrow flow channels obtained for the connected structure, which correspond to very high flow rates. The pressure head field is also strongly influence by texture,

in combination with the prescribed boundary conditions and borehole drawdown. North corresponds to an angle of approximately 120° in the simulated borehole coordinates, and based on the boundary conditions should be the point of maximum inflow for a homogenous fracture. The south-eastern edge (y-axis at x = 10.24 m) corresponds to the lowest boundary pressure and should contribute the least flow. However, the variance in transmissivity seems to be a more dominant factor in influencing flow channeling, more influential than texture, and to the extent that the boundary pressure plays a less notable role. For the cases of small heterogeneity $Y = 1$, only small to moderate channeling is observed for the connected and disconnected textures (not shown).

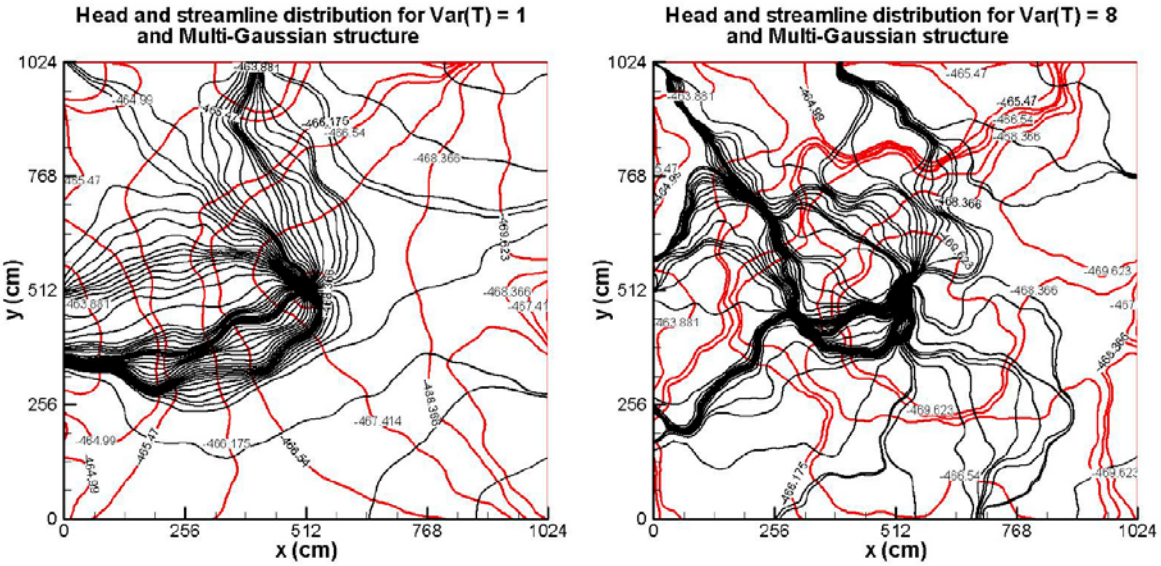

Figure 5-24. *Simulation results of the single 10 m × 10 m fracture with internal variability. The x-axis at y = 0 corresponds to Edge SW, and the y-axis at x = 0 corresponds to Edge NW; the highest boundary pressure occurs at (x, y) = (0,1024) cm and corresponds to the northernmost point. Showing the resulting head (red lines, units in cm) and streamline distribution (black lines) from a selected realisation of the multi-Gaussian (MG) structure with Var(T) = 1 (left) and Var(T) = 8 (right).*

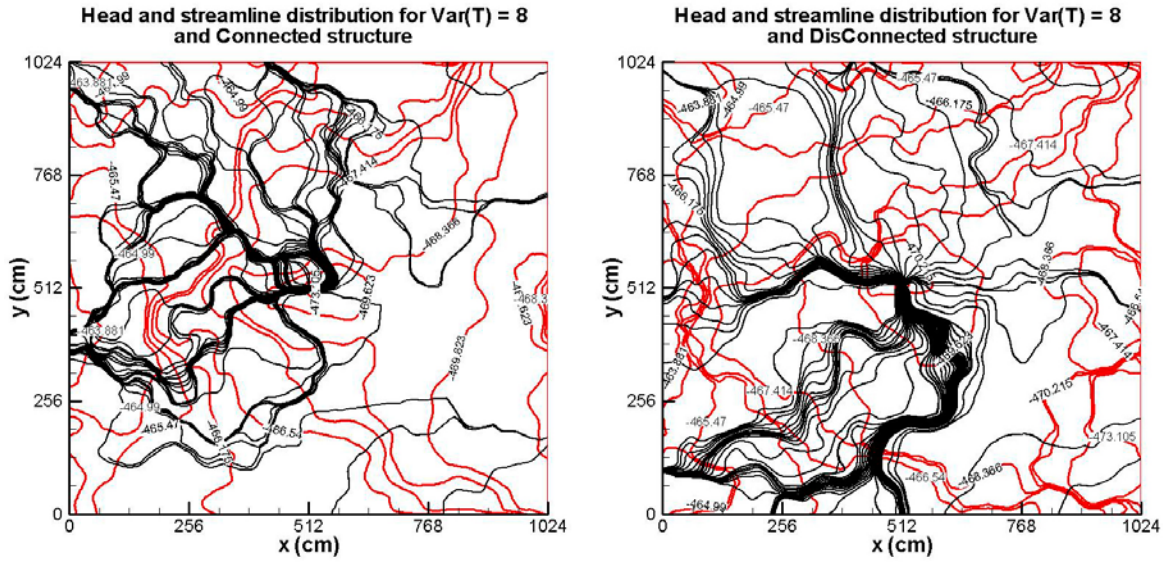

Figure 5-25. *Simulation results of the single 10 m × 10 m fracture with internal variability. Showing the resulting head (red lines) and streamline distribution (black lines) from a selected realisation of the Connected (CN, left) and Disconnected (DC, right) structures Var(T) = 8.*

The corresponding distributions of flow and velocity along the borehole circumference (entering the borehole) are shown in Figure 5-26 for the multi-Gaussian cases with $Y = 1$ and $Y = 8$, and Figure 5-27 for the connected and disconnected cases with $Y = 8$. The multi-Gaussian case with $Y = 1$ typically has a small variability in both flow and velocity around the borehole circumference, however for the increased heterogeneity case with $Y = 8$ regions of peak inflow can become pronounced (Figure 5-26). Both the connected and disconnected structures typically have a more pronounced peak-behaviour, usually concentrated to a relatively small segment of the borehole circumference (Figure 5-27). Note however this does not necessarily coincide with the northern direction (angle of 120°), and hence inflow is strongly influenced by the heterogeneity especially in the close vicinity of the borehole.

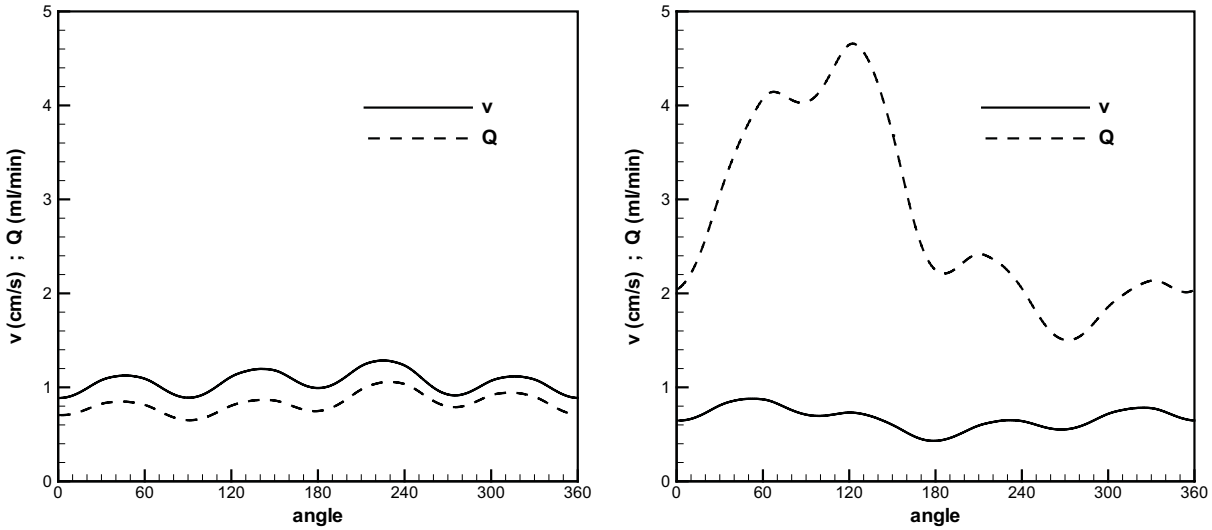

Figure 5-26. *Flow rate and velocity distribution in the borehole for a selected realisation; Var(T) = 1, n = 2, MG (left) and Var(T) = 8, n = 2, MG (right).*

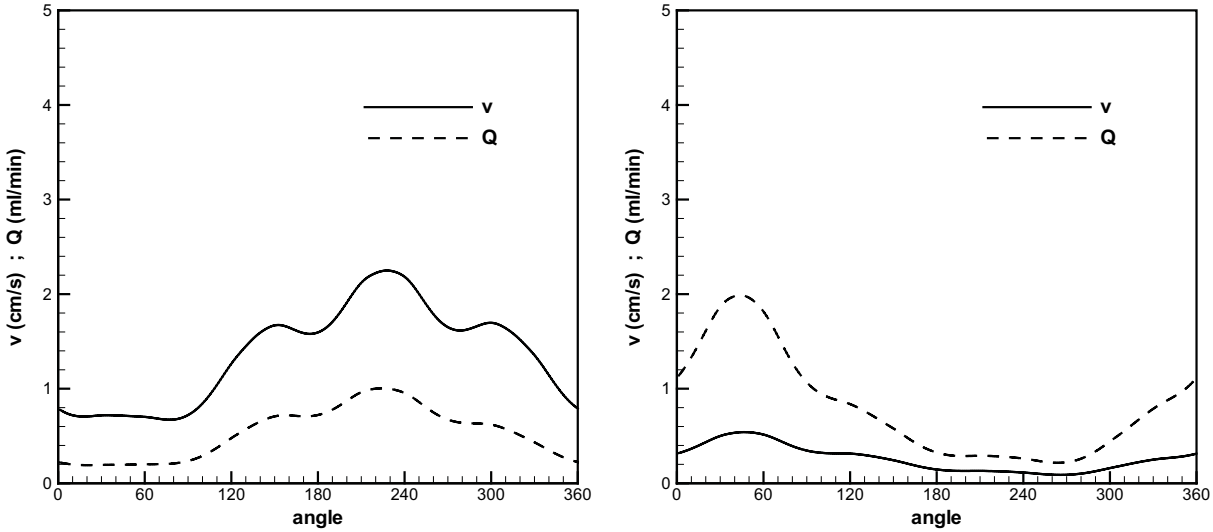

Figure 5-27. *Flow rate and velocity distribution in the borehole for a selected realisation; Var(T) = 8, n = 2, CN (left) and Var(T) = 8, n = 2, DN (right).*

A statistical analysis of the full distribution of inflow rates (into the borehole) can be seen from the sample ensemble of the multiple realisations. The resulting probability densities for all of the multi-Gaussian textures are shown in Figure 5-28. Large inflows (tail of the density) occur more frequently for the $Y = 8$ cases than the $Y = 1$ cases, which likely correspond to more distinct peak flows.

A comparison between textures for the $Y = 8$ case is shown in Figure 5-29. In terms of tailing behaviour and hence increased likelihood of large flows, the connected structure dominates, followed by the multi-Gaussian and finally the disconnected structure. As expected, flow rates are generally reduced for the lower T sensitivity case ($n = 3$). Based on the extended tails, the density distribution of flow rates appears to be non-Gaussian, at least for high variability cases, and the tailing behavior is notably influenced by structure and variability.

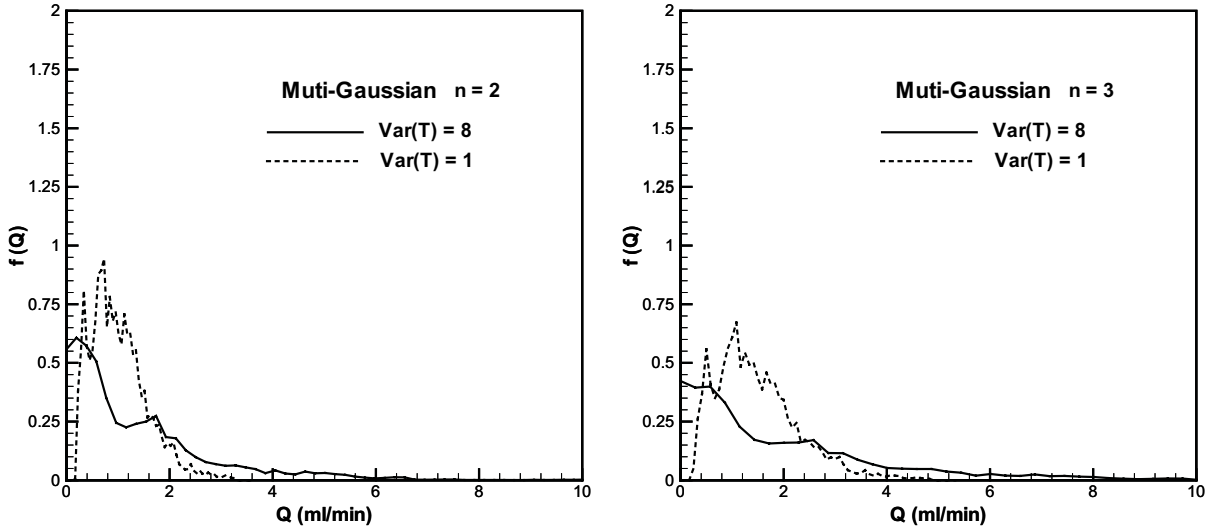

Figure 5-28. *Flow rate pdf; Var(T) = 1,8, n = 2, MG (left) and Var(T) = 1,8, n = 3, MG (right).*

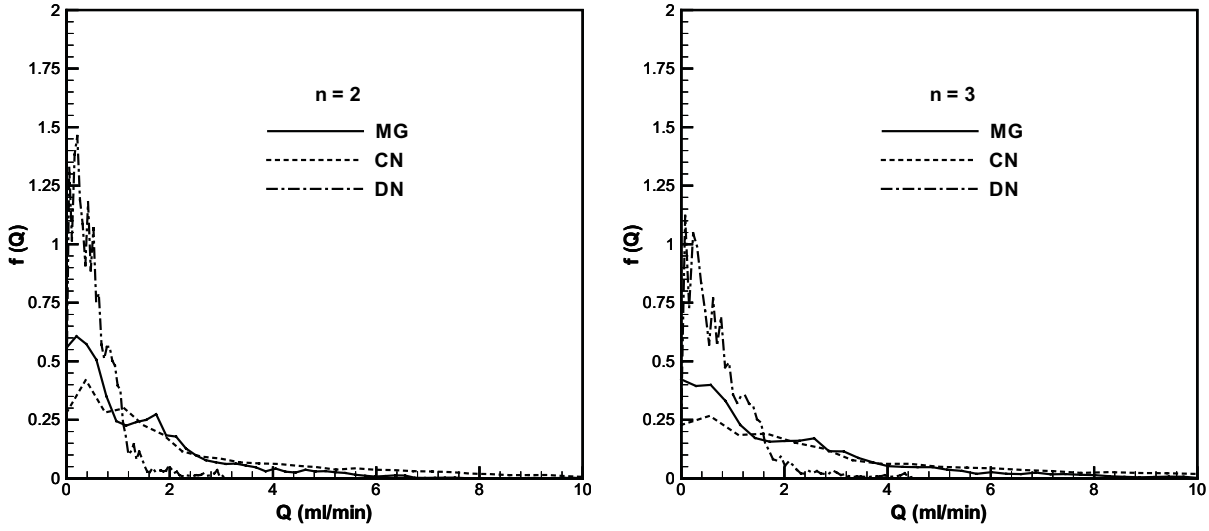

Figure 5-29. *Flow rate pdf for all structures; Var(T) = 8, n = 2 (left) and Var(T) = 8, n = 3 (right).*

A compilation of sample statistics showing the mean and variance in flow rates along small increments around the circumference of the borehole, as well as velocities and the total (cumulative) inflow into the borehole for all simulation scenarios considered is shown in Table 5-4 for the base mean *T* case and Table 5-5 for the reduced mean *T* case. The largest variance in all three measures occurs for the connected case (with $Y = 8$). The variance of the multi-Gaussian texture is somewhat smaller for all measures, followed by the variance of the disconnected texture. Whereas the total inflows vary significantly between cases, they are roughly one order of magnitude larger than the total inflow obtained from the large scale DFN simulation (cf. Table 5-3). Interestingly however, the total inflows are typically within the correct order of magnitude when compared against the field measured inflow (approx. 200 ml/min). Since only drawdown is specified as an internal constraint in pressure in the simulation, using the total inflow could be a means to further calibrate the effective transmissivity of the fracture.

Table 5-4. Mean and variance of volumetric flow rates Q and velocities v of water entering the borehole as well as the total (cumulative) volumetric flow rate Q_T of water entering the borehole obtained from multiple realisations of the base case mean T scenarios (n = 2).

n = 2	Mean <Q> (ml/min)	Var(Q) $(ml/min)^2$	Mean $<Q_T>$ (ml/min)	Var(Q_T) $(ml/min)^2$	Mean <v> (cm/s)	Var(v) $(cm/s)^2$
MG Var(T) = 1	1.47	0.64	378	33,651	0.47	1.60
MG Var(T) = 8	1.99	4.96	512	206,609	0.37	0.08
CN Var(T) = 8	3.48	16.43	892	512,059	0.69	0.27
DN Var(T) = 8	0.76	0.45	195	14,912	0.21	0.02

Table 5-5. Mean and variance of volumetric flow rates Q and velocities v of water entering the borehole as well as the total (cumulative) volumetric flow rate Q_T of water entering the borehole obtained from multiple realisations of the reduced mean T scenarios (n = 3).

n = 3	Mean <Q> (ml/min)	Var(Q) $(ml/min)^2$	Mean $<Q_T>$ (ml/min)	Var(Q_T) $(ml/min)^2$	Mean <v> (cm/s)	Var(v) $(cm/s)^2$
MG Var(T) = 1	1.01	0.29	260	15,710	0.97	0.05
MG Var(T) = 8	1.38	2.37	354	98,882	0.71	0.26
CN Var(T) = 8	2.41	7.69	617	235,703	1.26	0.69
DN Var(T) = 8	0.53	0.21	136	6,500	0.45	0.10

Although no comparison with field measurements for directional flows in boreholes are made, it could in principle be possible to use such field information in order to restrict or set bounds on feasible or non-feasible textures and heterogeneity classes. For example, by considering the range of inflow rates into the borehole and dominant inflow/outflow directions it could be possible to identify or reduce the range or possible parameterisation variables. However, it is likely that the spatial resolution of field measured inflows into borehole-fracture intersections is notably larger (coarser) than what is obtainable by simulation. Another potential issue is that it may be difficult to distinguish between equally probable realisations of a certain simulated fracture configuration; however, here the use of larger-scale boundary conditions obtained from the fracture network simulations may play a role in helping to constrain the inflow variability along the borehole circumference, at least if lower variability cases are assumed.

To conclude this section, further analysis would be needed to evaluate the possibility of setting constraints to simulation configurations. The use of the improved/detailed PFL measurements may be helpful in further setting bounds on parameter ranges or structural classes. Also, the use of other field information, such as tracer tests, may provide additional constraints such as when considering

streamlines and entry velocities. Nevertheless, a combined use of borehole inflow distribution and flow distributions along fractures intersecting the tunnel perimeter of tunnels and ventilation shafts may provide useful information on fracture heterogeneity at different and distinct scales (cm and m). There may however be technical advantages with considering borehole inflow distribution since complications involving unsaturated flow in the interface between fractures and tunnel walls or technical construction issues such as inadvertent infill material (cf. cement dust) are of course not an issue.

5.6 Discussion and conclusions

5.6.1 Discussion of results

Based on the results of the distribution of inflow to the shaft (Figure 5-10 through Figure 5-12), it seems the low variability case of $\mathrm{Var}(Y) = 1$, where $Y = \ln(T)$ is the natural logarithm of transmissivity, may be a poor representation of heterogeneity for this fracture, regardless of texture. It seems clear that the higher variability cases are generally more consistent with field measurements in that such cases produce fewer high peaks as well as baseline flow rates below the measurement limit. Also, even though the Multi-Gaussian texture with high variability can produce sufficiently high peaks, the flow distributions within these peaks are generally broader than what may be expected from field measurements. Both the Disconnected and Connected textures can produce distinct, narrow peaks, consistent with field measurements. The Multi-Gaussian texture could be further investigated by experimentation with various correlation lengths. Here the correlation length is set to 0.5 m in order to be smaller than the fracture size of about 10 m × 10 m and larger than the discretization scale of about 0.01 m. Smaller correlation length are likely to produce less structure and more noise-like variability, which would be likely to cause weaker channelling effects. Larger correlation scales may contribute to stronger channelling effects, but at some point a too large correlation scale will cause the fracture to behave more or less as a homogeneous fracture, thereby also causing weaker channelling. Thus there may be an optimum range of correlation scales which produce greatest channelling for the Multi-Gaussian structure.

In terms of the total inflow only (cumulative flow along the shaft circumference) it would be difficult to distinguish between the variability classes and transmissivity sensitivity, as the effective T combined with a low variability may produce a similar total inflow as a reduced effective T with a higher variability. As such, field measurements of flow distributions can offer additional insight to heterogeneity.

The effect of the cement dust as a grouting material may significantly impact possible larger-scaled heterogeneity structures. Since the material influences the location of observation along the shaft wall by possibly sealing parts of the fracture, it may have a substantial impact in biasing measurements. Based on an extended but brief analysis of simulations attempting to account for this bias, lower values of $\mathrm{Var}(Y)$ can likely be assumed to produce results consistent with observation. Nevertheless, the level of $\mathrm{Var}(Y) = 1$ may be too low to capture field effects, but a plausible range could be restricted to between $\mathrm{Var}(Y) = 1$ and $\mathrm{Var}(Y) = 4$, at least for multi-Gaussian textures. Alternatively, the connected textures with lower variability may offer similar responses. It should however be noted that the analysis considering possible effects of grouting is brief and based solely on single realisations and only considering a subset of cases for heterogeneity parameterisation. The main observation though is that when including grouting effects in the simulation, smaller $\mathrm{Var}(Y)$ values may suffice.

Thus it may be difficult to clearly determine an optimal heterogeneity structure based on the available data set. A unique solution should of course not be expected as the experimental configuration and field data is insufficient to provide a well-constrained problem. However, the simulations may demonstrate that certain parameters may be expected to be ruled out, and may further identify certain constraints and plausible ranges. In particular, it seems a relatively high value of variability, up to $\mathrm{Var}(Y) = 4$ considering effects of possible grouting, and even up to $\mathrm{Var}(Y) = 8$ when not considering effects of possible grouting, should be expected to be consistent with the variability in observed outflows from this fracture. Also, it seems the Connected and Disconnected textures may be more consistent with field observations, however based on simulation cases without possible effects of grouting. Conclusive results may be difficult to determine from the current limited data set considered.

Once a heterogeneity structure is determined, the full probability density of flow magnitudes can be obtained from ensemble realisations. Furthermore, a full characterisation of other parameters of interest can be obtained, such as transport properties. Here the probability density of the β-parameter is shown. This is useful in order to classify fractures in terms of their transport properties. From the analysis conducted in this study, it is observed that there is a significant difference between a Connected and Disconnected field in terms of the β-distribution (which is not evident from flow distribution analysis alone). In fact, the texture type seems to have a greater impact than both variability and hydraulic law. Hence, it may be of significant importance to characterise single fractures in terms of connectivity in transmissivity. Also, further analysis is needed to evaluate the effects this may have on (non-inert) tracer transport.

5.6.2 Main conclusions

The main conclusions based on the sensitivity analysis of single fracture heterogeneity, using numerical flow simulations and compared with field measured inflows to a ventilation shaft as well as inflows to a water-saturated borehole, are discussed in the following.

A microstructural fracture model for heterogeneity is developed, which is based on a correlation texture and combined with a variability class. The model is believed to be consistent with current observations and a general understanding of internal fracture variability for commonly occurring, low-transmissive fractures, applicable for sparsely fractured crystalline rock.

A procedure has been demonstrated for using the field measured inflows along the shaft wall obtained from the 'Nappy experiments' as a simple yet direct data set for comparison with numerical flow simulations. Furthermore, a similar procedure has been developed and principally demonstrated for using borehole-scale inflow distribution measurements as potential data sets for comparison with numerical flow simulations in a downscaling mode, starting at a network scale with multiple homogenous fractures to a small single-fracture scale with internal heterogeneity.

Based on a sensitivity analysis of heterogeneity and comparison with the available, although limited, field measured inflows into the shaft, including considerations of possible grouting effects, the following observations are made.

- A very low and very high variability class might be less consistent with these field measured inflows, whereas the moderate variability class seems to be more consistent with field measured inflows;
- The Multi-Gaussian texture might be less consistent with these field measured inflows, whereas the Disconnected or Connected textures seem to be more consistent with field measured inflows;

In summary, preference is given to cases with moderate log-transmissivity variance, that is within a range $\mathrm{Var}(Y) = 1$ to $\mathrm{Var}(Y) = 4$, combined with a non-Gaussian texture, either as a Disconnected or Connected field. Note that the connected texture represents connectivity in high permeability values and the disconnected texture represents connectivity in low permeability values.

A connected-type texture is consistent with the following conceptual view of a single fracture embedded in a fracture network. Fracture intersections may represent high permeable features in the fracture plane, and contact regions and regions with infill material may represent low permeable regions of the fracture plane. Then the fracture should exhibit significant correlation in high-transmissivity values for regions representing intersections, and significant correlation in low-transmissivity values for regions representing contact points. Thus the main question for a particular single fracture feature may be whether correlated, high-transmissive intersections dominate, or if correlated, low-transmissive contact points dominate. This, in turn, may be relatable to network-scale observational information which impacts the frequency of intersections per fracture, such as fracture set density and lengths.

The resulting probability density distribution of the β-parameter depends mainly on the connectivity patterns in heterogeneity. This is relevant for tracer transport in single fractures, as the β-parameter strongly impacts retention. As such, determination of texture type is identified to be of significant importance for transport studies. In particular, a connected-type texture may have significant effects on non-inert tracer transport, and may potentially be more important than variability class and hydraulic law.

Downscaling simulations using large-scaled effectively homogeneous discrete fracture networks to small single-fracture scaled simulations with internal heterogeneity are feasible, and this may be a potential method for further constraining and conceptualising fracture heterogeneity. The approached developed may in principle be used with field information based on improved PFL flow measurements.

5.6.3 Evaluation and lessons learned

Both the conceptual model for describing fracture heterogeneity as well as the adopted numerical modelling approach are applications of novel methods recently developed in the scientific community.

The heterogeneity structures represent an approach of describing textures based on either superposition of log-normal distributions (the Multi-Gaussian texture), or allowing classes of permeability values to be correlated – the Connected texture allows high permeability values to be correlated over large distances, and the Disconnected texture allows low permeability values to be correlated over large distances. A Disconnected texture may be considered as straight-forward to relate with a conceptual understanding of fractures if shear and normal stresses of the rock mass are assumed to seal most of the fracture, allowing only minor irregularities to form a fracture void space. A connected texture on the other hand could be conceptualised as a media consisting of connected conduits, which could for example be representative of larger connected void spaces caused by fracture intersections.

The numerical method which is used can accurately resolve heterogeneity, as well as accurately solve for flow and particle transport in highly heterogeneous media. Hence, it is a particularly useful tool for studying the effects of structural heterogeneity, including cases of very high variability, where other numerical methods may fail to converge.

The modelling approach adopted is simple and relatively straight-forward, where comparisons are made between shaft inflows obtained from field measurements with corresponding inflows obtained from simulations. Here only a visual comparison is made between simulations and field data. This is mainly due to the relatively limited field data set available, which consists of an inflow distribution along a single fracture trace, which in effect only allows for direct comparisons. As such, the comparison approach could be improved in several minor details. For example, the support scale of size of the liquid collection contained (about 0.2 m) from the field measurements could be imposed on the distribution of simulated inflows, in order to make more consistent comparisons. Also, it would be desirable to make multiple comparisons for several single realisations. Here, it would be necessary to develop a means to compare the inflow distribution of a single realisation with the field measured inflow distribution. For example, the frequency and magnitude of peak flows could be compared. Also, statistical comparison tests for sample data sets could be adopted. In previous studies (Frampton and Cvetkovic 2010), the Kolmogorov-Smirnov and Kuiper tests (Kolmogorov 1933, Kuiper 1962, Press et al. 1992) for unbinned cumulative distributions of PFL flows from boreholes have been successfully used.

Furthermore, the current simulations allow for inflow along the entire circumference of the fracture, whereas there are indications that significant portions may be sealed with cement dust. This could potentially have altered the field-measured inflow distribution, such that inflow is re-routed to open parts of the fracture trace. Hence, an undisturbed distribution may be more evenly distributed and with decreased peaks, assuming the total inflow remains constant. This could potentially alter the evaluation of heterogeneity textures. A simulation configuration which accounts for sealing of parts of the shaft circumference could provide more insight if this has a significant effect in terms of heterogeneity structure and characterisation.

Finally, a downscaling approach has been developed and demonstrated which could in principle be used to constrain heterogeneity parameterisation in a way similar to the procedure adopted using shaft inflow measurements. Combining two distinct scales, that is the tunnel or shaft scale (a few metres) and a borehole scale (a few centimetres) may provide additional information in terms on constraining results, even though technical differences such as support scale of measurement and in situ conditions need to be considered.

6 Conclusions

A summary of the main conclusions and findings of the work conducted within Task 7 as a whole is provided in the following unified discussion of results. Also, the main lessons learned and implications for the Task 7 objectives are highlighted. Specific conclusions for Task 7A, Task 7B, and Task 7C are summarised in Section 3.5, Section 4.5, and Section 5.6 respectively.

6.1 The use of PFL measurements to reduce uncertainty

The Posiva Flow Log (PFL) measurement data provides additional and useful information about a hydrogeological system, which complements traditional hydraulic measurements. In fact, since the measurements are of flow rates, which is essentially a vector quantity, the information provided is potentially more useful than traditional pressure or hydraulic head measurements, which is essentially a scalar quantity.

More importantly, flow rates represent information which may be more closely related to the information of interest for a hydrogeological system, in particular in the context of performance and safety assessment, since flow is more closely related to transport pathways and hence characterisation of transport parameters. However, the additional flow information may be somewhat more challenging to incorporate in current hydrogeological models.

PFL flow measurements conducted under non-pumped conditions and PFL flow responses measured in observation boreholes during adjacent pumping are complicated by the need to account for flow directions in terms of flow entering of leaving the borehole. Analysis of PFL flow data for extensive data sets such as the KR14–KR18 cross-hole interference tests is made possible by using logarithmic flow plots which include flow direction as positive or negative values.

In order to apply PFL data to hydrogeological models, both flow magnitude and direction needs to be taken into account. In particular, the compartmentalized fracture growth model developed and used within Task 7B is determined to be a useful approach which can make extensive use of PFL flow data. This modelling approach can make use of both flow magnitude and direction, which is a unique characteristic of PFL flow data, and hence allows for direct comparison of field measurables. It is also shown that conceptual aspects of the DFN model can to some extent be constrained, even by simple conditioning against PFL data, and as such may improve conceptual aspects of the hydrogeological flow system. Hence, this approach may lead to bridging the gap between stochastic modelling of background fractures and deterministic modelling of hydraulic zones.

As such, PFL information may be seen as vital complementary information in order to produce more accurate groundwater flow models. Hence it can be said that PFL data can be used to reduce model uncertainty, at least qualitatively. A quantifiable reduction of uncertainty may be more challenging to demonstrate, but should be achievable in principle.

In the current work, mainly a scenario analysis based on conceptual alterations of model configurations is conducted, in some instances combined with sensitivity analysis of certain model parameters. This has been the only viable approach as no suitable conditioning methods have been available which are able to handle the complexity of discrete fracture network models. Thus there is a need to develop model conditioning methods which are able to account for both static information and vector information, that is, which are able to incorporate both hydraulic head and flow measurements, such as that obtained from the PFL instrument. In particular, there is a need for conditioning methods which are able to handle a discrete fracture network approach. However, using formal conditioning methods may not necessarily provide an improved conceptual understanding of the behaviour of a model. Scenario analysis based on model variations is therefore likely to be a necessary approach and building block for improved conceptual understanding, which in turn may aid in providing a reduction of uncertainty in hydrogeological system, even if formal conditioning methods are employed.

6.2 Influence of open boreholes

The inclusion of conductive open boreholes is important for improved model representations. It is observed from numerical simulations, primarily based on the work conducted within Task 7A and Task 7B, that there is a clear influence of open boreholes on the hydrogeological flow system. Specifically, the addition of open boreholes results in a homogenization of head responses, since the connectivity between previously isolated fracture compartments increases. That is, the conductive boreholes help connect the discrete fracture network flow system, creating a slightly less heterogeneous system. As a consequence, it should be noted that the PFL measurement data from open boreholes is based on a flow system which may potentially have greater connectivity than the natural or undisturbed flow system, that is, the system present prior to borehole drilling. For long-term performance and safety assessment, the influence of open boreholes may be important if these are not restored to a state consistent with the pre-borehole state, for example filled with grouting material.

6.3 Single fracture heterogeneity

For the single-fracture analysis, a conceptual model for microstructural fracture heterogeneity is developed. This is based on a correlation texture and combined with a variability class. The conceptual model is believed to be consistent with current observations and a general understanding of internal fracture variability for commonly occurring, low-transmissive fractures, applicable for sparsely fractured crystalline rock.

In order to evaluate the conceptual microstructural single-fracture model, a procedure has been adopted for using the field measured inflows along the wall of a ventilation shaft for comparison with corresponding inflows obtained from numerical flow simulations. In addition, a downscaling method has been developed and demonstrated which may be used for comparison of simulated and field measured directional flows in specific fracture-boreholes intersections. The numerical method used is a particularly useful tool for single-fracture analysis as it is able to accurately solve for flow and particle pathways even for cases of extreme heterogeneity. This is consistent with a general understanding of single fractures, as parts of the fracture void space can be conceptualised as small open channels, yielding high transmissive regimes, whereas other parts of the fracture must be closed yielding no-flow regimes. The numerical model is thereby used to as a tool to test various configurations of the fracture model, and comparisons with field measurable quantities therefore make it possible to distinguish between plausible and unlikely representations of the microstructural single-fracture model.

The main result from the single-fracture analysis indicates that the particular single fracture considered, which represents a class of low-transmissive background fractures, is expected to have a moderate to relatively high variance in transmissivity, combined with a non-Gaussian texture where low permeability values are relatively strongly correlated.

This is relevant for tracer transport in fractured media, as a non-Gaussian, connected-type texture may have significant effects on non-inert tracer transport. It is noted that this may potentially be more important than identification of variability class or hydraulic law. As such, determination of texture type is identified to be of significant importance for transport studies. This in turn will have impact on long term performance and safety assessment analysis.

6.4 Additional comments

Based on large-scale discrete fracture network simulations conducted within Task 7A, the major flow pathways seem to be towards the south-eastern part of the island, via two major fracture zones to the fracture zones beneath the sea bed, which in turn are in contact with the Baltic Sea.

Multiple forcing of a hydrogeological system, such as the experiments conducted in boreholes KR14–KR18 and used in Task 7B, yields significantly more information in terms of constraining a model configuration than if pumping in a single borehole with a semi-radial drawdown only were considered. Here, the PFL instrument is particularly useful, since it is able to log flows in response

boreholes relatively quickly and efficiently, and provides a significant amount of useful information of the hydrogeological system. By combining this with suitable modelling approaches, an improved understanding of hydrogeological flow system is achievable.

In particular, the fracture growth model developed and used for work conducted within Task 7B is relatively simple, essentially based on a minimalistic approach at configuring and constraining a discrete fractured network based on extensive hydrogeological flow data such as that obtained with the PFL instrument. For example, only fractures with PFL measurable flows are used, which are thereafter evaluated against PFL flows at the locations of fractures intersecting boreholes. The main unknown parameters are fracture sizes, which in turn are constrained by the distance between neighbouring boreholes. Internal fracture heterogeneity is also a significant unknown, as the PFL inferred transmissivity is based on using homogenization assumptions. So far, the approach is adopted in a simplified manner. Despite this, it is shown to be useful in being able to discard certain aspects of possible simulation configurations and increase the confidence in others. Also, it is shown to be a useful tool in understanding fundamental conceptual features of the system, such as the main flow pathways.

Nevertheless, several improvements to the approach would be desirable and should be further investigated. In particular, the technical implementation of the fracture growth model used in this analysis is based on fixed geometrical domains surrounding boreholes. As such, it is based on a radial length scale from the borehole locations. It would be preferable to have a more physically-based implementation, such as by extending fractures until their first intersection with neighbouring fractures, that is, regardless of a fixed radial distance. Also, if fractures are dated by for example lithology, it would be possible to introduce fracture hierarchies, for example by allow younger fractures to terminate at older fractures, or based on other similar rules inspired from suitable understanding of the behaviour of rock mechanics.

Also, more advanced means of introducing fracture heterogeneity, and especially exerting control over fracture intersections would be useful to further analyse the system in terms of flow directions and flow continuity between boreholes. Here, additional information of the system could also be adopted. For example, incorporating hydraulic testing with packed-off boreholes should provide more detailed information on internal compartmentalization of the model, especially along the vertical extent of the domain.

This should also be put in context of the understanding of internal fracture heterogeneity gained from the work conducted in Task 7C. The heterogeneity structure of the fracture studied seems to be more consistent with a description of a non-Gaussian connected-type texture, where connectivity may exist between high or low permeable sections of the fracture. The fracture studied is assumed to be a single fracture, however in order to produce flow it cannot be isolated, so at certain locations must be connected to the larger fracture network. Thus, a connected-type texture is consistent with the conceptual view that single fractures embedded in a fracture network may exhibit strong correlation in high and/or low transmissivity values, representing for example fracture intersections and contact points respectively.

References

SKB's (Svensk Kärnbränslehantering AB) publications can be found at www.skb.com/publications.

Cvetkovic V, Frampton A, 2010. Transport and retention from single to multiple fractures in crystalline rock at Äspö (Sweden): 2. Fracture network simulations and generic retention model. Water Resources Research 46, W05506. doi:10.1029/2009WR008030

Cvetkovic V, Dagan G, Cheng H, 1998. Contaminant transport in aquifers with spatially variable hydraulic and sorpion properties. Proceedings: Mathematical, Physical and Engineering Sciences 454, 2173–2207.

Cvetkovic V, Selroos J-O, Cheng H, 1999. Transport of reactive tracers in rock fractures. Journal of Fluid Mechanics 378, 335–356.

Cvetkovic V, Painter S, Outters N, Selroos J-O, 2004. Stochastic simulation of radionuclide migration in discretely fractured rock near the Äspö Hard Rock Laboratory. Water Resources Research 40. doi:10.1029/2003WR002655

Cvetkovic V, Cheng H, Widestrand H, Byegård J, Winberg A, Andersson P, 2007. Sorbing tracer experiments in a crystalline rock fracture at Äspö (Sweden): 2. Transport model and effective parameter estimation. Water Resources Research 43. doi:10.1029/2006WR005278

Dershowitz W, Winberg A, Hermanson J, Bygård J, Tullborg E-L, Andersson P, Mazurek M, 2003. Äspö Hard Rock Laboratory. Äspö Task Force on modelling of groundwater flow and transport of solutes. Task 6c. A semi-synthetic model of block scale conductive structures at the Äspö HRL. SKB IPR-03-13, Svensk Kärnbränslehantering AB.

Frampton A, Cvetkovic V, 2009. Significance of injection modes and heterogeneity on spatial and temporal dispersion of advecting particles in two-dimensional discrete fracture networks. Advances in Water Resources 32, 649–658.

Frampton A, Cvetkovic V, 2010. Inference of field scale fracture transmissivities in crystalline rock using flow log measurements. Water Resources Research 46. doi:10.1029/2009WR008367

Gotovac H, 2009. A multi-resolution approach for modeling flow and solute transport in heterogeneous porous media. PhD thesis. Royal Institute of Technology (KTH), Stockholm, Sweden.

Gotovac H, Andricevic R, Gotovac B, 2007. Multi-resolution adaptive modeling of groundwater flow and transport problems. Advances in Water Resources 30, 1105–1126.

Gotovac H, Cvetkovic V, Andricevic R, 2009a. Adaptive Fup multi-resolution approach to flow and advective transport in highly heterogeneous porous media: methodology, accuracy and convergence. Advances in Water Resources 32, 885–905.

Gotovac H, Cvetkovic V, Andricevic R, 2009b. Flow and travel time statistics in highly heterogeneous porous media. Water Resources Research 45, W07402. doi:10.1029/2008WR007168

Hartley L, Holton D, 2008a. CONNECTFLOW Release 9.4. Technical summary document. 150 Harwell IBC, Didcot, Oxfordshire OX11 0RA, United Kingdom.

Hartley L, Holton D, 2008b. CONNECTFLOW Release 9.5. Technical summary document. 150 Harwell IBC, Didcot, Oxfordshire OX11 0RA, United Kingdom.

Hartley L, Holton D, 2008c. CONNECTFLOW Release 9.6. Technical summary document. 150 Harwell IBC, Didcot, Oxfordshire OX11 0RA, United Kingdom.

Hartley L, Holton D, Hoch A R, 2008a. NAPSAC Release 9.4. Technical summary document. 150 Harwell IBC, Didcot, Oxfordshire OX11 0RA, United Kingdom.

Hartley L, Holton D, Hoch A R, 2008b. NAPSAC Release 9.5. Technical summary document. 150 Harwell IBC, Didcot, Oxfordshire OX11 0RA, United Kingdom.

Hartley L, Holton D, Hoch A R, 2008c. NAPSAC Release 9.6. Technical summary document. 150 Harwell IBC, Didcot, Oxfordshire OX11 0RA, United Kingdom.

Kolmogorov A, 1933. Sulla determinazione empirica di una legge di distribuzione [On the empirical determination of a distribution function]. Giornale dell'Istituto Italiano degli Attuari 4, 83–91. (In Italian.)

Koyama T, 2007. Stress, flow and particle transport in rock fractures. PhD thesis. Royal Institute of Technology (KTH), Stockholm, Sweden.

Kuiper N H, 1962. Tests concerning random points on a circle. Proceedings of the Koninklijke Nederlandse Akademie van Wetenschappen, Series A 63, 38–47.

Press W H, Teukolsky S A, Vetterling W T, Flannery B P, 1992. Numerical recipes in Fortran 77: the art of scientific computing. 2nd ed. Cambridge: Cambridge University Press.

Pöllänen J, Rouhiainen P, 2001. Difference flow measurements in borehole KOV01 at Oskarshamn. SKB R-01-59, Svensk Kärnbränslehantering AB.

Rouhiainen P, Sokolnicki M, 2005. Oskarshamn site investigation. Difference flow logging of borehole KLX04. Subarea Laxemar. SKB P-05-68, Svensk Kärnbränslehantering AB.

Vidstrand P (ed), Ahokas H, Bockgård N, Dershowitz W, Holton D, Lanyon W, Poteri A, Koskinen L, 2015. SKB Task Force GWFTS – Task 7. Descriptions for hydrogeological modelling of Olkiluoto, Finland. Compilation of all task descriptions assessed within the Task 7 of the SKB Task Force on modelling of groundwater flow and transport of solutes. SKB P-12-21, Svensk Kärnbränslehantering AB.

Zinn B, Harvey C F, 2003. When good statistical models of aquifer heterogeneity go bad: a comparison of flow, dispersion, and mass transfer in connected and multivariate Gaussian hydraulic conductivity fields. Water Resources Research 39, 1051. doi:10.1029/2001WR001146.

Öhberg A, Rouhiainen P, 2000. Groundwater flow measuring techniques. Posiva 2000-12, Posiva Oy, Finland.